


Measurement of the azimuthal anisotropy of charged particles in $\sqrt{s_{NN}} = 5.36$ TeV $^{16}\text{O} + ^{16}\text{O}$ and $^{20}\text{Ne} + ^{20}\text{Ne}$ collisions with the ATLAS detector

G. Aad *et al.**
(ATLAS Collaboration)

 (Received 8 September 2025; accepted 10 December 2025; published 13 April 2026)

This paper presents the first measurements of the azimuthal anisotropy coefficients v_n , which quantify the n th-order Fourier modulation of charged-particle azimuthal distributions, for $n = 2-4$ in $\sqrt{s_{NN}} = 5.36$ TeV $^{16}\text{O} + ^{16}\text{O}$ and $^{20}\text{Ne} + ^{20}\text{Ne}$ collisions recorded with the ATLAS detector at the CERN Large Hadron Collider in 2025. The v_n coefficients are measured as a function of transverse momentum (p_T), collision centrality, and event multiplicity. They are extracted using two complementary methods: two-particle correlations with a template-fit subtraction of short-range nonflow contributions, and four-particle subevent cumulants, which intrinsically suppress nonflow effects and provide sensitivity to flow fluctuations. The results show a clear hierarchy $v_2 > v_3 > v_4$ and a nonmonotonic dependence on p_T , reaching a maximum around 2 GeV, consistent with trends observed in heavy-ion collisions. Detailed comparisons between the two collision systems reveal an enhanced v_2 in central $^{20}\text{Ne} + ^{20}\text{Ne}$ collisions, consistent with theory expectations based on the predicted prolate deformation of neon nuclei, in contrast to the slightly tetrahedral structure predicted for oxygen. The four-particle cumulant results highlight strong event-by-event fluctuations and provide the greatest sensitivity to nuclear shape effects. These measurements can place new constraints on the initial geometry and the hydrodynamic response in light-ion collisions, offering valuable input for models of nuclear structure.

DOI: [10.1103/xqxz-8bhf](https://doi.org/10.1103/xqxz-8bhf)

I. INTRODUCTION

A hot and dense state of nuclear matter in which the relevant degrees of freedom are strongly coupled quarks and gluons is known as the quark-gluon plasma (QGP). This state can be created transiently in collisions of heavy nuclei at high-energy colliders, such as the BNL Relativistic Heavy Ion Collider (RHIC) and the CERN Large Hadron Collider (LHC) [1–11]. The QGP produced in heavy-ion collisions undergoes collective expansion driven by strong pressure gradients, which convert initial-state spatial anisotropies into momentum anisotropies of the final-state hadron distribution [1–3,12]. This phenomenon, commonly referred to as collective flow, is well described by nearly inviscid relativistic hydrodynamics and constitutes a key signature of QGP formation (see Ref. [13] and references therein).

The anisotropy of particle distributions in heavy-ion collisions is quantitatively characterized by a Fourier series in the azimuthal angle ϕ [14]:

$$\frac{dN}{d\phi} \propto 1 + 2 \sum_{n=1}^{\infty} v_n \cos[n(\phi - \Psi_n)], \quad (1)$$

where v_n and Ψ_n represent the magnitude and orientation of the n th-order anisotropy, respectively. The v_n are commonly referred to as “flow harmonics,” while the Ψ_n are referred to as “event-plane angles.” The v_n depend on transverse momentum p_T , pseudorapidity¹ (η), and event multiplicity, and they fluctuate event-by-event (EbE) [15–18]. These EbE fluctuations arise primarily from variations in the initial geometry and energy density of the nuclear overlap region, which are driven by the fluctuating positions of nucleons and by the subnucleonic structure, collectively referred to as geometric fluctuations. Among these coefficients, elliptic flow (v_2) is the largest due to the lenticular geometry of the average overlap region. This is typically followed by triangular flow (v_3), which typically has no contribution from the average geometry and is therefore generated entirely by EbE geometric fluctuations. For higher orders ($n \geq 4$), the flow harmonics are influenced not only by the initial geometry but also by nonlinear mode coupling from lower-order harmonics, such as v_4 from v_2^2 and v_5 from $v_2 v_3$ [19]. These contributions make the higher-order harmonics sensitive to both the geometry and the medium’s collective response. Extensive studies of v_n and their EbE fluctuations have provided important constraints on

*Full author list given at the end of the article.

Published by the American Physical Society under the terms of the [Creative Commons Attribution 4.0 International](https://creativecommons.org/licenses/by/4.0/) license. Further distribution of this work must maintain attribution to the author(s) and the published article’s title, journal citation, and DOI. Open access publication funded by CERN.

¹ATLAS uses a right-handed coordinate system with its origin at the nominal interaction point (IP) in the center of the detector and the z axis along the beam pipe. The x axis points from the IP to the center of the LHC ring, and the y axis points upwards. Cylindrical coordinates (r, ϕ) are used in the transverse plane, with ϕ being the azimuthal angle around the z axis. The pseudorapidity is defined in terms of the polar angle θ as $\eta = -\ln \tan(\theta/2)$.

the initial-state geometry and on transport properties of the QGP in nuclear collisions, such as the shear viscosity to entropy density ratio η/s (see Ref. [13] and references therein).

The observation of collective flow was initially regarded as an exclusive signature of QGP formation in collisions of heavy nuclei, such as Au + Au or Pb + Pb systems. However, experiments at the LHC and the RHIC have revealed large v_n signals in much smaller collision systems, including pp and $p + \text{Pb}$ at the LHC [20–23] and $p/d/{}^3\text{He} + \text{Au}$ at the RHIC [24–27]. Remarkably, the observed v_n hierarchy in these small systems follows patterns consistent with expectations based on geometrical differences between their initial conditions. Detailed theory studies suggest that the measured v_n in small systems can be explained by the collective expansion of the matter produced in the collision, driven by the shape and fluctuations of the initial overlap region [28,29]. Nevertheless, substantial uncertainties remain regarding the precise nature and properties of the produced matter in small collision systems. These uncertainties arise primarily from the incomplete understanding of the initial conditions in small systems, which are sensitive not only to the spatial distribution of nucleons within nuclei but also to the internal structure of individual nucleons [24,30]. Consequently, precise characterization of the initial conditions in small systems is essential to improve the extraction of medium properties such as shear viscosity, prehydrodynamic evolution effects, and initial-state momentum anisotropies [31–33].

To address these uncertainties, a promising experimental strategy is to compare v_n harmonics in collisions of nuclei with similar mass numbers but distinct nucleon arrangements [34–36]. Such systems are expected to produce matter with comparable bulk properties and similar final-state collective responses. Therefore, the ratios of v_n between the two systems are expected to be primarily sensitive to differences between their initial conditions [37]. Analogous comparisons have previously been used to study the influence of nuclear structure in large collision systems [38–40]. A key advantage of applying this approach in small collision systems is that the initial-state differences are governed by nucleon distributions that can, in principle, be calculated using state-of-the-art *ab initio* nuclear structure theories [41], providing a theoretical foundation for interpreting experimental observations.

An ideal pair of collision systems for such comparative studies is ${}^{16}\text{O} + {}^{16}\text{O}$ and ${}^{20}\text{Ne} + {}^{20}\text{Ne}$. Low-energy experiments and theory calculations indicate that ${}^{16}\text{O}$ has a near-spherical tetrahedral shape, whereas ${}^{20}\text{Ne}$ is predicted to consist of a ${}^4\text{He}$ cluster “orbiting” an ${}^{16}\text{O}$ core [42,43]. Hydrodynamic simulations incorporating nuclear configurations from *ab initio* calculations predict significant enhancements in v_2 and v_3 for central ${}^{20}\text{Ne} + {}^{20}\text{Ne}$ collisions compared with central ${}^{16}\text{O} + {}^{16}\text{O}$ collisions² [44]. Furthermore, nuclear structure effects are also predicted to modify the E_{bE} fluctuations of v_2 and v_3 between the two systems [45], providing additional discriminatory power for theory models.

This paper presents measurements of anisotropic flow coefficients v_n for $n = 2$ to 4 in $\sqrt{s_{NN}} = 5.36$ TeV O + O and Ne + Ne collisions recorded by the ATLAS detector at the LHC in 2025. The analysis employs both two- and four-particle correlation methods [22,46], which probe different moments of the v_n distributions. These measurements provide valuable constraints on the final-state collective response and on the properties of the produced medium in each system individually, while their comparison offers unique insights into the initial-state geometry and nucleon distributions within these light nuclei. After this paper was submitted for publication, related measurements from the ALICE and CMS Collaborations [47,48] were also submitted.

II. EXPERIMENTAL CONFIGURATION

The ATLAS detector [49,50] at the LHC covers nearly the entire solid angle around the collision point. It consists of an inner tracking detector surrounded by a thin superconducting solenoid, electromagnetic and hadronic calorimeters, and a muon spectrometer incorporating three large superconducting air-core toroidal magnets. The primary subsystems relevant to this study include the inner detector (ID), the calorimeter, and the trigger and data acquisition infrastructure.

The ID is immersed in a 2-T axial magnetic field and provides charged-particle tracking in the range $|\eta| < 2.5$. The high-granularity silicon pixel detector covers the vertex region and typically provides four measurements per track, the first hit generally being in the insertable B-layer (IBL). It is followed by the semiconductor tracker (SCT), which usually provides eight measurements per track. These silicon detectors are complemented by the transition radiation tracker (TRT), which enables radially extended track reconstruction up to $|\eta| = 2.0$.

The calorimetry system includes several components: a liquid argon (LAr) electromagnetic calorimeter covering $|\eta| < 3.2$; a steel-scintillator sampling hadronic calorimeter covering $|\eta| < 1.7$; an additional LAr-based hadronic calorimeter for the region $1.5 < |\eta| < 3.2$; and forward LAr calorimeters (FCal) designed to measure both electromagnetic and hadronic activity in the range $3.2 < |\eta| < 4.9$. Forward neutrons produced from the breakup of nuclei in both hadronic and electromagnetic interactions are measured by compact tungsten sampling zero degree calorimeters (ZDCs) positioned at $z = \pm 140$ m from the ATLAS interaction point.

Event collection is handled by a two-tiered trigger system [51]. The first level (L1) is implemented through a combination of custom hardware and programmable logic, while the high-level trigger (HLT) uses software algorithms to refine the selection using more detailed detector information.

A software suite [52] is used in data simulation, in the reconstruction and analysis of real and simulated data, in detector operations, and in the trigger and data acquisition systems of the experiment.

III. DATASETS, EVENT, AND TRACK SELECTION

The O + O and Ne + Ne data used in this paper were collected in July 2025. The datasets correspond to integrated

²For simplicity, ${}^{16}\text{O}$ and ${}^{20}\text{Ne}$ are hereafter denoted as O and Ne, respectively.

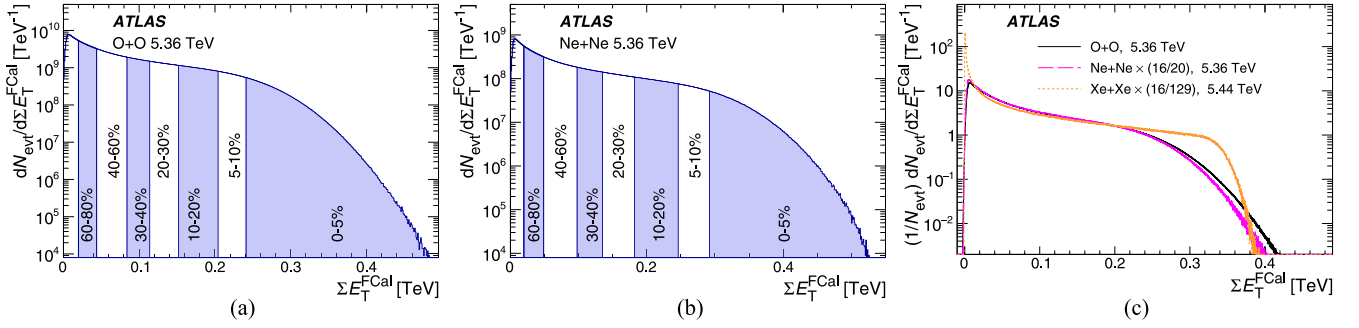


FIG. 1. The ΣE_T^{FCal} distribution in minimum-bias events, together with the thresholds for a few centrality intervals for (a) O + O collisions and (b) Ne + Ne collisions. (c) Comparison to Xe + Xe collisions [7], where the ΣE_T^{FCal} distributions of the Xe + Xe and Ne + Ne systems are scaled by the relative number of nucleons to oxygen. The Ne + Ne and Xe + Xe ΣE_T^{FCal} distributions in panel (c) are normalized to have the same integral as the O + O distribution above 30 GeV.

luminosities of 2 nb^{-1} for O + O and 0.5 nb^{-1} for Ne + Ne collisions, respectively. Minimum-bias events were selected with an L1 trigger based on the TRT “FastOR” algorithm [53], which required at least one TRT azimuthal sector above threshold, together with an HLT requirement of at least one reconstructed charged-particle track. To increase statistics for the highest-activity events, an additional trigger was used that required the TRT FastOR at L1 and at least 290 reconstructed tracks with $p_T > 200 \text{ MeV}$ at the HLT. A similar trigger with a requirement of 100 reconstructed tracks with $p_T > 200 \text{ MeV}$ at the HLT was employed to supplement the intermediate-activity region. In addition, a trigger requiring an L1 calorimeter transverse energy threshold of 20 GeV, followed by at least one reconstructed track with $p_T > 200 \text{ MeV}$ at the HLT, was also included.

In the offline analysis, the z position of the primary vertex [54] was required to lie within 10 cm of the nominal interaction point (i.e., within 10 cm of the center of ATLAS). In the recorded O + O and Ne + Ne data, there are sizable contributions from pileup events, in which two or more inelastic collisions occur in the same bunch crossing. The majority of the pileup events are removed by requiring only a single high-quality reconstructed vertex per event. A high-quality vertex is defined as one that is well constrained in position, having a z -position variance of less than 0.02 mm^2 ; such vertices have many associated tracks pointing to a common origin. Additional background is suppressed by removing events with significantly smaller track multiplicities than expected relative to the total transverse energy recorded in the FCal (ΣE_T^{FCal}) [55]. Similarly, correlations between the energy deposited in the ZDCs and ΣE_T^{FCal} are used to suppress additional pileup by rejecting events for which the energy deposited in the ZDCs is significantly higher than that in the majority of collisions. The estimated residual pileup after these selections is found to be at most 0.2%.

As in earlier ATLAS studies of heavy-ion collisions, events are categorized into centrality percentiles based on the ΣE_T^{FCal} [5,7,15]. To relate the ΣE_T^{FCal} distribution to the sampled fraction of the total inelastic O + O and Ne + Ne cross sections, a Glauber-model-based calculation [56,57] is used to fit the data, to extract the fraction of events selected above a minimum ΣE_T^{FCal} threshold, and to estimate the systematic uncertainties on that fraction [5,7,15]. Additionally, the

Glauber model is used to extract primary collision characteristics, such as the average number of participating nucleons, $\langle N_{\text{part}} \rangle$, for each centrality interval. The distribution of ΣE_T^{FCal} observed in data, along with the threshold values defining various centrality intervals, is illustrated in Fig. 1. Figure 1(c) shows the comparison of the ΣE_T^{FCal} distributions in O + O and Ne + Ne collisions to that in Xe + Xe collisions (from Ref. [7]). The comparison is done after scaling the Ne + Ne and Xe + Xe ΣE_T^{FCal} distributions by the number of nucleons relative to oxygen. While the Xe + Xe distribution exhibits a sharper fall-off at a scaled $\Sigma E_T^{\text{FCal}} \approx 0.34 \text{ TeV}$ and a narrower tail beyond this point, the O + O and Ne + Ne distributions show a significantly more pronounced high- ΣE_T^{FCal} tail. This behavior reflects the larger relative event-by-event fluctuations in particle production in the smaller O + O and Ne + Ne systems compared to Xe + Xe.

Charged-particle tracks and collision vertices are reconstructed from hits in the ID using standard methods [58]. For the nominal analysis, the reconstructed tracks are required to have $p_T > 0.5 \text{ GeV}$, $|\eta| < 2.5$, and at least one pixel hit, with the additional requirement of a hit in the IBL when one is expected.³ If a hit in the IBL is not expected, then a hit is required in the next-to-innermost pixel layer, if such a hit is expected. The tracks are required to have at least six SCT hits. To suppress secondary contributions, the transverse impact parameter of the track with respect to the beamline, d_0 , and the longitudinal impact parameter of the track relative to the primary vertex, $z_0 \sin(\theta)$, are required to satisfy $|d_0| < 1.5 \text{ mm}$ and $|z_0 \sin(\theta)| < 1.5 \text{ mm}$. The quantity $N_{\text{ch}}^{\text{rec}}$ is defined as the number of charged-particle tracks in an event that satisfy these selection criteria and have $p_T > 0.5 \text{ GeV}$. An alternate set of more restrictive selections are used to evaluate systematic uncertainties in the measurement. For these “tight” selections, the number of pixel and SCT hits are raised to two and eight, respectively, a requirement of at most one missing hit in the SCT is imposed, and the d_0 and $z_0 \sin(\theta)$ impact parameter

³A hit is expected if the extrapolated track crosses an active region of a silicon-sensor module (pixel or SCT) that has not been disabled, and a hit is said to be “missing” when it is expected but not found. If a track crosses a disabled module, then for the purposes of hit counting, the disabled module is counted as a hit.

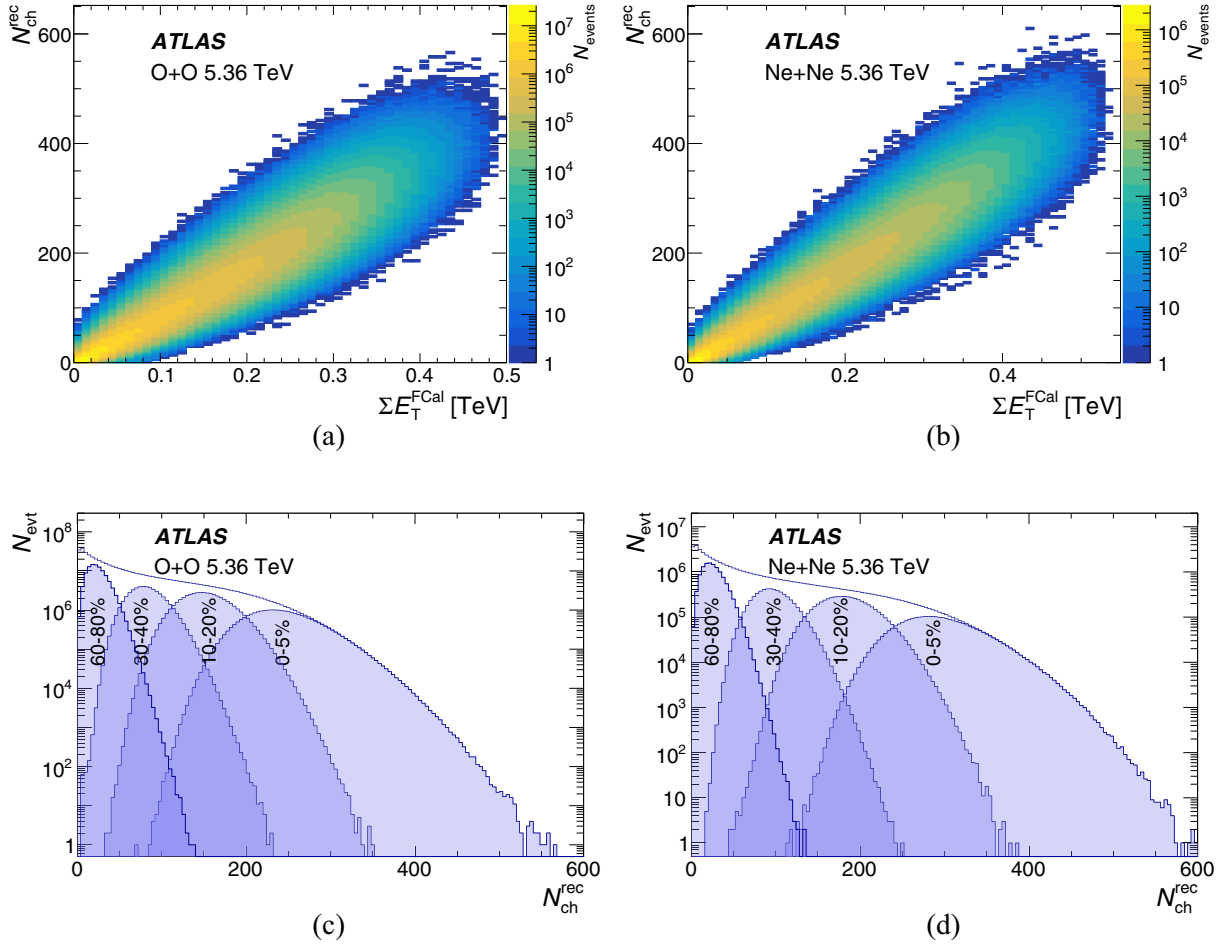


FIG. 2. Correlation between $N_{\text{ch}}^{\text{rec}}$ and $\Sigma E_{\text{T}}^{\text{FCal}}$ in minimum-bias events for (a) O + O and (b) Ne + Ne collisions, and distributions of $N_{\text{ch}}^{\text{rec}}$ in minimum-bias events for (c) O + O and (d) Ne + Ne collisions, including the distributions for several centrality intervals.

selections are decreased to 1 mm. Furthermore, the χ^2 per degree of freedom of the reconstructed track trajectory is required to be less than 6.

Figures 2(a) and 2(b) show the correlation between $\Sigma E_{\text{T}}^{\text{FCal}}$ and $N_{\text{ch}}^{\text{rec}}$ in minimum-bias O + O and Ne + Ne events, respectively. These two measures of event activity are found to be well correlated. Figures 2(c) and 2(d) show the $N_{\text{ch}}^{\text{rec}}$ distributions in minimum-bias O + O and Ne + Ne events, together with the distributions for several centrality intervals from Fig. 1.

To study the detector performance, a sample of 7×10^6 minimum-bias O + O Monte Carlo (MC) events was generated using the HIJING event generator version 1.38b [59]. Since HIJING does not have any intrinsic mechanism to generate flow, the latter is added after the initial particle generation step using an “afterburner” procedure [60], which slightly shifts the ϕ positions of generated particles to mimic flow. The generated sample was then passed through a full simulation of the ATLAS detector [61] using GEANT4 [62], and the MC events were reconstructed by the same algorithms as the data. The reconstructed particles in the MC events were used to calculate the reconstruction efficiency—the fraction of the generated charged particles that are successfully reconstructed and selected—as a function of p_{T} and η , denoted

by $\epsilon(p_{\text{T}}, \eta)$ below. With the criteria imposed in this analysis, the efficiency at $p_{\text{T}} = 1$ GeV varies between $\approx 65\%$ at $|\eta| = 2.5$ and $\approx 75\%$ at $|\eta| = 2$ and $\approx 85\%$ at $|\eta| = 0$. At midrapidity ($|\eta| < 1$) the efficiency is $\approx 80\%$ at $p_{\text{T}} = 0.5$ GeV and increases to $\approx 90\%$ at a p_{T} of 5 GeV. The rate of fake tracks, tracks that do not correspond to any generated particle, denoted by $f(p_{\text{T}}, \eta)$, is also estimated from the MC and stays below $\approx 2\%$ across the p_{T} and η ranges used in this measurement. The reconstructed event multiplicity $N_{\text{ch}}^{\text{rec}}$ is corrected for reconstruction efficiency and fake tracks by weighting each track with

$$\frac{1 - f(p_{\text{T}}, \eta)}{\epsilon(p_{\text{T}}, \eta)}, \quad (2)$$

where the numerator accounts for fake-track removal and the denominator for the reconstruction efficiency. This efficiency- and fake-corrected multiplicity is referred to as N_{ch} .

IV. METHODOLOGY

Due to the limited multiplicity per event, the v_n cannot be reliably measured on an EbE basis. Instead, the flow harmonics v_n are estimated from multiparticle correlations, which average over many events and provide access to different

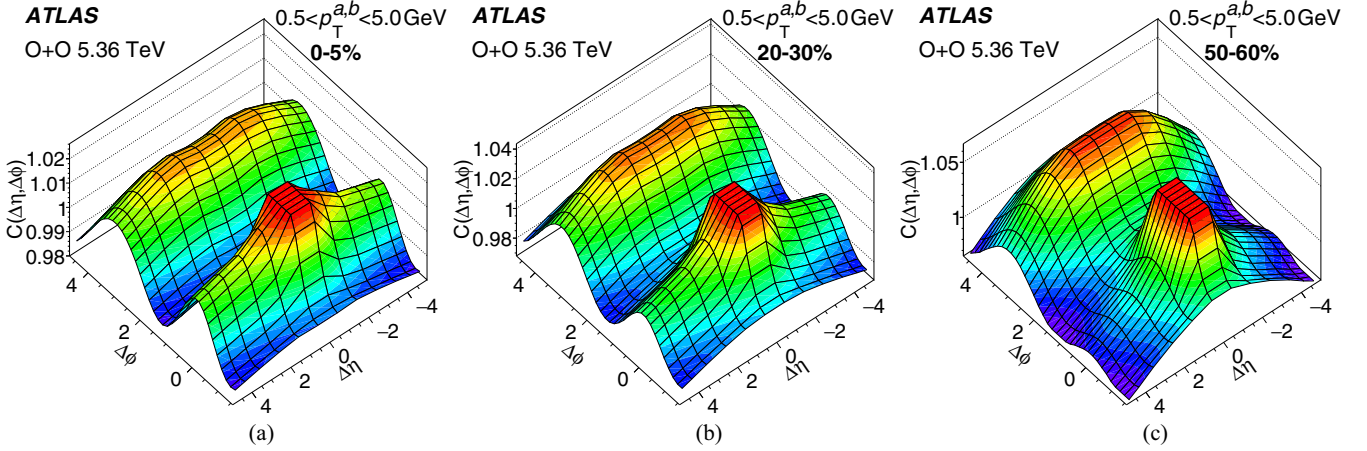


FIG. 3. Two-particle $\Delta\eta$ - $\Delta\phi$ correlations in O + O collisions for the (a) 0–5%, (b) 20–30%, and (c) 50–60% centrality intervals. The plots are for $0.5 < p_T^{a,b} < 5$ GeV. The distributions are truncated along the z axis to suppress the peak at $\Delta\eta = \Delta\phi = 0$ and are plotted over $|\Delta\eta| < 4.5$ to avoid statistical fluctuations at larger $|\Delta\eta|$.

moments of the EbE v_n distributions. However, correlations unrelated to collective flow can contaminate the measurement and must be suppressed or removed. For example, jet production and resonance decays produce strongly correlated collinear particles ($|\Delta\eta|, |\Delta\phi| < 1$) and weaker but equally important back-to-back correlations at $\Delta\phi \approx \pi$ that persist even at large $\Delta\eta$. These few-particle, nonglobal correlations are referred to as “nonflow.” This section describes two approaches for estimating flow harmonics: the two-particle correlations (2PC) method, including its improved template-fit implementation, and the multiparticle cumulant method. In the 2PC approach, a template fit is used to subtract nonflow contributions based on the lowest-multiplicity events, while the multiparticle cumulant method applies a subevent technique to suppress nonflow effects.

A. Two-particle correlations and template fit

The 2PC method has been widely used for flow measurements at the RHIC and the LHC [6,9,15,16,21,22,63–71]. Correlations between pairs of charged particles are studied as a function of their relative pseudorapidity, $\Delta\eta = \eta^a - \eta^b$, and relative azimuthal angle, $\Delta\phi = \phi^a - \phi^b$. The indices a and b denote the two particles in the pair, whose kinematic selections may differ. To account for detector acceptance effects, the correlation function is defined as the ratio of the “same-event” pair distribution S , where both particles are taken from the same event, to the “mixed-event” distribution B , where they are taken from different events [15]:

$$C(\Delta\eta, \Delta\phi) = \frac{S(\Delta\eta, \Delta\phi)}{B(\Delta\eta, \Delta\phi)}.$$

The same-event distribution contains both genuine physical correlations and contributions from detector acceptance, inefficiencies, and nonuniformities that are not related to the underlying physics. The mixed-event distribution reflects only these nonphysical effects, so that their ratio isolates the genuine physical correlations [63]. To ensure this, events used for the B distribution are required to have similar centrality (or

multiplicity) and vertex position. When constructing S and B , corrections for track reconstruction inefficiency and fake tracks are applied using a per-pair weight [see Eq. (2)]:

$$\frac{[1 - f(p_T^a, \eta^a)][1 - f(p_T^b, \eta^b)]}{\epsilon(p_T^a, \eta^a)\epsilon(p_T^b, \eta^b)}.$$

Examples of $C(\Delta\eta, \Delta\phi)$ are shown in Fig. 3, normalized such that the integral of $B(\Delta\eta, \Delta\phi)$ matches that of $S(\Delta\eta, \Delta\phi)$ for $|\Delta\eta| > 2$. In all cases, a prominent peak is observed at $\Delta\eta = \Delta\phi = 0$, arising from short-range correlations such as jet fragmentation, resonance decays, or Hanbury Brown–Twiss (HBT) correlations [72]. At large $\Delta\eta$, long-range correlations are visible both on the near side ($\Delta\phi \sim 0$) and the away side ($\Delta\phi \sim \pi$). The near-side correlation, commonly referred to as the “ridge,” originates primarily from collective flow. The away-side correlation receives contributions from both collective flow and back-to-back dijets.

One-dimensional correlation functions, $C(\Delta\phi)$, are obtained by integrating the S and B distributions over the range $2 < |\Delta\eta| < 5$:

$$C(\Delta\phi) = \frac{\int_2^5 S(|\Delta\eta|, \Delta\phi) d|\Delta\eta|}{\int_2^5 B(|\Delta\eta|, \Delta\phi) d|\Delta\eta|} \equiv \frac{S(\Delta\phi)}{B(\Delta\phi)},$$

where the $|\Delta\eta| > 2$ requirement is imposed to suppress nonflow correlations arising from the peak at $\Delta\eta = \Delta\phi = 0$ seen in Fig. 3 [21,22,64]. The $C(\Delta\phi)$ ’s are normalized to have an average value of unity. Similar to the single-particle distribution [Eq. (1)], the $C(\Delta\phi)$ is parametrized with a Fourier series [15]:

$$C(\Delta\phi) = C_0 [1 + 2\sum_{n=1}^{\infty} v_{n,n}(p_T^a, p_T^b) \cos(n\Delta\phi)]. \quad (3)$$

To suppress residual nonflow contributions that persist over $|\Delta\eta| > 2$, primarily on the away side ($\Delta\phi \sim \pi$), a commonly used template-fit procedure is employed [22,24,66,73]. In this method, the shape of the nonflow component is estimated from low-multiplicity (peripheral) events and assumed to be unchanged in higher-multiplicity (more central) events. For this analysis, the peripheral reference correlation $C^{\text{periph}}(\Delta\phi)$

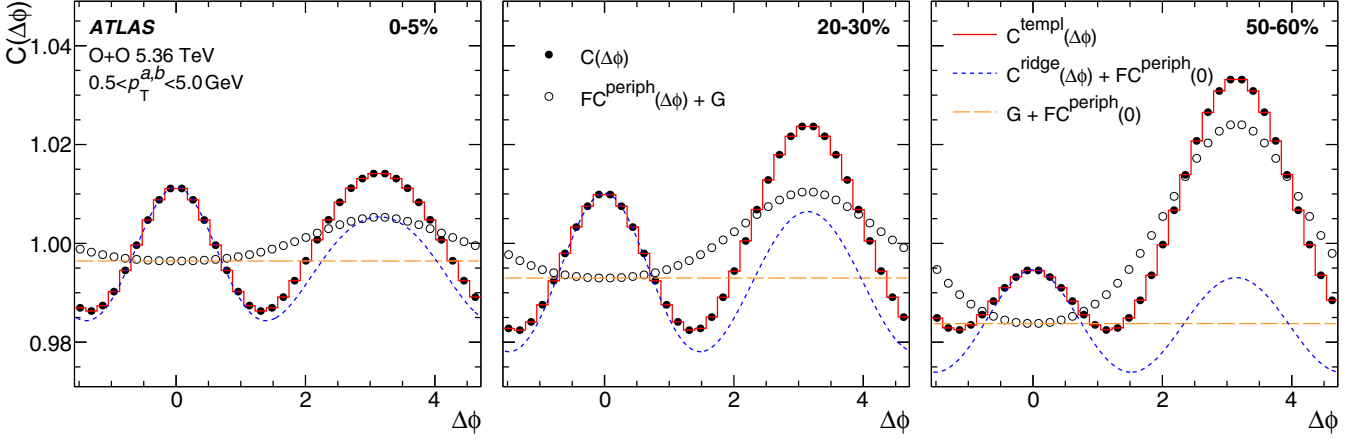


FIG. 4. Template fits to correlation functions measured in O + O collisions for the (left) 0–5%, (center) 20–30%, and (right) 50–60% centrality intervals. The plots are for $0.5 < p_T^{a,b} < 5$ GeV. The solid points indicate the measured $C(\Delta\phi)$, and the continuous red line indicates the template fit $C^{\text{templ}}(\Delta\phi)$. The open points and dashed curves indicate the different components of the template fit, which are shifted along the y axis by G or by $FC^{\text{periph}}(0)$, where necessary, for presentation.

is constructed from events of the same collision species (O + O or Ne + Ne) with centrality greater than 80%. The measured correlation $C(\Delta\phi)$ is then parametrized as the sum of this nonflow reference and an azimuthally modulated pedestal, $C^{\text{ridge}}(\Delta\phi)$, that encodes the collective anisotropy:

$$C(\Delta\phi) = FC^{\text{periph}}(\Delta\phi) + C^{\text{ridge}}(\Delta\phi), \quad (4)$$

with

$$C^{\text{ridge}}(\Delta\phi) \equiv G \left[1 + 2 \sum_{n=2}^5 v_{n,n}(p_T^a, p_T^b) \cos(n\Delta\phi) \right]. \quad (5)$$

The parameters F , G , and $v_{n,n}$ are determined by the template fit, with F and G constrained such that the integrals of both sides of Eq. (4) are equal. Fourier terms up to fifth order ($v_{2,2}$ – $v_{5,5}$) are included in the fit.

Figure 4 shows examples of template fits for O + O collisions, where the template fit is denoted as $C^{\text{templ}}(\Delta\phi)$. In the measured correlations, the away-side peak is the largest in the 50–60% centrality interval and decreases systematically in the 20–30% and 0–5% intervals. A significant fraction of the away-side correlation is described by the scaled peripheral reference [$FC^{\text{periph}}(\Delta\phi)$ term in Eq. (4)]. The relative contribution of this term decreases monotonically toward mid-central and central events, indicating that nonflow correlations are most important in peripheral collisions. The $C^{\text{ridge}}(\Delta\phi)$ component of the template fit is double-peaked in all intervals, reflecting the dominant contribution from the $v_{2,2}$ term in Eq. (5).

If the pair distribution is entirely determined by a global single-particle distribution, like in Eq. (1), the Fourier coefficients of the $C(\Delta\phi)$ [or $C^{\text{ridge}}(\Delta\phi)$] factorize into the product of single-particle anisotropies [63] as $v_{n,n}(p_T^a, p_T^b) = v_n(p_T^a)v_n(p_T^b)$ and thus

$$v_n(p_T^b) = \frac{v_{n,n}(p_T^a, p_T^b)}{v_n(p_T^a)} = \frac{v_{n,n}(p_T^a, p_T^b)}{\sqrt{v_{n,n}(p_T^a, p_T^a)}}. \quad (6)$$

For all the 2PC results in this analysis, the $v_n(p_T^b)$'s are evaluated using Eq. (6) with $0.5 < p_T^a < 5$ GeV. The upper limit on p_T^a is chosen to suppress nonflow, which increases at high p_T . The template-fit method provides a more reliable treatment of nonflow effects and is therefore regarded as the primary measurement method. Results obtained with the 2PC method are also included in this paper to illustrate the impact of nonflow removal achieved by the template-fit procedure.

B. Four-particle cumulants

Multiparticle cumulants extract higher-order azimuthal correlations, providing information about EbE flow fluctuations. The cumulant measurements have the advantage of suppressing correlations from jets and dijets, instead of relying on an explicit procedure to correct v_n as discussed in Sec. IV A. The cumulant of order $2k$, where k is an integer, involves correlations between $2k$ particles and suppresses all correlations involving less than $2k$ particles, including nonflow correlations [74]. The framework for the cumulant measurements is described in Refs. [75–77], but a concise description is provided here for completeness.

As mentioned before, the cumulant method involves the calculation of $2k$ -particle azimuthal correlations $\langle\{2k\}_n\rangle$ and $2k$ -particle cumulants $c_n\{2k\}$ for the n th-order flow harmonics, where k equals either 1 or 2 in this paper. The two- or four-particle azimuthal correlations in one event are evaluated as follows [75–77]:

$$\langle\{2\}_n\rangle = \langle e^{in(\phi_1 - \phi_2)} \rangle, \quad (7)$$

$$\langle\{4\}_n\rangle = \langle e^{in(\phi_1 + \phi_2 - \phi_3 - \phi_4)} \rangle, \quad (8)$$

where “ $\langle \cdot \rangle$ ” denotes a single-event average over all pairs or quadruplets of distinct particles, respectively. The averages from Eqs. (7) and (8) are expanded into products of per-particle normalized flow vectors [78]:

$$\langle q_n \rangle = \langle e^{in(\phi)} \rangle, \quad (9)$$

which provides an efficient calculation of multiparticle correlations. The exact details of this procedure follow Ref. [46]. These flow vectors are constructed with per-particle weights that correct for detector nonuniformities, tracking inefficiency, and contributions from fake tracks, similar to Eq. (2) but with additional ϕ -dependent corrections applied.

In the “standard” cumulant method described so far, all $2k$ -particle multiplets involved in the calculations of $\langle\{2k\}_n\rangle$ are selected using the entire detector acceptance. To further suppress the nonflow correlations, which typically involve particles emitted within a localized region in η , the particles can be grouped into several “subevents,” each covering a nonoverlapping η interval [77]. The multiparticle correlations are then constructed by correlating particles between different subevents (two and three in this case), further reducing nonflow correlations. For two-subevent correlations, particles 1 and 2 in Eq. (7) are selected from different regions of η . Similarly, in Eq. (8), the pair of particles 1 and 2 are selected from one region of η , and the pair of particles 3 and 4 are selected from another region. For the three-subevent correlations, permutations of different choices are made and combined (see Ref. [46] for details). For the results presented here, the subevents used for the two-subevent method cover $-2.5 < \eta < 0$ and $0 < \eta < 2.5$, and those for the three-subevent method cover $-2.5 < \eta < -2.5/3$, $-2.5/3 < \eta < 2.5/3$, and $2.5/3 < \eta < 2.5$.

The two- and four-particle cumulants are then obtained from the azimuthal correlations as

$$c_n\{2\} = \langle\langle\{2\}_n\rangle\rangle, \quad (10)$$

$$c_n\{4\} = \langle\langle\{4\}_n\rangle\rangle - 2\langle\langle\{2\}_n\rangle\rangle^2, \quad (11)$$

where “ $\langle\langle\cdot\rangle\rangle$ ” represents the average of $\langle\{2k\}_n\rangle$ over an event ensemble. In the absence of nonflow correlations, $c_n\{2k\}$ reflects the moments of the distribution of the flow coefficient v_n :

$$\begin{aligned} c_n\{2\} &= \langle v_n^2 \rangle, \\ c_n\{4\} &= \langle v_n^4 \rangle - 2\langle v_n^2 \rangle^2. \end{aligned} \quad (12)$$

The v_n measured by the two-particle cumulants is defined as $v_n\{2\} = \sqrt{c_n\{2\}}$. In the absence of nonflow effects, the v_n measured by the two-particle cumulant is identical to that measured using the 2PC method. However, nonflow contributions lead to differences between the two. Henceforth, the v_n 's measured with the 2PC and template-fit methods are denoted as $v_n^{2PC}\{2\}$ and $v_n^{\text{sub}}\{2\}$, respectively. When making general statements without reference to a specific method, v_n obtained from any two-particle correlation technique is denoted simply as $v_n\{2\}$.

Under the Gaussian model of eccentricity fluctuations [78], the two- and four-particle cumulants can be expressed in terms of an average geometry-driven component, \bar{x}_n , and a fluctuation component, Δ_n , as

$$c_n\{4\} = -\bar{x}_n^4, \quad c_n\{2\} \equiv \langle v_n^2 \rangle = \bar{x}_n^2 + \Delta_n^2. \quad (13)$$

This implies $c_n\{4\} < 0$, and a positive $c_n\{4\}$ signals the onset of non-Gaussian flow fluctuations, or significant nonflow contamination. If the sign constraints are obeyed, the

corresponding four-particle flow coefficient is then defined as

$$v_n\{4\} = \sqrt[4]{-c_n\{4\}} \quad (14)$$

and measures the contribution to the flow from the average-geometry component only.

A comparison of the results of the standard and the two- and three-subevent cumulants in the O + O and Ne + Ne collisions shows that the two- and three-subevent results are consistent. This demonstrates that both subevent methods effectively suppress nonflow in the measured phase-space region. For this reason, the $v_n\{4\}$ results presented in this paper use the two-subevent method.

V. SYSTEMATIC UNCERTAINTIES

The systematic uncertainties of the measured v_n using the 2PC, template-fit, and multiparticle cumulant methods are described in this section. The following sources of systematic uncertainty are considered.

- (i) MC closure: The MC-closure test compares v_n^{gen} , obtained from MC-generated particles, with v_n^{reco} , obtained by applying the full analysis procedure to reconstructed tracks in the MC simulation, as done in the data analysis. The difference between the two is within 1% across the p_T and multiplicity ranges considered in this analysis and is conservatively assigned as a systematic uncertainty. This uncertainty accounts for residual reconstruction effects not corrected in the data analysis.
- (ii) Track selection: The track selection criteria control the relative contributions of genuine charged particles and fake tracks entering the analysis. The stability of the results with respect to the track selections is evaluated by varying the requirements applied to reconstructed tracks and including the resulting variation in v_n as a systematic uncertainty. The results obtained with the nominal selections are compared with those using the tighter criteria described in Sec. II. The differences depend on the harmonic order and are between 0.5 and 1.5%.
- (iii) Tracking efficiency: The uncertainty in the reconstruction efficiency and fake-rate due to ID material modeling in the GEANT4 simulation is accounted for by evaluating the efficiency and fake rates in alternate MC samples. In each sample, a single modification is applied to the ATLAS ID geometry: the passive material of the ID is increased by 5%, the passive material of the IBL is increased by 10%, or the passive material in the services region is increased by 25%. These variations capture the full range of data-MC differences observed in dedicated studies of the ID material [79]. The variation in the results when using these alternative models is taken as a systematic uncertainty. This uncertainty is less than 0.25%.

- (iv) Centrality definition: The centrality definitions used to classify the events into centrality percentiles have an $\approx 1\%$ (2%) uncertainty associated with them in the O + O (Ne + Ne) measurements. This arises from uncertainties in the fraction of the inelastic O + O and Ne + Ne cross sections accepted by the triggers used in this analysis and is estimated from the Glauber fits to the ΣE_T^{FCal} distributions [5,6]. The impact of this uncertainty on the v_n is evaluated by varying the ΣE_T^{FCal} thresholds that define the centrality intervals, reevaluating the v_n , and assigning the observed variation as a systematic uncertainty. This uncertainty is negligible in most central collisions and increases systematically for more peripheral collisions.
- (v) Residual pileup: Pileup events dilute the measured v_n as there are no correlations between independent collisions. The estimated residual pileup is at most 0.2% in any centrality or multiplicity interval considered in this paper. Because the maximum possible dilution cannot exceed the pileup rate, the entire residual pileup rate of 0.2% is conservatively assigned as a systematic uncertainty on the v_n .
- (vi) Event mixing: As mentioned before, the 2PC method uses event mixing to account for detector acceptance effects. The nominal mixing matches events that are within a z_{Vtx} separation of less than 20 mm. Alternate mixing criteria, where the matching is restricted to within 10 mm and relaxed to 200 mm, are used, and the maximum variation in the results is included as a systematic uncertainty. This uncertainty is of order 1% and only affects the 2PC and template-fit measurements.
- (vii) Peripheral reference: For the centrality-dependent measurements, the nominal template-fit procedure uses events more peripheral than 80% for building the peripheral reference $C^{\text{periph}}(\Delta\phi)$. For the multiplicity-dependent results, the peripheral references are built from events from the same collision system that have $N_{\text{ch}}^{\text{rec}}$ less than 20. For evaluating uncertainties associated with the assumptions made in the template-fit analysis, the centrality- and multiplicity-dependent measurements are repeated with the peripheral reference built from 5.02-TeV pp events with $N_{\text{ch}}^{\text{rec}}$ less than 20, as was done in Ref. [7]. The difference between the results with this alternate choice of peripheral reference are included as a systematic uncertainty. This uncertainty is relevant only for the template-fit method. This uncertainty is the dominant contribution in peripheral centralities. In this region, the measured correlation $C(\Delta\phi)$ becomes very similar in shape to the peripheral reference correlation $C^{\text{periph}}(\Delta\phi)$ used in Eq. (4). As a result, the template decomposition becomes increasingly sensitive to small differences between the two, leading to a large relative uncertainty in the extracted v_n .
- (viii) Flattening procedure: The cumulant measurements use a flattening procedure to remove detector

TABLE I. The contributions to the systematic uncertainty of v_n in O + O collisions from different sources, as a function of centrality. The contributions are expressed in percentages. Items 1–5 are common to all the methods used here (2PC, template-fit, and cumulants). Item 6 is specific to the 2PC and template-fit methods. Item 7 is specific to the template-fit method. Item 8 is specific to the cumulant method. The uncertainties are shown for the integrated p_T interval of 0.5–5 GeV.

Source	Harmonic order	0–40% (%)	40–70% (%)
1. MC closure	v_2-v_4	1	1
	v_2	0.5	0.5
2. Track selection	v_3	0.75	0.75
	v_4	1.5	1.5
3. Tracking efficiency	v_2-v_4	0.25	0.25
	v_2	0.2	0.2–0.6
4. Centrality definition	v_3	0.2–1.0	1–2
	v_4	0.2	0.2–0.6
5. Residual pileup	v_2-v_4	0.2	0.2
	v_2	0.25	0.25
6. Event mixing	v_3	0.5	0.5
	v_4	1	1
	v_2	0.5	0.5–3
7. Peripheral reference	v_3	0.75–3.5	3.5–12
	v_4	1.0–4.5	4.5–20
8. Flattening procedure	v_2-v_3	0.25	0.25

nonuniformities in ϕ [46]. As a conservative estimate of the systematic related to the flattening procedure, the measurements were repeated with the flattening removed, and the resulting variations of $\approx 0.25\%$ are included as a systematic uncertainty on the $v_n\{4\}$.

Table I summarizes the final systematic uncertainties for the integrated p_T interval of 0.5–5.0 GeV in the O + O measurements. Except for the uncertainties related to the peripheral reference and centrality definition, all other uncertainties are conservatively taken to be constant and sufficiently large to cover the variations across all centrality (or multiplicity) and p_T intervals studied here. The dominant uncertainties are the uncertainties related to the MC closure and the peripheral reference variation. For Ne + Ne, the assigned uncertainties are taken to be the same as those for O + O, with values chosen large enough to cover both systems, except for the centrality-definition uncertainty, which is about twice as large. These individual uncertainties are added in quadrature to obtain total uncertainties. For ratios of the Ne + Ne to O + O v_n measurements, all sources of systematic uncertainty are treated as correlated, with the exception of the residual pileup. The latter is not considered correlated, since pileup rates can differ between the two systems due to their distinct running conditions. The remaining systematic uncertainties are treated as correlated between the two collision systems. The charged-particle multiplicities in Ne + Ne are only about 20% higher than those in O + O, leading to very similar detector occupancy and reconstruction conditions. Consequently, the

systematic effects related to tracking and detector acceptance, namely, the MC-closure, track-selection, tracking-efficiency, event-mixing, and flattening uncertainties, are expected to be identical in both systems. The peripheral reference related uncertainty is evaluated by using an identical low-multiplicity pp reference for both systems and is also treated as a correlated uncertainty. In addition, the centrality-definition uncertainty is treated as correlated, as it is dominated by the modeling of nucleon distributions in the Glauber calculation—such as the choice between hard-sphere and diffuse nucleons, or the inclusion of nucleon clustering—which affects both collision systems in the same way.

VI. RESULTS

Figure 5 shows the measured $v_n^{\text{sub}}\{2\}$ and the $v_n^{2\text{PC}}\{2\}$ as a function of p_T^b in O + O and Ne + Ne collisions at $\sqrt{s_{NN}} = 5.36$ TeV. Comparing the template fit v_n and the 2PC v_n , a large potential nonflow contribution is observed in the 2PC results, particularly at higher p_T^b and in peripheral collisions. The v_2 results exhibit a linear rise at low p_T^b , followed by a decrease in the range of 2–4 GeV for the 0–5% and 20–30% centrality intervals. This behavior is qualitatively similar to what is observed in other collision systems, from Pb + Pb to pp [6,7,22,66]. A hierarchy is also observed, with the magnitude of v_n decreasing as n increases, in agreement with observations from other systems. In peripheral events (50–60% centrality), or at p_T above approximately 3 GeV, significant differences are observed between the 2PC and template-fit measurements, highlighting the impact of non-flow background correlations on the 2PC method.

The hydrodynamic response to the initial geometry is best studied as a function of variables that are directly impacted by it, chiefly charged-particle multiplicity and centrality. Figure 6(a) shows $v_n^{\text{sub}}\{2\}$ and $v_n\{4\}$ for charged particles with $0.5 < p_T < 5.0$ GeV in O + O and Ne + Ne collisions as a function of N_{ch} . In both systems, $v_n^{\text{sub}}\{2\}$ is observed to exceed $v_n\{4\}$ for the same harmonic order n , which reflects the positive contribution of fluctuations to $v_n\{2\}$ as described in Eq. (13). The difference between the $v_2\{2\}$ and $v_2\{4\}$ increases with increasing multiplicity, indicating the increased role of the fluctuation component Δ_2^2 in Eq. (13) relative to the mean geometry component \bar{x}_2^2 going from peripheral to central collisions.

To compare O + O and Ne + Ne v_n 's directly, their ratio is plotted in Fig. 6(b). For the elliptic flow v_2 , there is a growing enhancement in Ne + Ne collisions with increasing N_{ch} . These can be attributed to centrality-dependent changes in the overlap geometry and neon's deformed nuclear structure, which is further discussed below, in the context of the centrality-dependent results. Conversely, there is a striking similarity of $v_3^{\text{sub}}\{2\}$ in O + O and Ne + Ne collisions as a function of N_{ch} . This provides evidence that the hydrodynamic response and the fluctuation-driven component of the initial-state geometry depend primarily on the particle density. The residual difference and systematically smaller $v_3\{4\}$ may be an indication of differing average triangularity in the initial-state geometry.

To compare the geometric aspects of oxygen and neon nuclei, Fig. 7(a) presents the results as a function of collision centrality, using the same kinematic requirements and analysis techniques as those in Fig. 6. Although light-ion collisions have large initial-state geometry fluctuations and possibly nuclear deformations, a large contribution to the elliptic geometry is the event-averaged lenticular shape. This event-averaged shape depends on the ratio of the impact parameter to the nuclear radius, which is highly correlated with centrality. For this reason, there is closer agreement observed between O + O and Ne + Ne as a function of centrality than N_{ch} . Thus, the ratio of Ne + Ne to O + O flow harmonics is calculated as a function of centrality, in an attempt to remove these average geometric effects. This ratio is shown in Fig. 7(b). For both $v_2^{\text{sub}}\{2\}$ and $v_2\{4\}$, a relatively centrality-independent ratio is observed for centralities more peripheral than 10%, as opposed to the ratios as a function of N_{ch} [Fig. 6(b)]. However, over the 0–10% centrality interval, a growing enhancement appears toward the most-central collisions. This enhancement is more pronounced in the four-particle cumulant measurement. A similar behavior is observed for the triangular moment: the $v_3^{\text{sub}}\{2\}$ ratio exhibits a sudden decrease in the 0–10% centrality interval. For the $v_3\{4\}$ ratio, the statistical uncertainties are too large to observe clear trends.

Figure 8 shows the comparisons of the measured $v_n^{\text{sub}}\{2\}$ with the template-fit method to $v_n\{2\}$ calculations from the model described in Ref. [80]. The model combines the projected generator coordinate method (PGCM), an *ab initio* nuclear structure model for oxygen and neon, with the IP-Glasma framework, including JIMWLK evolution [81], to calculate the initial energy densities of the colliding nuclei. These energy densities are then evolved using viscous relativistic hydrodynamics (MUSIC [82]). Finally, a hadronic afterburner (UrQMD [83,84]) is applied to obtain the v_n . The centrality is determined with the charged-particle multiplicity at midrapidity. The model is denoted as “Hydro + IPGlasma + PGCM” in the figure. The calculations overpredict the v_2 and v_3 in central collisions, but are consistent within uncertainties with the measurements in more peripheral collisions. These comparisons indicate that the light-ion measurements can provide additional constraints for tuning existing theory models.

Figure 9 shows comparisons of the measured ratios for $v_n\{2\}$ between Ne + Ne and O + O collisions to two theory calculations. The first is the Hydro + IPGlasma + PGCM model introduced above. The second model is described in Ref. [44] and uses PGCM [85] to determine the nuclear configurations of both oxygen and neon, which are then collided, generating initial-state energy densities with the Trento model [86]. These events are then simulated with the trajectory hydrodynamic framework [87,88]. This model is labeled as “Hydro + Trento + PGCM.” The model uses midrapidity multiplicity to determine centrality. The fluctuations in the model calculations are statistical in nature. The measured $v_n\{2\}$ ratios are obtained from the template-fit method. The event-averaged eccentricity, a quantification of the magnitude of ellipticity ϵ_2 and the triangularity ϵ_3 , ratios for a particular Trento parameter set [89] are also shown in Fig. 9. The data

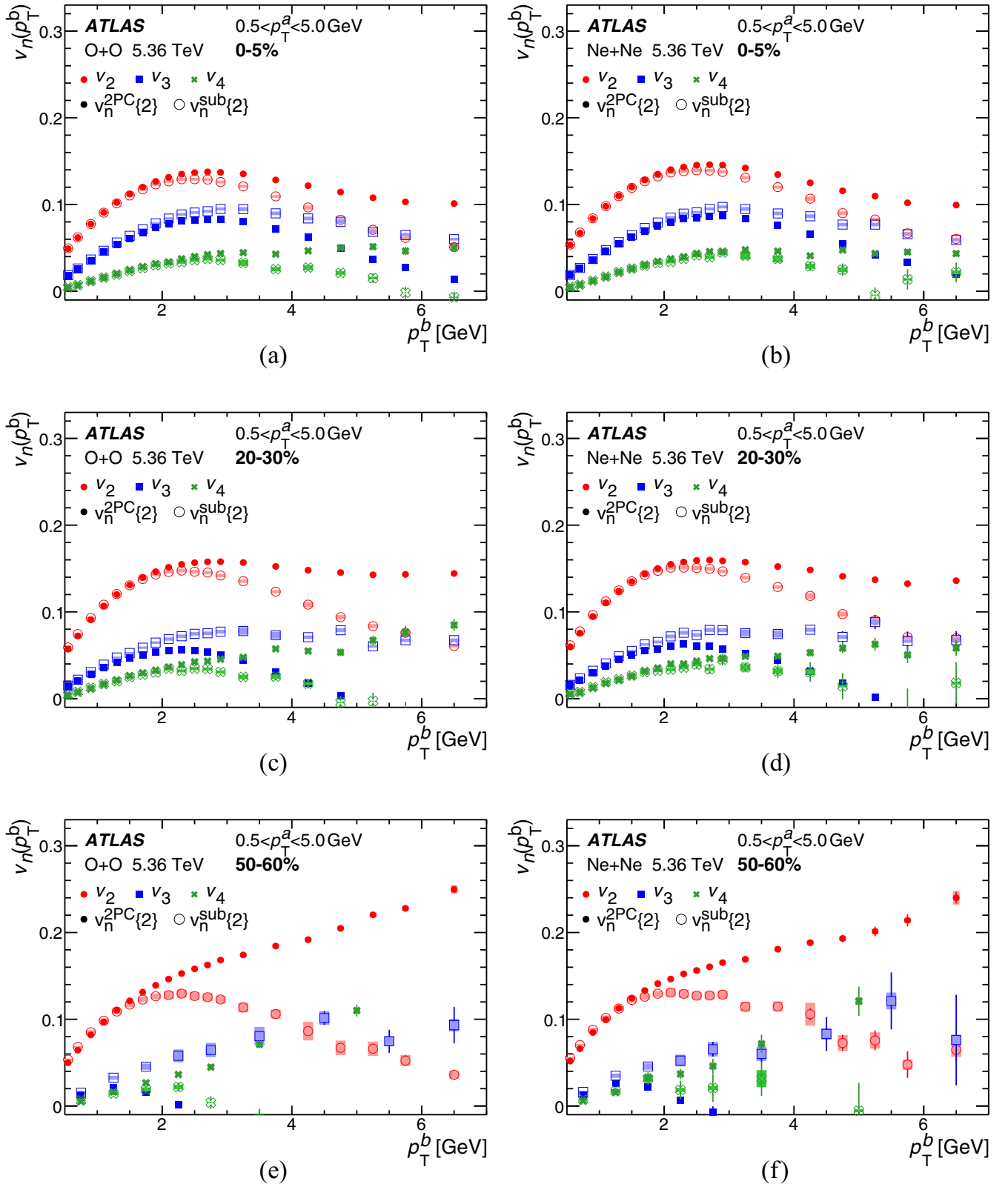


FIG. 5. The p_T^b dependence of the $v_n^{2PC\{2\}}$ and $v_n^{sub\{2\}}$ in the (a), (c), (e) O + O and (b), (d), (f) Ne + Ne collisions, for the (a), (b) 0–5%, (c), (d) 20–30%, and (e), (f) 50–60% centrality intervals. The solid and open points show the results obtained using the 2PC and the template-fit methods, respectively. The vertical lines and vertical bars indicate statistical and systematic uncertainties, respectively.

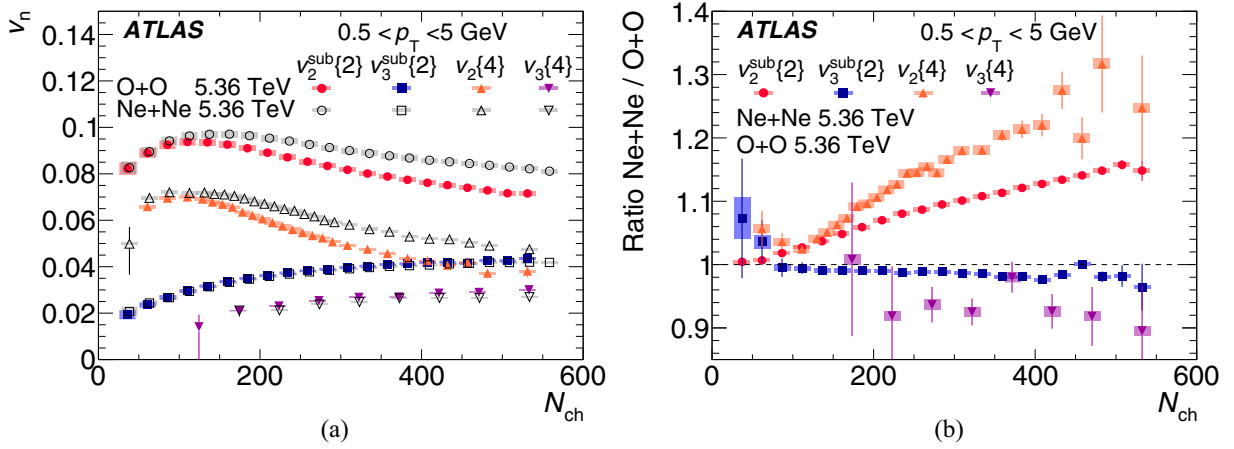


FIG. 6. (a) Flow harmonics $v_n^{sub\{2\}}$ and $v_n\{4\}$ for the elliptic and triangular moments in O + O collisions (colored solid markers) and Ne + Ne collisions (open black markers) at $\sqrt{s_{NN}} = 5.36$ TeV, shown as a function of N_{ch} . The Ne + Ne points are slightly displaced along the horizontal axis for visual clarity. (b) Ratios of the flow coefficients in Ne + Ne to those in O + O collisions, corresponding to the results in panel (a). Ratios are shown only for the 0–50% centrality range to suppress large statistical fluctuations in more peripheral intervals. The vertical lines and vertical bars indicate statistical and systematic uncertainties, respectively. For the ratios, systematic uncertainties correlated between the O + O and Ne + Ne measurements largely cancel.

and the Hydro + Trento + PGCM model agree quantitatively, at the edge of the theory uncertainties, in $v_2\{2\}$ in central collisions. The large enhancement in the $v_2\{2\}$ ratio in the 0–10% central collisions observed in the hydrodynamic theory calculation is attributed to the elongated shape of the neon nucleus, leading to an elliptic initial state, as can be seen in the $\epsilon_2\{2\}$ ratio. The qualitative behavior of the measured $v_2\{2\}$ ratio supports this picture. The Hydro + IPGlasma + PGCM calculation does not capture this proposed geometrically driven behavior in the 0–10% centrality range. This inability to capture geometric effects in the latter calculation is also reflected in the data-theory disagreement in Fig. 8. In both Ne + Ne and O + O collisions, the measured v_2

decreases in the most central collisions, but this trend is not predicted by the model. Because the nuclear structure model PGCM can capture geometric effects, as seen in the Hydro + Trento + PGCM v_2 ratio agreement with the data, the disagreement with the Hydro + IPGlasma + PGCM calculations could arise in the IPGlasma-with-JIMWLK portion of the initial-state model. It has been noted [80] that this aspect of the model creates large multiplicity fluctuations, reducing the correlation between the centrality and the impact parameter. This can lead to the inability of the model to reproduce the centrality dependence trends observed in Figs. 8 and 9. For both model comparisons presented in Fig. 9, the experimental uncertainties are significantly smaller than

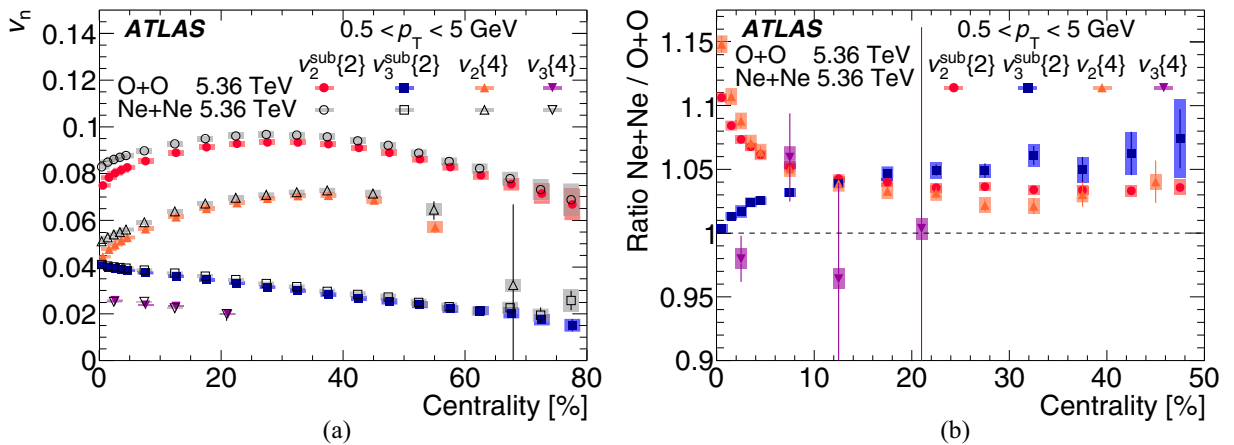


FIG. 7. (a) Flow harmonics $v_n^{sub\{2\}}$ and $v_n\{4\}$ for the elliptic and triangular moments in O + O collisions (colored solid markers) and Ne + Ne collisions (open black markers) at $\sqrt{s_{NN}} = 5.36$ TeV, shown as a function of centrality. The Ne + Ne points are slightly displaced along the horizontal axis for visual clarity. (b) Ratios of the flow coefficients in Ne + Ne to those in O + O collisions, corresponding to the results in panel (a). The vertical lines and vertical bars indicate statistical and systematic uncertainties, respectively. For the ratios, systematic uncertainties correlated between the O + O and Ne + Ne measurements largely cancel.

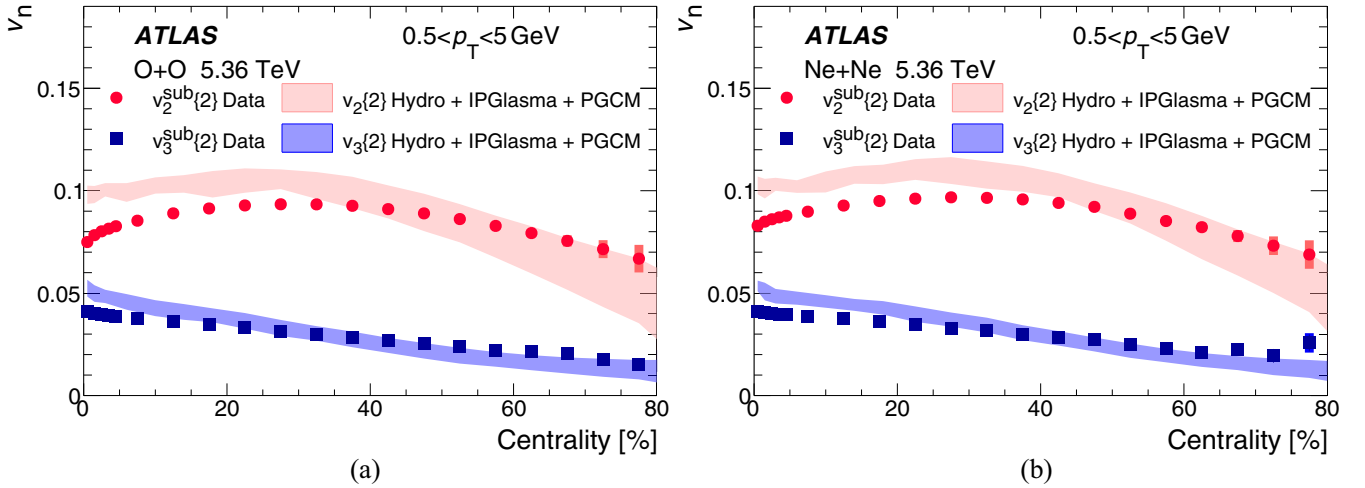


FIG. 8. Comparison of $v_2^{\text{sub}\{2\}}$ and $v_3^{\text{sub}\{2\}}$ with theory calculations from the model described in Ref. [80], for (a) O + O and (b) Ne + Ne collisions. The theory calculations are labeled as “Hydro + IPGlasma + PGCM.” For the data, the vertical lines and vertical bars indicate statistical and systematic uncertainties, respectively. The data uncertainties are sometimes too small to be visible. The bands for the theory calculations represent the combined statistical and systematic uncertainties.

the statistical and systematic uncertainties associated with the model calculations. Consequently, further refinement of the theory predictions is required to fully capitalize on the precision of the data.

Figure 10 shows comparisons of $v_n^{\text{sub}\{2\}}$ measurements in O + O and Ne + Ne collisions to previous $v_n^{2\text{PC}\{2\}}$ results in Xe + Xe collisions at 5.44 TeV and Pb + Pb collisions at 5.02 TeV from Ref. [7], as a function of centrality. In heavy-ion collisions, the v_2 is largely determined by the elliptic geometry of the nuclear overlap, which is strongly correlated with centrality and thus drives the pronounced centrality dependence of v_2 . By contrast, the v_2 in light-ion systems shows a much weaker centrality dependence, highlighting the dominant role of Ebe geometry fluctuations in these systems.

The v_3 in Xe + Xe and Pb + Pb collisions exhibits a non-monotonic centrality dependence, increasing from central to mid-central collisions and then decreasing. In light-ion collisions, however, the v_3 decreases monotonically from central to peripheral events. Figure 11 shows similar comparisons of $v_n^{\text{sub}\{2\}}$ as a function of the reconstructed charged-particle multiplicity $N_{\text{ch}}^{\text{rec}}$, including results from p + Pb collisions at 5.02 TeV. The most notable feature is the very similar magnitude and $N_{\text{ch}}^{\text{rec}}$ dependence of v_3 in both light- and heavy-ion collisions. This stands in stark contrast to the centrality dependence of v_3 , which differs strongly between light- and heavy-ion systems. Interestingly, the p + Pb v_3 is also comparable in magnitude to the light- and heavy-ion results at the

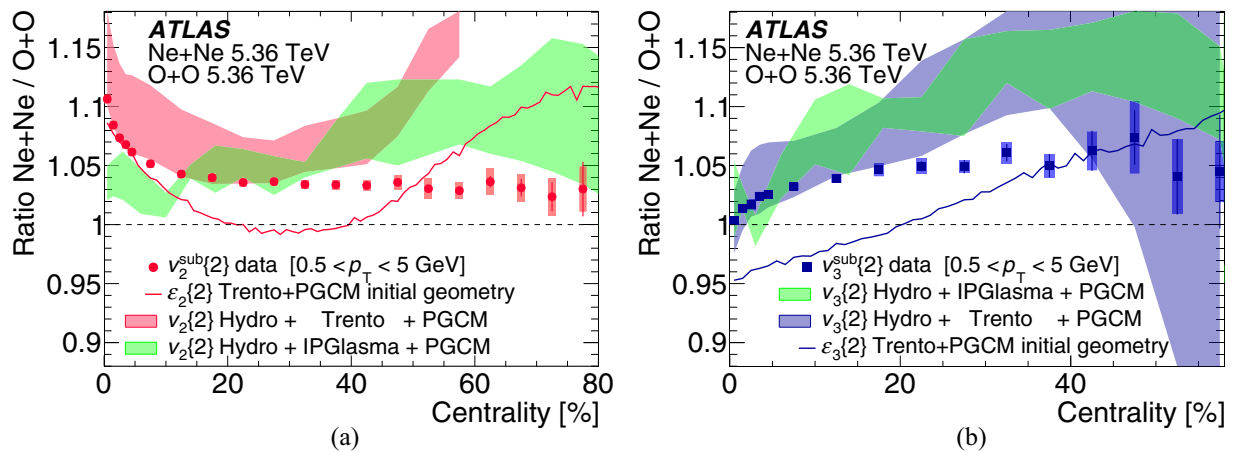


FIG. 9. Comparison of the measurements to theory predictions for the ratio of (a) $v_2\{2\}$ and (b) $v_3\{2\}$ between Ne + Ne and O + O. The $v_n\{2\}$ ratios in the data are obtained from the template-fit method. The Hydro + Trento + PGCM theory is taken from Ref. [44] ($0.3 < p_T < 3.0$ GeV) and the Hydro + IPGlasma + PGCM is an extension of Ref. [80] ($0.5 < p_T < 5.0$ GeV). The ratios are also shown for the eccentricities, a quantification of the elliptic (ε_2) or triangular (ε_3) shape of the initial-state energy density, using the Trento + PGCM model. For the data, the vertical lines and vertical bars indicate statistical and systematic uncertainties, respectively. The bands for the theory calculations represent combined statistical and systematic uncertainties.

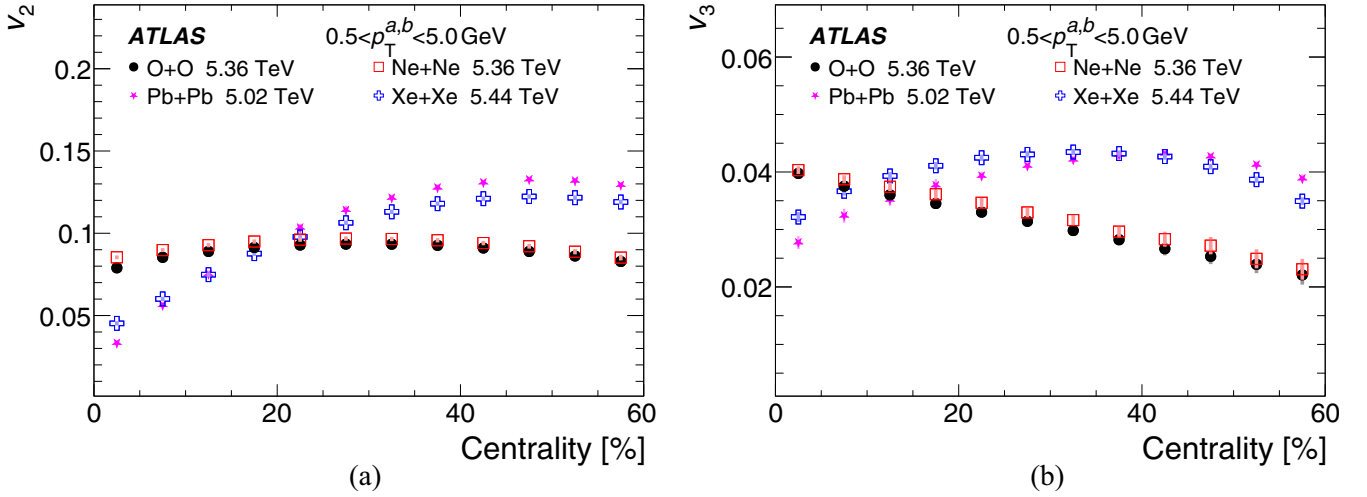


FIG. 10. Comparisons of the (a) v_2 and (b) v_3 measured by the template-fit method in O + O and Ne + Ne collisions with prior measurements in Xe + Xe and Pb + Pb collisions from Ref. [7], as a function of centrality. The Xe + Xe and Pb + Pb results are obtained with the 2PC method. The plots are for $0.5 < p_T^{a,b} < 5$ GeV. The vertical lines and vertical bars indicate statistical and systematic uncertainties, respectively.

same multiplicities and shows a qualitatively similar multiplicity dependence.

VII. CONCLUSION

This paper presents the first comprehensive measurements of anisotropic flow coefficients v_n ($n = 2-4$) in $\sqrt{s_{NN}} = 5.36$ TeV O + O and Ne + Ne collisions with the ATLAS detector at the LHC. The results are obtained using two-particle (template-fit) and four-particle (subevent cumulant) methods, and they explore the dependence of v_n on transverse momentum, multiplicity, and centrality in each system. To isolate the role of initial-state geometry, ratios of Ne + Ne to O + O v_n are also studied.

The measurements reveal a characteristic rise and fall of v_2 with p_T , peaking at 2–4 GeV, large event-by-event fluctuations in the most-central collisions, and a clear hierarchy $v_2 > v_3 > v_4$, consistent with hydrodynamic expectations. Multiplicity- and centrality-dependent ratios of $v_2\{2\}$ and $v_2\{4\}$, taken between Ne + Ne and O + O collisions, reveal a marked enhancement in Ne + Ne, consistent with the elongated nuclear shape of neon and reproduced by model calculations. For v_2 , the four-particle cumulant ratios provide the greatest sensitivity to these geometric effects. For $v_3\{2\}$, the Ne + Ne values exceed those in O + O for most centralities, except in the 0–1% most-central events where they are comparable. Detailed comparisons of these measurements with model predictions may also provide new sensitivity to α -clustering in the oxygen nucleus [90]. Com-

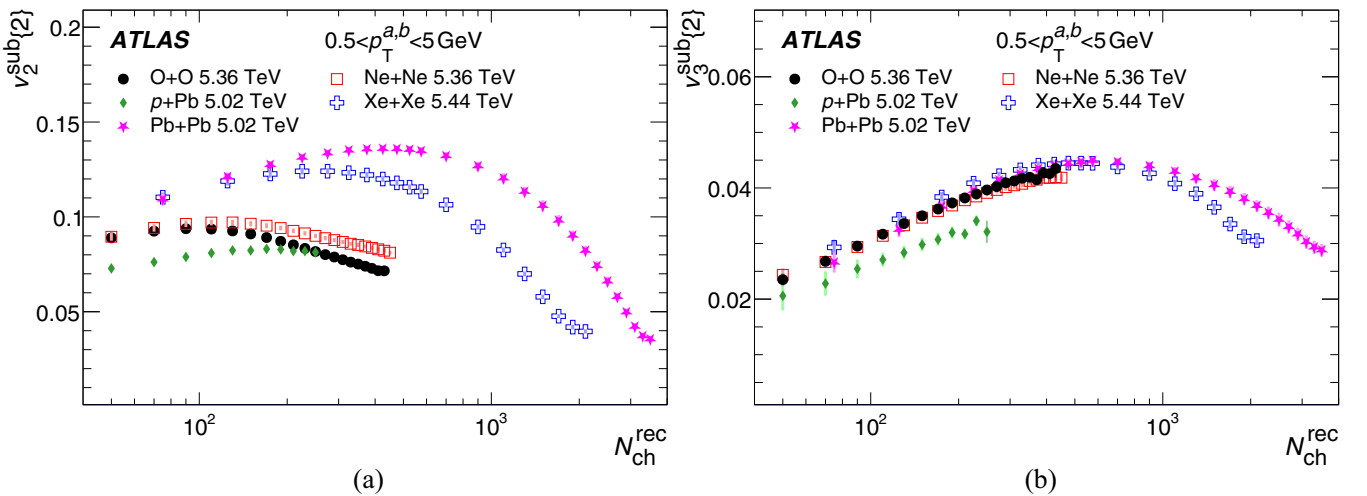


FIG. 11. Comparison of (a) $v_2^{\text{sub}}\{2\}$ and (b) $v_3^{\text{sub}}\{2\}$ measured in O + O and Ne + Ne collisions with prior measurements in p + Pb, Xe + Xe, and Pb + Pb collisions from Ref. [7], as a function of the reconstructed charged-particle multiplicity ($N_{\text{ch}}^{\text{rec}}$). The vertical lines and vertical bars indicate statistical and systematic uncertainties, respectively, and are often too small to be visible.

pared to heavy-ion collisions, the v_2 values in light ions show a much weaker centrality dependence, underscoring the enhanced role of EbE geometry fluctuations in these systems. As a function of event multiplicity, the v_3 values in O + O and Ne + Ne are quantitatively similar to those measured in Pb + Pb, Xe + Xe, and p + Pb collisions.

These light-ion results offer stringent constraints on hydrodynamic models incorporating *ab initio* nuclear structure inputs and provide unique insight into how nucleon-level geometry influences collective flow in small QGP droplets. Future comparisons with detailed model calculations could further constrain key medium and geometric properties, including the temperature dependence of η/s , the role of the prehydrodynamic phase, mechanisms of energy deposition in hadronic collisions, and other initial-state effects.

ACKNOWLEDGMENTS

We thank CERN for the very successful operation of the LHC and its injectors, as well as the support staff at CERN and at our institutions worldwide without whom ATLAS could not be operated efficiently.

The crucial computing support from all WLCG partners is acknowledged gratefully, in particular, from CERN, the ATLAS Tier-1 facilities at TRIUMF/SFU (Canada), NDGF (Denmark, Norway, Sweden), CC-IN2P3 (France), KIT/GridKA (Germany), INFN-CNAF (Italy), NL-T1 (Netherlands), PIC (Spain), RAL (UK), BNL (USA), the Tier-2 facilities worldwide, and large non-WLCG resource providers. Major contributors of computing resources are listed in Ref. [91].

We gratefully acknowledge the support of ANPCyT, Argentina; YerPhI, Armenia; ARC, Australia; BMWFW and FWF, Austria; ANAS, Azerbaijan; CNPq and FAPESP, Brazil; NSERC, NRC, and CFI, Canada; CERN; ANID, Chile; CAS, MOST, and NSFC, China; Minciencias, Colombia; MEYS CR, Czech Republic; DNRF and DNSRC, Denmark; IN2P3-CNRS and CEA-DRF/IRFU, France; SRNSFG, Georgia; BMFTR, HGF, and MPG, Germany; GSRI, Greece; RGC and Hong Kong SAR, China; ICHEP and Academy of Sciences and Humanities, Israel; INFN, Italy; MEXT and JSPS, Japan; CNRST, Morocco; NWO, Netherlands; RCN, Norway; MNiSW, Poland; FCT, Portugal; MNE/IFA, Romania; MSTDI, Serbia; MSSR, Slovakia; ARIS and MVZI, Slovenia; DSI/NRF, South Africa; MICIU/AEI, Spain; SRC and Wallenberg Foundation, Sweden; SERI, SNSF, and Cantons of Bern and Geneva, Switzerland; NSTC, Taipei; TENMAK, Turkey; STFC/UKRI, United Kingdom; and DOE and NSF, USA.

Individual groups and members have received support from BCKDF, CANARIE, CRC, and DRAC, Canada; CERN-CZ, FORTE, and PRIMUS, Czech Republic; COST, ERC, ERDF, Horizon 2020, ICSC-NextGenerationEU, and Marie Skłodowska-Curie Actions, European Union; Investissements d'Avenir Labex, Investissements d'Avenir Idex, and ANR, France; DFG and AvH Foundation, Germany; Herakleitos, Thales, and Aristeia programmes cofinanced by EU-ESF and the Greek NSRF, Greece; BSF-NSF and MINERVA, Israel; NCN and NAWA, Poland; La Caixa Banking Foundation,

CERCA Programme Generalitat de Catalunya, PROMETEO, and GenT Programmes Generalitat Valenciana, Spain; Göran Gustafssons Stiftelse, Sweden; and The Royal Society and Leverhulme Trust, United Kingdom.

In addition, individual members wish to acknowledge support from CERN: European Organization for Nuclear Research (CERN DOCT); Chile: Agencia Nacional de Investigación y Desarrollo (FONDECYT 1230812, FONDECYT 1240864, Fondecyt 3240661, Fondecyt Regular 1240721); China: Chinese Ministry of Science and Technology (MOST-2023YFA1605700, MOST-2023YFA1609300), National Natural Science Foundation of China (NSFC-12175119, NSFC-12275265); Czech Republic: Czech Science Foundation (GACR-24-11373S), Ministry of Education Youth and Sports (ERC-CZ-LL2327, FORTE CZ.02.01.01/00/22_008/0004632), PRIMUS Research Programme (PRIMUS/21/SCI/017); EU: H2020 European Research Council (ERC-101002463); European Union: European Research Council (BARD No. 101116429, ERC-948254, ERC-101089007), European Regional Development Fund (SMASH COFUND 101081355, SLO ERDF), European Union, Future Artificial Intelligence Research (FAIR-NextGenerationEU PE00000013), Italian Center for High Performance Computing, Big Data and Quantum Computing (ICSC, NextGenerationEU); France: Agence Nationale de la Recherche (ANR-21-CE31-0022, ANR-22-EDIR-0002, ANR-24-CE31-0504-01); Germany: Deutsche Forschungsgemeinschaft (DFG-469666862, DFG-CR 312/5-2); China: Research Grants Council (GRF); Italy: Istituto Nazionale di Fisica Nucleare (ICSC, NextGenerationEU), Ministero dell'Università e della Ricerca (NextGenEU 153D23001490006 M4C2.1.1, NextGenEU I53D23000820006 M4C2.1.1, NextGenEU I53D23001490006 M4C2.1.1, SOE2024_0000023); Japan: Japan Society for the Promotion of Science (JSPS KAKENHI JP22H01227, JSPS KAKENHI JP22H04944, JSPS KAKENHI JP22KK0227, JSPS KAKENHI JP24K23939, JSPS KAKENHI JP24KK0251, JSPS KAKENHI JP25H00650, JSPS KAKENHI JP25H01291, JSPS KAKENHI JP25K01023); Norway: Research Council of Norway (RCN-314472); Poland: Ministry of Science and Higher Education (IDUB AGH, POB8, D4 No. 9722), Polish National Science Centre (NCN 2021/42/E/ST2/00350, NCN OPUS 2023/51/B/ST2/02507, NCN UMO-2019/34/E/ST2/00393, UMO-2022/47/O/ST2/00148, UMO-2023/49/B/ST2/04085, UMO-2023/51/B/ST2/00920, UMO-2024/53/N/ST2/00869); Portugal: Foundation for Science and Technology (FCT); Spain: Generalitat Valenciana (ASFAE/2022/008), Ministry of Science and Innovation (MCIN & NextGenEU PCI2022-135018-2, MICIN & FEDER PID2021-125273NB, RYC2019-028510-I, RYC2020-030254-I, RYC2021-031273-I, RYC2022-038164-I), Ministerio de Ciencia, Innovación y Universidades/Agencia Estatal de Investigación (PID2022-142604OB-C22); Sweden: Carl Trygger Foundation (Carl Trygger Foundation CTS 22:2312), Swedish Research Council (Swedish Research Council 2023-04654, VR 2021-03651, VR 2022-03845, VR 2022-04683, VR 2023-03403, VR 2024-05451), Knut and Alice Wallenberg Foundation (KAW 2018.0458, KAW 2022.0358, KAW

2023.0366); Switzerland: Swiss National Science Foundation (SNSF-PCEFP2_194658); United Kingdom: Royal Society (NIF-R1-231091); USA: U.S. Department of Energy (ECA DE-AC02-76SF00515) and Neubauer Family Foundation.



DATA AVAILABILITY

The data for the paper are now publicly available at [92].

-
- [1] STAR Collaboration, Experimental and theoretical challenges in the search for the quark gluon plasma: The STAR collaboration's critical assessment of the evidence from RHIC collisions, *Nucl. Phys. A* **757**, 102 (2005).
- [2] PHOBOS Collaboration, The PHOBOS perspective on discoveries at RHIC, *Nucl. Phys. A* **757**, 28 (2005).
- [3] PHENIX Collaboration, Formation of dense partonic matter in relativistic nucleus-nucleus collisions at RHIC: Experimental evaluation by the PHENIX Collaboration, *Nucl. Phys. A* **757**, 184 (2005).
- [4] BRAHMS Collaboration, Quark-gluon plasma and color glass condensate at RHIC? The perspective from the BRAHMS experiment, *Nucl. Phys. A* **757**, 1 (2005).
- [5] ATLAS Collaboration, Measurement of the pseudorapidity and transverse momentum dependence of the elliptic flow of charged particles in lead-lead collisions at $\sqrt{s_{NN}} = 2.76$ TeV with the ATLAS detector, *Phys. Lett. B* **707**, 330 (2012).
- [6] ATLAS Collaboration, Measurement of the azimuthal anisotropy of charged particles produced in $\sqrt{s_{NN}} = 5.02$ TeV Pb+Pb collisions with the ATLAS detector, *Eur. Phys. J. C* **78**, 997 (2018).
- [7] ATLAS Collaboration, Measurement of the azimuthal anisotropy of charged-particle production in Xe+Xe collisions at $\sqrt{s_{NN}} = 5.44$ TeV with the ATLAS detector, *Phys. Rev. C* **101**, 024906 (2020).
- [8] CMS Collaboration, Measurement of the elliptic anisotropy of charged particles produced in PbPb collisions at $\sqrt{s_{NN}} = 2.76$ TeV, *Phys. Rev. C* **87**, 014902 (2013).
- [9] CMS Collaboration, Charged-particle angular correlations in XeXe collisions at $\sqrt{s_{NN}} = 5.44$ TeV, *Phys. Rev. C* **100**, 044902 (2019).
- [10] ALICE Collaboration, Elliptic flow of charged particles in Pb-Pb collisions at $\sqrt{s_{NN}} = 2.76$ TeV, *Phys. Rev. Lett.* **105**, 252302 (2010).
- [11] ALICE Collaboration, Anisotropic flow in Xe-Xe collisions at $\sqrt{s_{NN}} = 5.44$ TeV, *Phys. Lett. B* **784**, 82 (2018).
- [12] J.-Y. Ollitrault, Anisotropy as a signature of transverse collective flow, *Phys. Rev. D* **46**, 229 (1992).
- [13] W. Busza, K. Rajagopal, and W. van der Schee, Heavy ion collisions: The big picture, and the big questions, *Annu. Rev. Nucl. Part. Sci.* **68**, 339 (2018).
- [14] B. H. Alver, C. Gombeaud, M. Luzum, and J.-Y. Ollitrault, Triangular flow in hydrodynamics and transport theory, *Phys. Rev. C* **82**, 034913 (2010).
- [15] ATLAS Collaboration, Measurement of the azimuthal anisotropy for charged particle production in $\sqrt{s_{NN}} = 2.76$ TeV lead-lead collisions with the ATLAS detector, *Phys. Rev. C* **86**, 014907 (2012).
- [16] ATLAS Collaboration, Measurement of the distributions of event-by-event flow harmonics in lead-lead collisions at $\sqrt{s_{NN}} = 2.76$ TeV with the ATLAS detector at the LHC, *J. High Energy Phys.* **11** (2013) 183.
- [17] CMS Collaboration, Non-Gaussian elliptic-flow fluctuations in PbPb collisions at $\sqrt{s_{NN}} = 5.02$ TeV, *Phys. Lett. B* **789**, 643 (2019).
- [18] ALICE Collaboration, Energy dependence and fluctuations of anisotropic flow in Pb-Pb collisions at $\sqrt{s_{NN}} = 5.02$ and 2.76 TeV, *J. High Energy Phys.* **07** (2018) 103.
- [19] ATLAS Collaboration, Measurement of event-plane correlations in $\sqrt{s_{NN}} = 2.76$ TeV lead-lead collisions with the ATLAS detector, *Phys. Rev. C* **90**, 024905 (2014).
- [20] ALICE Collaboration, Long-range angular correlations on the near and away side in p -Pb collisions at $\sqrt{s_{NN}} = 5.02$ TeV, *Phys. Lett. B* **719**, 29 (2013).
- [21] ATLAS Collaboration, Observation of associated near-side and away-side long-range correlations in $\sqrt{s_{NN}} = 5.02$ TeV proton-lead collisions with the ATLAS detector, *Phys. Rev. Lett.* **110**, 182302 (2013).
- [22] ATLAS Collaboration, Observation of long-range elliptic azimuthal anisotropies in $\sqrt{s} = 13$ and 2.76 TeV pp collisions with the ATLAS detector, *Phys. Rev. Lett.* **116**, 172301 (2016).
- [23] CMS Collaboration, Evidence for collectivity in pp collisions at the LHC, *Phys. Lett. B* **765**, 193 (2017).
- [24] STAR Collaboration, Measurement of flow coefficients in high-multiplicity $p + Au$, $d + Au$, and $^3\text{He} + Au$ collisions at $\sqrt{s_{NN}} = 200$ GeV, *Phys. Rev. C* **110**, 064902 (2024).
- [25] STAR Collaboration, Measurements of the elliptic and triangular azimuthal anisotropies in central $^3\text{He} + Au$, $d + Au$ and $p + Au$ collisions at $\sqrt{s_{NN}} = 200$ GeV, *Phys. Rev. Lett.* **130**, 242301 (2023).
- [26] PHENIX Collaboration, Kinematic dependence of azimuthal anisotropies in $p + Au$, $d + Au$, and $^3\text{He} + Au$ at $\sqrt{s_{NN}} = 200$ GeV, *Phys. Rev. C* **105**, 024901 (2022).
- [27] PHENIX Collaboration, Creation of quark-gluon plasma droplets with three distinct geometries, *Nat. Phys.* **15**, 214 (2019).
- [28] R. D. Weller and P. Romatschke, One fluid to rule them all: Viscous hydrodynamic description of event-by-event central p+p, p+Pb and Pb+Pb collisions at $\sqrt{s} = 5.02$ TeV, *Phys. Lett. B* **774**, 351 (2017).
- [29] A. Bzdak, B. Schenke, P. Tribedy, and R. Venugopalan, Initial-state geometry and the role of hydrodynamics in proton-proton, proton-nucleus, and deuteron-nucleus collisions, *Phys. Rev. C* **87**, 064906 (2013).
- [30] H. Mäntysaari and B. Schenke, Evidence of strong proton shape fluctuations from incoherent diffraction, *Phys. Rev. Lett.* **117**, 052301 (2016).
- [31] G. Giacalone, J. Noronha-Hostler, M. Luzum, and J.-Y. Ollitrault, Hydrodynamic predictions for 5.44 TeV Xe+Xe collisions, *Phys. Rev. C* **97**, 034904 (2018).
- [32] V. E. Ambrus, S. Schlichting, and C. Werthmann, Collective dynamics in heavy and light-ion collisions. II. Determining the origin of collective behavior in high-energy collisions, *Phys. Rev. D* **111**, 054025 (2025).

- [33] J. Noronha, B. Schenke, C. Shen, and W. Zhao, Progress and challenges in small systems, *Int. J. Mod. Phys. E* **33**, 2430005 (2024).
- [34] Z. Citron, *et al.*, Future physics opportunities for high-density QCD at the LHC with heavy-ion and proton beams, *CERN Yellow Rep. Monogr.* **7**, 1159 (2019).
- [35] J. Jia, *et al.*, Imaging the initial condition of heavy-ion collisions and nuclear structure across the nuclide chart, *Nucl. Sci. Tech.* **35**, 220 (2024).
- [36] STAR Collaboration, Search for the chiral magnetic effect with isobar collisions at $\sqrt{s_{NN}} = 200$ GeV by the STAR collaboration at the BNL Relativistic Heavy Ion Collider, *Phys. Rev. C* **105**, 014901 (2022).
- [37] G. Giacalone, J. Jia, and V. Somà, Accessing the shape of atomic nuclei with relativistic collisions of isobars, *Phys. Rev. C* **104**, L041903 (2021).
- [38] ATLAS Collaboration, Correlations between flow and transverse momentum in Xe+Xe and Pb+Pb collisions at the LHC with the ATLAS detector: A probe of the heavy-ion initial state and nuclear deformation, *Phys. Rev. C* **107**, 054910 (2023).
- [39] ALICE Collaboration, Exploring nuclear structure with multi-particle azimuthal correlations at the LHC, *Phys. Lett. B* **869**, 139855 (2025).
- [40] STAR Collaboration, Imaging shapes of atomic nuclei in high-energy nuclear collisions, *Nature (London)* **635**, 67 (2024).
- [41] H. Hergert, A guided tour of *ab initio* nuclear many-body theory, *Front. Phys.* **8**, 379 (2020).
- [42] K. Wei, Y.-L. Ye, and Z.-H. Yang, Clustering in nuclei: Progress and perspectives, *Nucl. Sci. Tech.* **35**, 216 (2024).
- [43] J. Hiura, Y. Abe, S. Saitō, and O. Endō, Alpha-cluster plus ^{16}O -core model for ^{20}Ne and neighboring nuclei, *Prog. Theor. Phys.* **42**, 555 (1969).
- [44] G. Giacalone, *et al.*, Exploiting ^{20}Ne isotopes for precision characterizations of collectivity in small systems, *Phys. Rev. Lett.* **135**, 012302 (2025).
- [45] H.-C. Wang, S.-J. Li, L.-M. Liu, J. Xu, and Z.-Z. Ren, Deformation probes for light nuclei in their collisions at relativistic energies, *Phys. Rev. C* **110**, 034909 (2024).
- [46] ATLAS Collaboration, Measurement of long-range multiparticle azimuthal correlations with the subevent cumulant method in pp and $p + \text{Pb}$ collisions with the ATLAS detector at the CERN Large Hadron Collider, *Phys. Rev. C* **97**, 024904 (2018).
- [47] ALICE Collaboration, Evidence of nuclear geometry-driven anisotropic flow in OO and Ne-Ne collisions at $\sqrt{s_{NN}} = 5.36$ TeV, [arXiv:2509.06428](https://arxiv.org/abs/2509.06428).
- [48] CMS Collaboration, Observation of long-range collective flow in OO and NeNe collisions and implications for nuclear structure studies, [arXiv:2510.02580](https://arxiv.org/abs/2510.02580).
- [49] ATLAS Collaboration, The ATLAS experiment at the CERN Large Hadron Collider, *JINST* **3**, S08003 (2008).
- [50] ATLAS Collaboration, The ATLAS experiment at the CERN Large Hadron Collider: A description of the detector configuration for run 3, *JINST* **19**, P05063 (2024).
- [51] ATLAS Collaboration, The ATLAS trigger system for LHC run 3 and trigger performance in 2022, *JINST* **19**, P06029 (2024).
- [52] ATLAS Collaboration, Software and computing for run 3 of the ATLAS experiment at the LHC, *Eur. Phys. J. C* **85**, 234 (2025).
- [53] ATLAS Collaboration, The ATLAS transition radiation detector (TRT) fast-OR trigger, technical report no. ATL-INDET-PUB-2009-002, CERN, Geneva, 2009, <https://cds.cern.ch/record/1229213>.
- [54] ATLAS Collaboration, Vertex reconstruction performance of the ATLAS detector at $\sqrt{s} = 13$ TeV, technical report no. ATL-PHYS-PUB-2015-026, CERN, Geneva, 2015.
- [55] ATLAS Collaboration, Measurement of flow harmonics with multi-particle cumulants in Pb+Pb collisions at $\sqrt{s_{NN}} = 2.76$ TeV with the ATLAS detector, *Eur. Phys. J. C* **74**, 3157 (2014).
- [56] M. L. Miller, K. Reygers, S. J. Sanders, and P. Steinberg, Glauber modeling in high-energy nuclear collisions, *Annu. Rev. Nucl. Part. Sci.* **57**, 205 (2007).
- [57] C. Loizides, Glauber predictions for oxygen and neon collisions at LHC, *Phys. Rev. C* **113**, 014914 (2026).
- [58] ATLAS Collaboration, Performance of the ATLAS track reconstruction algorithms in dense environments in LHC run 2, *Eur. Phys. J. C* **77**, 673 (2017).
- [59] X.-N. Wang and M. Gyulassy, hijing: A Monte Carlo model for multiple jet production in pp , pA , and AA collisions, *Phys. Rev. D* **44**, 3501 (1991).
- [60] J. Jia and S. Mohapatra, Disentangling flow and nonflow correlations via Bayesian unfolding of the event-by-event distributions of harmonic coefficients in ultrarelativistic heavy-ion collisions, *Phys. Rev. C* **88**, 014907 (2013).
- [61] ATLAS Collaboration, The ATLAS simulation infrastructure, *Eur. Phys. J. C* **70**, 823 (2010).
- [62] S. Agostinelli, *et al.*, GEANT4—a simulation toolkit, *Nucl. Instrum. Methods Phys. Res., Sect. A* **506**, 250 (2003).
- [63] PHENIX Collaboration, Dihadron azimuthal correlations in Au+Au collisions at $\sqrt{s_{NN}} = 200$ GeV, *Phys. Rev. C* **78**, 014901 (2008).
- [64] ATLAS Collaboration, Measurement of long-range pseudorapidity correlations and azimuthal harmonics in $\sqrt{s_{NN}} = 5.02$ TeV proton-lead collisions with the ATLAS detector, *Phys. Rev. C* **90**, 044906 (2014).
- [65] ATLAS Collaboration, Measurement of the correlation between flow harmonics of different order in lead-lead collisions at $\sqrt{s_{NN}} = 2.76$ TeV with the ATLAS detector, *Phys. Rev. C* **92**, 034903 (2015).
- [66] ATLAS Collaboration, Measurements of long-range azimuthal anisotropies and associated Fourier coefficients for pp collisions at $\sqrt{s} = 5.02$ and 13 TeV and $p + \text{Pb}$ collisions at $\sqrt{s_{NN}} = 5.02$ TeV with the ATLAS detector, *Phys. Rev. C* **96**, 024908 (2017).
- [67] CMS Collaboration, Centrality dependence of dihadron correlations and azimuthal anisotropy harmonics in PbPb collisions at $\sqrt{s_{NN}} = 2.76$ TeV, *Eur. Phys. J. C* **72**, 2012 (2012).
- [68] CMS Collaboration, Long-range and short-range dihadron angular correlations in central PbPb collisions at $\sqrt{s_{NN}} = 2.76$ TeV, *J. High Energy Phys.* **07** (2011) 076.
- [69] CMS Collaboration, Studies of azimuthal dihadron correlations in ultra-central PbPb collisions at $\sqrt{s_{NN}} = 2.76$ TeV, *J. High Energy Phys.* **02** (2014) 088.
- [70] ALICE Collaboration, Harmonic decomposition of two-particle angular correlations in Pb-Pb collisions at $\sqrt{s_{NN}} = 2.76$ TeV, *Phys. Lett. B* **708**, 249 (2012).
- [71] ALICE Collaboration, Measurements of long-range two-particle correlation over a wide pseudorapidity range in $p - \text{Pb}$ collisions at $\sqrt{s_{NN}} = 5.02$ TeV, *J. High Energy Phys.* **01** (2024) 199.
- [72] M. A. Lisa, S. Pratt, R. Soltz, and U. Wiedemann, Femtoscopy in relativistic heavy ion collisions: Two decades of progress, *Annu. Rev. Nucl. Part. Sci.* **55**, 357 (2005).

- [73] ATLAS Collaboration, Measurement of long-range two-particle azimuthal correlations in Z-boson tagged pp collisions at $\sqrt{s} = 8$ and 13 TeV, *Eur. Phys. J. C* **80**, 64 (2020).
- [74] N. Borghini, P. M. Dinh, and J.-Y. Ollitrault, Flow analysis from multiparticle azimuthal correlations, *Phys. Rev. C* **64**, 054901 (2001).
- [75] A. Bilandzic, C. H. Christensen, K. Gulbrandsen, A. Hansen, and Y. Zhou, Generic framework for anisotropic flow analyses with multiparticle azimuthal correlations, *Phys. Rev. C* **89**, 064904 (2014).
- [76] A. Bilandzic, R. Snellings, and S. Voloshin, Flow analysis with cumulants: Direct calculations, *Phys. Rev. C* **83**, 044913 (2011).
- [77] J. Jia, M. Zhou, and A. Trzupek, Revealing long-range multiparticle collectivity in small collision systems via subevent cumulants, *Phys. Rev. C* **96**, 034906 (2017).
- [78] S. A. Voloshin, A. M. Poskanzer, A. Tang, and G. Wang, Elliptic flow in the Gaussian model of eccentricity fluctuations, *Phys. Lett. B* **659**, 537 (2008).
- [79] ATLAS Collaboration, Study of the material of the ATLAS inner detector for run 2 of the LHC, *JINST* **12**, P12009 (2017).
- [80] H. Mäntysaari, B. Schenke, C. Shen, and W. Zhao, Collision-energy dependence in heavy-ion collisions from nonlinear QCD evolution, *Phys. Rev. Lett.* **135**, 022302 (2025).
- [81] B. Schenke, P. Tribedy, and R. Venugopalan, Fluctuating Glasma initial conditions and flow in heavy ion collisions, *Phys. Rev. Lett.* **108**, 252301 (2012).
- [82] B. Schenke, S. Jeon, and C. Gale, (3+1)D hydrodynamic simulation of relativistic heavy-ion collisions, *Phys. Rev. C* **82**, 014903 (2010).
- [83] M. Bleicher, *et al.*, Relativistic hadron-hadron collisions in the ultra-relativistic quantum molecular dynamics model, *J. Phys. G* **25**, 1859 (1999).
- [84] S. A. Bass, *et al.*, Microscopic models for ultrarelativistic heavy ion collisions, *Prog. Part. Nucl. Phys.* **41**, 255 (1998).
- [85] D. Lee, Lattice simulations for few- and many-body systems, *Prog. Part. Nucl. Phys.* **63**, 117 (2009).
- [86] J. S. Moreland, J. E. Bernhard, and S. A. Bass, Alternative ansatz to wounded nucleon and binary collision scaling in high-energy nuclear collisions, *Phys. Rev. C* **92**, 011901 (2015).
- [87] G. Nijs, W. van der Schee, U. Gürsoy, and R. Snellings, Bayesian analysis of heavy ion collisions with the heavy ion computational framework Trajectum, *Phys. Rev. C* **103**, 054909 (2021).
- [88] G. Nijs and W. van der Schee, Predictions and postdictions for relativistic lead and oxygen collisions with the computational simulation code Trajectum, *Phys. Rev. C* **106**, 044903 (2022).
- [89] G. Giacalone, G. Nijs, and W. van der Schee, Determination of the neutron skin of ^{208}Pb from ultrarelativistic nuclear collisions, *Phys. Rev. Lett.* **131**, 202302 (2023).
- [90] Y. Wang, S. Zhao, B. Cao, H.-j. Xu, and H. Song, Exploring the compactness of α clusters in ^{16}O nuclei with relativistic $^{16}\text{O} + ^{16}\text{O}$ collisions, *Phys. Rev. C* **109**, L051904 (2024).
- [91] ATLAS Collaboration, ATLAS computing acknowledgements, technical report no. ATL-SOFT-PUB-2025-001, CERN, Geneva, 2025, <https://cds.cern.ch/record/2922210/>.
- [92] <https://www.hepdata.net/record/ins2967110>.

G. Aad ¹⁰³, E. Aakvaag ¹⁷, B. Abbott ¹²², S. Abdelhameed ^{118a}, K. Abeling ⁵⁵, N. J. Abicht ⁴⁹, S. H. Abidi ³⁰, M. Aboelela ⁴⁵, A. Aboulhorma ^{36e}, H. Abramowicz ¹⁵⁶, Y. Abulaiti ¹¹⁹, B. S. Acharya ^{69a,69b,a}, A. Ackermann ^{63a}, C. Adam Bourdarios ⁴, L. Adamczyk ^{86a}, S. V. Addepalli ¹⁴⁸, M. J. Addison ¹⁰², J. Adelman ¹¹⁷, A. Adiguzel ^{22c}, T. Adye ¹³⁶, A. A. Affolder ¹³⁸, Y. Afik ⁴⁰, M. N. Agaras ¹³, A. Aggarwal ¹⁰¹, C. Agheorghiesei ^{28c}, F. Ahmadov ^{39,b}, S. Ahuja ⁹⁶, S. Ahuja ¹⁶⁸, X. Ai ^{142b}, G. Aielli ^{76a,76b}, A. Aikot ¹⁶⁸, M. Ait Tamlit ^{36e}, B. Aitbenchikh ^{36a}, T. P. A. Åkesson ⁹⁹, A. V. Akimov ¹⁵⁰, D. Akiyama ¹⁷³, N. N. Akolkar ²⁵, S. Aktas ¹⁷¹, G. L. Alberghi ^{24b}, J. Albert ¹⁷⁰, U. Alberti ²⁰, P. Albicocco ⁵³, G. L. Albouy ⁶⁰, S. Alderweireldt ⁵², Z. L. Alegria ¹²³, M. Aleksa ³⁷, I. N. Aleksandrov ³⁹, C. Alexa ^{28b}, T. Alexopoulos ¹⁰, F. Alfonsi ^{24b}, M. Algren ⁵⁶, M. Alhroob ¹⁷², B. Ali ¹³⁴, H. M. J. Ali ^{92,c}, S. Ali ³², S. W. Alibocus ⁹³, M. Aliev ^{34c}, G. Alimonti ^{71a}, W. Alkhamis ⁵⁵, C. Allaire ⁶⁶, B. M. M. Allbrooke ¹⁵¹, D. R. Allen ¹²³, J. S. Allen ¹⁰², J. F. Allen ⁵², P. P. Allport ²¹, A. Aloisio ^{72a,72b}, F. Alonso ⁹¹, C. Alpigiani ¹⁴¹, Z. M. K. Alsolami ⁹², A. Alvarez Fernandez ¹⁰¹, M. Alves Cardoso ⁵⁶, M. G. Alviggi ^{72a,72b}, M. Aly ¹⁰², Y. Amaral Coutinho ^{82b}, A. Ambler ¹⁰⁵, C. Amelung ³⁷, M. Amerl ¹⁰², C. G. Ames ¹¹⁰, T. Amezza ¹²⁹, D. Amidei ¹⁰⁷, B. Amini ⁵⁴, K. Amirie ¹⁶⁰, A. Amirkhanov ³⁹, S. P. Amor Dos Santos ^{132a}, K. R. Amos ¹⁶⁸, D. Amperiadou ¹⁵⁷, S. An ⁸³, C. Anastopoulos ¹⁴⁴, T. Andeen ¹¹, J. K. Anders ⁹³, A. C. Anderson ⁵⁹, A. Andreazza ^{71a,71b}, S. Angelidakis ⁹, A. Angerami ⁴², A. V. Anisenkov ³⁹, A. Annovi ^{74a}, C. Antel ³⁷, E. Antipov ¹⁵⁰, M. Antonelli ⁵³, F. Anulli ^{75a}, M. Aoki ⁸³, T. Aoki ¹⁵⁸, M. A. Aparo ¹⁵¹, L. Aperio Bella ⁴⁸, M. Apicella ³¹, C. Appelt ¹⁵⁶, A. Apyan ²⁷, M. Arampatzi ¹⁰, S. J. Arbiol Val ⁸⁷, C. Arcangeletti ⁵³, A. T. H. Arce ⁵¹, J.-F. Arguin ¹⁰⁹, S. Argyropoulos ¹⁵⁷, J.-H. Arling ⁴⁸, O. Arnaez ⁴, H. Arnold ¹⁵⁰, G. Artoni ^{75a,75b}, H. Asada ¹¹², K. Asai ¹²⁰, S. Asatryan ¹⁷⁸, N. A. Asbah ³⁷, R. A. Ashby Pickering ¹⁷², A. M. Aslam ⁹⁶, K. Assamagan ³⁰, R. Astalos ^{29a}, K. S. V. Astrand ⁹⁹, S. Atashi ¹⁶⁴, R. J. Atkin ^{34a}, H. Atmani ^{36f}, P. A. Atlasiddha ¹³⁰, K. Augsten ¹³⁴, A. D. Auriol ⁴¹, V. A. Austrup ¹⁰², A. S. Avad ⁹⁵, G. Avolio ³⁷, K. Axiotis ⁵⁶, A. Azzam ¹³, D. Babal ^{29b}, H. Bachacou ¹³⁷, K. Bachas ^{157,d}, A. Bachiu ³⁵, E. Bachmann ⁵⁰, M. J. Backes ^{63a}, A. Badae ⁴⁰, T. M. Baer ¹⁰⁷, P. Bagnaia ^{75a,75b}, M. Bahmani ¹⁹, D. Bahner ⁵⁴, K. Bai ¹²⁵, J. T. Baines ¹³⁶, L. Baines ⁹⁵, O. K. Baker ¹⁷⁷, E. Bakos ¹⁶, D. Bakshi Gupta ⁸, L. E. Balabram Filho ^{82b}, V. Balakrishnan ¹²², R. Balasubramanian ⁴, E. M. Baldin ³⁸, P. Balek ^{86a}, E. Ballabene ^{24a,24b}, F. Balli ¹³⁷, L. M. Baltes ^{63a}, W. K. Balunas ³³, J. Balz ¹⁰¹, I. Bamwidhi ^{118b}, E. Banas ⁸⁷, M. Bandieramonte ¹³¹, A. Bandyopadhyay ²⁵, S. Bansal ²⁵, L. Barak ¹⁵⁶, M. Barakat ⁴⁸, E. L. Barberio ¹⁰⁶, D. Barberis ^{18b}, M. Barbero ¹⁰³, M. Z. Barel ¹¹⁶, T. Barillari ¹¹¹, M.-S. Barisits ³⁷, T. Barklow ¹⁴⁸

- P. Baron ¹³⁵ D. A. Baron Moreno ¹⁰² A. Baroncelli ⁶² A. J. Barr ¹²⁸ J. D. Barr ⁹⁷ F. Barreiro ¹⁰⁰
 J. Barreiro Guimarães da Costa ¹⁴ M. G. Barros Teixeira ^{132a} S. Barsov ³⁸ F. Bartels ^{63a} R. Bartoldus ¹⁴⁸
 A. E. Barton ⁹² P. Bartos ^{29a} M. Baselga ⁴⁹ S. Bashiri ⁸⁷ A. Bassalat ^{66,e} M. J. Basso ^{161a} S. Bataju ⁴⁵ R. Bate ¹⁶⁹
 R. L. Bates ⁵⁹ S. Batlamou, ¹⁰⁰ M. Battaglia ¹³⁸ D. Battulga ¹⁹ M. Bauce ^{75a,75b} M. Bauer ⁷⁹ P. Bauer ²⁵
 L. T. Bayer ⁴⁸ L. T. Bazzano Hurrell ³¹ J. B. Beacham ¹¹¹ T. Beau ¹²⁹ J. Y. Beaucamp ⁹¹ P. H. Beauchemin ¹⁶³
 P. Bechtel ²⁵ H. P. Beck ^{20,f} K. Becker ¹⁷² A. J. Beddall ⁸¹ V. A. Bednyakov ³⁹ C. P. Bee ¹⁵⁰ L. J. Beemster ¹⁶
 M. Begalli ^{82d} M. Begel ³⁰ J. K. Behr ⁴⁸ J. F. Beirer ³⁷ F. Beisiegel ²⁵ M. Belfkir ^{118b} G. Bella ¹⁵⁶
 L. Bellagamba ^{24b} A. Bellerive ³⁵ C. D. Bellgraph ⁶⁸ P. Bellos ²¹ K. Beloborodov ³⁸ I. Benaoumeur ²¹
 D. Benckekroun ^{36a} F. Bendebba ^{36a} Y. Benhammou ¹⁵⁶ K. C. Benkendorfer ⁶¹ L. Beresford ⁴⁸ M. Beretta ⁵³
 E. Bergeaas Kuutmann ¹⁶⁶ N. Berger ⁴ B. Bergmann ¹³⁴ J. Beringer ^{18a} G. Bernardi ⁵ C. Bernius ¹⁴⁸
 F. U. Bernlochner ²⁵ A. Berrocal Guardia ¹³ T. Berry ⁹⁶ P. Berta ¹³⁵ A. Berti ^{132a} R. Bertrand ¹⁰³ S. Bethke ¹¹¹
 A. Betti ^{75a,75b} A. J. Bevan ⁹⁵ L. Bezio ⁵⁶ N. K. Bhalla ⁵⁴ S. Bharthuar ¹¹¹ S. Bhatta ¹⁵⁰ P. Bhattarai ¹⁴⁸
 Z. M. Bhatti ¹¹⁹ K. D. Bhide ⁵⁴ V. S. Bhopatkar ¹²³ R. M. Bianchi ¹³¹ G. Bianco ^{24a,24b} O. Biebel ¹¹⁰
 M. Biglietti ^{77a} C. S. Billingsley ⁴⁵ Y. Bimgdi ^{36f} M. Bindi ⁵⁵ A. Bingham ¹⁷⁶ A. Bingul ^{22b} C. Bini ^{75a,75b}
 G. A. Bird ³³ M. Birman ¹⁷⁴ M. Biros ¹³⁵ S. Biryukov ¹⁵¹ T. Bisanz ⁴⁹ E. Bisceglie ^{24a,24b} J. P. Biswal ¹³⁶
 D. Biswas ¹⁴⁶ I. Bloch ⁴⁸ A. Blue ⁵⁹ U. Blumenschein ⁹⁵ V. S. Bobrovnikov ³⁹ L. Boccardo ^{57a,57b} M. Boehler ⁵⁴
 B. Boehm ¹⁷¹ D. Bogavac ¹³ A. G. Bogdanchikov ³⁸ L. S. Boggia ¹²⁹ V. Boisvert ⁹⁶ P. Bokan ³⁷ T. Bold ^{86a}
 M. Bomben ⁵ M. Bona ⁹⁵ M. Boonekamp ¹³⁷ A. G. Borbély ⁵⁹ I. S. Bordulev ³⁸ G. Borissov ⁹² D. Bortoletto ¹²⁸
 D. Boscherini ^{24b} M. Bosman ¹³ K. Bouaouda ^{36a} N. Bouchhar ¹⁶⁸ L. Boudet ⁴ J. Boudreau ¹³¹
 E. V. Bouhova-Thacker ⁹² D. Boumediene ⁴¹ R. Bouquet ^{57a,57b} A. Boveia ¹²¹ J. Boyd ³⁷ D. Boye ³⁰
 I. R. Boyko ³⁹ L. Bozianu ⁵⁶ J. Bracik ²¹ N. Brahimi ⁴ G. Brandt ¹⁷⁶ O. Brandt ³³ B. Brau ¹⁰⁴ J. E. Brau ¹²⁵
 R. Brenner ¹⁷⁴ L. Brenner ¹¹⁶ R. Brenner ¹⁶⁶ S. Bressler ¹⁷⁴ G. Brianti ^{78a,78b} D. Britton ⁵⁹ D. Britzger ¹¹¹
 I. Brock ²⁵ R. Brock ¹⁰⁸ G. Brooijmans ⁴² A. J. Brooks ⁶⁸ E. M. Brooks ^{161b} E. Brost ³⁰ L. M. Brown ^{161a,170}
 L. E. Bruce ⁶¹ T. L. Bruckler ¹²⁸ P. A. Bruckman de Renstrom ⁸⁷ B. Brüers ⁴⁸ A. Bruni ^{24b} G. Bruni ^{24b}
 D. Brunner ^{47a,47b} M. Bruschi ^{24b} N. Bruscino ^{75a,75b} T. Buanes ¹⁷ Q. Buat ¹⁴¹ D. Buchin ¹¹¹ A. G. Buckley ⁵⁹
 O. Bulekov ⁸¹ B. A. Bullard ¹⁴⁸ S. Burdin ⁹³ C. D. Burgard ⁴⁹ A. M. Burger ⁹⁰ B. Burghgrave ⁸ O. Burlayenko ⁵⁴
 J. Bureson ¹⁶⁷ J. C. Burzynski ¹⁴⁷ E. L. Busch ⁴² V. Büscher ¹⁰¹ P. J. Bussey ⁵⁹ O. But ²⁵ J. M. Butler ²⁶
 C. M. Buttar ⁵⁹ J. M. Butterworth ⁹⁷ W. Buttinger ¹³⁶ C. J. Buxo Vazquez ¹⁰⁸ A. R. Buzyaev ³⁹
 S. Cabrera Urbán ¹⁶⁸ L. Cadamuro ⁶⁶ H. Cai ³⁷ Y. Cai ^{113c,24a,24b} Y. Cai ^{113a} V. M. M. Cairo ³⁷ O. Cakir ^{3a}
 N. Calace ³⁷ P. Calafiura ^{18a} G. Calderini ¹²⁹ P. Calfayan ³⁵ L. Calic ⁹⁹ G. Callea ⁵⁹ L. P. Caloba ^{82b} D. Calvet ⁴¹
 S. Calvet ⁴¹ R. Camacho Toro ¹²⁹ S. Camarda ³⁷ D. Camarero Munoz ²⁷ P. Camarri ^{76a,76b} C. Camincher ¹⁷⁰
 M. Campanelli ⁹⁷ A. Camplani ⁴³ V. Canale ^{72a,72b} A. C. Canbay ^{3a} E. Canonero ⁹⁶ J. Cantero ¹⁶⁸ Y. Cao ¹⁶⁷
 F. Capocasa ²⁷ M. Capua ^{44a,44b} A. Carbone ^{71a,71b} R. Cardarelli ^{76a} J. C. J. Cardenas ⁸ M. P. Cardiff ²⁷
 G. Carducci ^{44a,44b} T. Carli ³⁷ G. Carlino ^{72a} J. I. Carlotto ¹³ B. T. Carlson ^{131,g} E. M. Carlson ¹⁷⁰ J. Carmignani ⁹³
 L. Carminati ^{71a,71b} A. Carnelli ⁴ M. Carnesale ³⁷ S. Caron ¹¹⁵ E. Carquin ^{139g} I. B. Carr ¹⁰⁶ S. Carrá ^{73a,73b}
 G. Carratta ^{24a,24b} C. Carrion Martinez ¹⁶⁸ A. M. Carroll ¹²⁵ M. P. Casado ^{13,h} P. Casolaro ^{72a,72b} M. Caspar ⁴⁸
 W. R. Castiglioni ⁴⁰ F. L. Castillo ⁴ L. Castillo Garcia ¹³ V. Castillo Gimenez ¹⁶⁸ N. F. Castro ^{132a,132e}
 A. Catinaccio ³⁷ J. R. Catmore ¹²⁷ T. Cavaliere ⁴ V. Cavaliere ³⁰ L. J. Cavedes Betancourt ^{23b} E. Celebi ⁸¹
 S. Cella ³⁷ V. Cepaitis ⁵⁶ K. Cerny ¹²⁴ A. S. Cerqueira ^{82a} A. Cerri ^{74a,i} L. Cerrito ^{76a,76b} F. Cerutti ^{18a}
 B. Cervato ^{71a,71b} A. Cervelli ^{24b} G. Cesarini ⁵³ S. A. Cetin ⁸¹ P. M. Chabrilat ¹²⁹ R. Chakkappai ⁶⁶
 S. Chakraborty ¹⁷² A. Chambers ⁶¹ J. Chan ^{18a} W. Y. Chan ¹⁵⁸ J. D. Chapman ³³ E. Chapon ¹³⁷
 B. Chargeishvili ^{154b} D. G. Charlton ²¹ C. Chauhan ¹³⁵ Y. Che ^{113a} S. Chekanov ⁶ G. A. Chelkov ^{39,j} B. Chen ¹⁵⁶
 B. Chen ¹⁷⁰ H. Chen ³⁰ J. Chen ^{143a} J. Chen ¹⁴⁷ M. Chen ¹²⁸ S. Chen ⁸⁸ S. J. Chen ^{113a} X. Chen ^{143a}
 X. Chen ^{15,k} Z. Chen ⁶² C. L. Cheng ¹⁷⁵ H. C. Cheng ^{64a} S. Cheong ¹⁴⁸ A. Cheplakov ³⁹ E. Cherepanova ¹¹⁶
 R. Cherkaoui El Moursli ^{36e} E. Cheu ⁷ K. Cheung ⁶⁵ L. Chevalier ¹³⁷ V. Chiarella ⁵³ G. Chiarelli ^{74a}
 G. Chiodini ^{70a} A. S. Chisholm ²¹ A. Chitan ^{28b} M. Chitishvili ¹⁶⁸ M. V. Chizhov ^{39,i} K. Choi ¹¹ Y. Chou ¹⁴¹
 E. Y. S. Chow ¹¹⁵ K. L. Chu ¹⁷⁴ M. C. Chu ^{64a} X. Chu ^{113c,14} Z. Chubinidze ⁵³ J. Chudoba ¹³³
 J. J. Chwastowski ⁸⁷ D. Cieri ¹¹¹ K. M. Ciesla ^{86a} V. Cindro ⁹⁴ A. Ciocio ^{18a} F. Ciotto ^{72a,72b} Z. H. Citron ¹⁷⁴
 M. Citterio ^{71a} D. A. Ciubotaru ^{28b} A. Clark ⁵⁶ P. J. Clark ⁵² N. Clarke Hall ⁹⁷ C. Clarry ¹⁶⁰ S. E. Clawson ⁴⁸
 C. Clement ^{47a,47b} L. Clissa ^{24a,24b} Y. Coadou ¹⁰³ M. Cobal ^{69a,69c} A. Coccaro ^{57b} R. F. Coelho Barrue ^{132a}
 R. Coelho Lopes De Sa ¹⁰⁴ S. Coelli ^{71a} M. M. Cohen ¹³⁰ L. S. Colangeli ¹⁶⁰ B. Cole ⁴² P. Collado Soto ¹⁰⁰
 J. Collot ⁶⁰ R. Coluccia ^{70a,70b} P. Conde Muiño ^{132a,132g} M. P. Connell ^{34c} S. H. Connell ^{34c} E. I. Conroy ¹²⁸
 M. Contreras Cossio ¹¹ F. Conventi ^{72a,m} A. M. Cooper-Sarkar ¹²⁸ L. Corazzina ^{75a,75b} F. A. Corchia ^{24a,24b}
 A. Cordeiro Oudot Choi ¹⁴¹ L. D. Corpe ⁴¹ M. Corradi ^{75a,75b} F. Corriveau ^{105,n} A. Cortes-Gonzalez ¹⁵⁸
 M. J. Costa ¹⁶⁸ F. Costanza ⁴ D. Costanzo ¹⁴⁴ J. Couthures ⁴ G. Cowan ⁹⁶ K. Cranmer ¹⁷⁵ L. Cremer ⁴⁹
 D. Cremonini ^{24a,24b} S. Crépe-Renaudin ⁶⁰ F. Crescioli ¹²⁹ T. Cresta ^{73a,73b} M. Cristinziani ¹⁴⁶
 M. Cristoforetti ^{78a,78b} E. Critelli ⁹⁷ V. Croft ¹¹⁶ G. Crosetti ^{44a,44b} A. Cueto ¹⁰⁰ H. Cui ⁹⁷ Z. Cui ⁷
 B. M. Cunnnett ¹⁵¹ W. R. Cunningham ⁵⁹ F. Curcio ¹⁶⁸ J. R. Curran ⁵² M. J. Da Cunha Sargedas De Sousa ^{57a,57b}

- J. V. Da Fonseca Pinto ^{82b} C. Da Via ¹⁰² W. Dabrowski ^{86a} T. Dado ³⁷ S. Dahbi ¹⁵³ T. Dai ¹⁰⁷ D. Dal Santo ²⁰
 C. Dallapiccola ¹⁰⁴ M. Dam ⁴³ G. D'amen ³⁰ V. D'Amico ¹¹⁰ J. R. Dandoy ³⁵ M. D'Andrea ^{57a,57b}
 D. Dannheim ³⁷ G. D'anniballe ^{74a,74b} M. Danninger ¹⁴⁷ V. Dao ¹⁵⁰ G. Darbo ^{57b} S. J. Das ³⁰ F. Dattola ⁴⁸
 S. D'Auria ^{71a,71b} A. D'Avanzo ^{72a,72b} T. Davidek ¹³⁵ J. Davidson ¹⁷² I. Dawson ⁹⁵ K. De ⁸
 C. De Almeida Rossi ¹⁶⁰ R. De Asmundis ^{72a} N. De Biase ⁴⁸ S. De Castro ^{24a,24b} N. De Groot ¹¹⁵ P. de Jong ¹¹⁶
 H. De la Torre ¹¹⁷ A. De Maria ^{113a} A. De Salvo ^{75a} U. De Sanctis ^{76a,76b} F. De Santis ^{70a,70b} A. De Santo ¹⁵¹
 J. B. De Vivie De Regie ⁶⁰ J. Debevc ⁹⁴ D. V. Dedovich ³⁹ J. Degens ⁹³ A. M. Deiana ⁴⁵ J. Del Peso ¹⁰⁰
 L. Delagrangé ¹²⁹ F. Deliot ¹³⁷ C. M. Delitzsch ⁴⁹ M. Della Pietra ^{72a,72b} D. Della Volpe ⁵⁶ A. Dell'Acqua ³⁷
 L. Dell'Asta ^{71a,71b} M. Delmastro ⁴ C. C. Delogu ^{57a,57b} P. A. Delsart ⁶⁰ S. Demers ¹⁷⁷ M. Demichev ³⁹
 S. P. Denisov ³⁸ H. Denizli ^{22a,o} M. G. Depala ⁹³ L. D'Eramo ⁴¹ D. Derendarz ⁸⁷ F. Derue ¹²⁹ P. Dervan ^{93,p}
 A. M. Desai ¹ K. Desch ²⁵ F. A. Di Bello ^{74a,74b} A. Di Ciaccio ^{76a,76b} L. Di Ciaccio ⁴ A. Di Domenico ^{75a,75b}
 C. Di Donato ^{72a,72b} A. Di Girolamo ³⁷ G. Di Gregorio ⁶⁶ A. Di Luca ^{78a,78b} B. Di Micco ^{77a,77b} R. Di Nardo ^{77a,77b}
 K. F. Di Petrillo ⁴⁰ M. Diamantopoulou ³⁵ F. A. Dias ¹¹⁶ M. A. Diaz ^{139a,139b} A. R. Didenko ³⁹ M. Didenko ¹⁶⁸
 S. D. Diefenbacher ^{18a} E. B. Diehl ¹⁰⁷ S. Díez Cornell ⁴⁸ C. Díez Pardos ¹⁴⁶ C. Dimitriadi ¹⁴⁹ A. Dimitrievska ²¹
 A. Dimri ¹⁵⁰ Y. Ding ⁶² J. Dingfelder ²⁵ T. Dingley ¹²⁸ I.-M. Dinu ^{28b} S. J. Dittmeier ^{63b} F. Dittus ³⁷ M. Divisek ¹³⁵
 B. Dixit ⁹³ F. Djama ¹⁰³ T. Djobava ^{154b} C. Doglioni ^{102,99} A. Dohnalova ^{29a} Z. Dolezal ¹³⁵ K. Domijan ^{86a}
 K. M. Dona ⁴⁰ M. Donadelli ^{82d} B. Dong ¹⁰⁸ J. Donini ⁴¹ A. D'Onofrio ^{72a,72b} M. D'Onofrio ⁹³ J. Dopke ¹³⁶
 A. Doria ^{72a} N. Dos Santos Fernandes ^{132a} I. A. Dos Santos Luz ^{82e} P. Dougan ¹⁰² M. T. Dova ⁹¹ A. T. Doyle ⁵⁹
 M. P. Drescher ⁵⁵ E. Dreyer ¹⁷⁴ I. Drivas-koulouris ¹⁰ M. Drnevic ¹¹⁹ D. Du ⁶² T. A. du Pree ¹¹⁶ Z. Duan ^{113a}
 M. Dubau ⁴ F. Dubinin ³⁹ M. Dubovsky ^{29a} E. Duchovni ¹⁷⁴ G. Duckeck ¹¹⁰ P. K. Duckett ⁹⁷ O. A. Ducu ^{28b}
 D. Duda ⁵² A. Dudarev ³⁷ M. M. Dudek ⁸⁷ E. R. Duden ²⁷ M. D'uffizi ¹⁰² L. Dufлот ⁶⁶ M. Dührssen ³⁷
 I. Duminica ^{28g} A. E. Dumitriu ^{28b} M. Dunford ^{63a} K. Dunne ^{47a,47b} A. Duperrin ¹⁰³ H. Duran Yildiz ^{3a}
 A. Durglishvili ^{154b} G. I. Dyckes ^{18a} M. Dyndal ^{86a} B. S. Dziedzic ³⁷ Z. O. Earnshaw ¹⁵¹ G. H. Eberwein ¹²⁸
 B. Eckerova ^{29a} S. Eggebrecht ⁵⁵ E. Egidio Purcino De Souza ^{82e} G. Eigen ¹⁷ K. Einsweiler ^{18a} T. Ekelof ¹⁶⁶
 P. A. Ekman ⁹⁹ S. El Farkh ^{36b} Y. El Ghazali ⁶² H. El Jarrari ¹⁰⁵ A. El Moussaouy ^{36a} D. Elitez ³⁷ M. Ellert ¹⁶⁶
 F. Ellinghaus ¹⁷⁶ T. A. Elliot ⁹⁶ N. Ellis ³⁷ J. Elmsheuser ³⁰ M. Elsayy ^{118a} M. Elsing ³⁷ D. Emelianov ¹³⁶
 Y. Enari ⁸³ S. Epari ¹⁰⁹ D. Ernani Martins Neto ⁸⁷ F. Ernst ³⁷ M. Escalier ⁶⁶ C. Escobar ¹⁶⁸ E. Etzion ¹⁵⁶
 G. Evans ^{132a,132b} H. Evans ⁶⁸ L. S. Evans ⁴⁸ A. Ezhilov ³⁸ S. Ezzarqtouni ^{36a} F. Fabbri ^{24a,24b} L. Fabbri ^{24a,24b}
 G. Facini ⁹⁷ V. Fadeyev ¹³⁸ R. M. Fakhruddinov ³⁸ D. Fakoudis ¹⁰¹ S. Falciano ^{75a} L. F. Falda Ulhoa Coelho ²⁷
 F. Fallavollita ¹¹¹ G. Falsetti ^{44a,44b} J. Faltova ¹³⁵ C. Fan ¹⁶⁷ K. Y. Fan ^{64b} Y. Fan ¹⁴ Y. Fang ^{113c,14}
 M. Fanti ^{71a,71b} M. Faraj ^{69a,69b} Z. Farazpay ⁹⁸ A. Farbin ⁸ A. Farilla ^{77a} K. Farman ¹⁵³ T. Farooque ¹⁰⁸
 J. N. Farr ¹⁷⁷ M. S. Farrington ⁶¹ S. M. Farrington ^{136,52} F. Fassi ^{36e} D. Fassouliotis ⁹ L. Fayard ⁶⁶ P. Federic ¹³⁵
 P. Federicova ¹³³ O. L. Fedin ^{38,j} M. Feickert ¹⁷⁵ L. Feligioni ¹⁰³ D. E. Fellers ^{18a} C. Feng ^{142a} Y. Feng ¹⁴
 Z. Feng ¹¹⁶ M. J. Fenton ¹⁶⁴ L. Ferencz ⁴⁸ B. Fernandez Barbadillo ⁹² P. Fernandez Martinez ⁶⁷ M. J. V. Fernoux ¹⁰³
 J. Ferrando ⁹² A. Ferrari ¹⁶⁶ P. Ferrari ^{115,116} R. Ferrari ^{73a} D. Ferrere ⁵⁶ C. Ferretti ¹⁰⁷ M. P. Fewell ¹
 D. Fiacco ^{75a,75b} F. Fiedler ¹⁰¹ P. Fiedler ¹³⁴ S. Filimonov ³⁹ M. S. Filip ^{28b,q} A. Filipčić ⁹⁴ E. K. Filmer ^{161a}
 F. Filthaut ¹¹⁵ M. C. N. Fiolhais ^{132a,132c,r} L. Fiorini ¹⁶⁸ W. C. Fisher ¹⁰⁸ T. Fitschen ¹⁰² P. M. Fitzhugh ¹³⁷
 I. Fleck ¹⁴⁶ P. Fleischmann ¹⁰⁷ T. Flick ¹⁷⁶ M. Flores ^{34d} L. R. Flores Castillo ^{64a} F. M. Follega ^{78a,78b} N. Fomin ³³
 J. H. Foo ¹⁶⁰ A. Formica ¹³⁷ A. C. Forti ¹⁰² E. Fortin ³⁷ A. W. Fortman ^{18a} L. Foster ^{18a} L. Fountas ^{9,s}
 D. Fournier ⁶⁶ H. Fox ⁹² P. Francavilla ^{74a,74b} S. Francescato ⁶¹ S. Franchellucci ⁵⁶ M. Franchini ^{24a,24b}
 S. Franchino ^{63a} D. Francis ³⁷ L. Franco ⁴⁸ L. Franconi ⁴⁸ M. Franklin ⁶¹ G. Frattari ²⁷ Y. Y. Frid ¹⁵⁶ J. Friend ⁵⁹
 N. Fritzsche ³⁷ A. Froch ⁵⁶ D. Froidevaux ³⁷ J. A. Frost ¹³⁶ Y. Fu ¹⁰⁸ S. Fuenzalida Garrido ^{139g} M. Fujimoto ¹⁵⁰
 K. Y. Fung ^{64a} E. Furtado De Simas Filho ^{82e} M. Furukawa ¹⁵⁸ M. Fuste Costa ⁴⁸ J. Fuster ¹⁶⁸ A. Gaa ⁵⁵
 A. Gabrielli ^{24a,24b} A. Gabrielli ¹⁶⁰ P. Gadov ³⁷ G. Gagliardi ^{57a,57b} L. G. Gagnon ^{18a} S. Gaid ^{84b} S. Galantzan ¹⁵⁶
 J. Gallagher ¹ E. J. Gallas ¹²⁸ A. L. Gallen ¹⁶⁶ B. J. Gallop ¹³⁶ K. K. Gan

S. González de la Hoz¹⁶⁸ M. V. Gonzalez Rodrigues⁴⁸ R. Gonzalez Suarez¹⁶⁶ S. Gonzalez-Sevilla⁵⁶
 L. Goossens³⁷ B. Gorini³⁷ E. Gorini^{70a,70b} A. Gorišek⁹⁴ T. C. Gosart¹³⁰ A. T. Goshaw⁵¹ M. I. Gostkin³⁹
 S. Goswami¹²³ C. A. Gottardo³⁷ S. A. Gotz¹¹⁰ M. Goughri^{36b} A. G. Goussiou¹⁴¹ N. Govender^{34c}
 R. P. Grabarczyk¹²⁸ I. Grabowska-Bold^{86a} K. Graham³⁵ E. Gramstad¹²⁷ S. Grancagnolo^{70a,70b} C. M. Grant¹
 P. M. Gravila^{28f} F. G. Gravili^{70a,70b} H. M. Gray^{18a} M. Greco¹¹¹ M. J. Green¹ C. Grefe²⁵ A. S. Grefsrud¹⁷
 I. M. Gregor⁴⁸ K. T. Greif¹⁶⁴ P. Grenier¹⁴⁸ S. G. Grewe¹¹¹ A. A. Grillo¹³⁸ K. Grimm³² S. Grinstein^{13,u}
 J.-F. Grivaz⁶⁶ E. Gross¹⁷⁴ J. Grosse-Knetter⁵⁵ L. H. Grossman^{18b} L. Guan¹⁰⁷ G. Guerrieri³⁷ R. Guevara¹²⁷
 R. Gugel¹⁰¹ J. A. M. Guhit¹⁰⁷ A. Guida¹⁹ E. Guilloton¹⁷² S. Guindon³⁷ F. Guo^{113c,14} J. Guo^{143a} L. Guo⁴⁸
 L. Guo^{113b,v} Y. Guo¹⁰⁷ Y. Guo⁴² A. Gupta⁴⁹ R. Gupta¹³¹ S. Gupta²⁷ S. Gurbuz²⁵ S. S. Gurdasani⁴⁸
 G. Gustavino^{75a,75b} P. Gutierrez¹²² L. F. Gutierrez Zagazeta¹³⁰ M. Gutsche⁵⁰ C. Gutschow⁹⁷ C. Gwenlan¹²⁸
 C. B. Gwilliam⁹³ E. S. Haaland¹²⁷ A. Haas¹¹⁹ M. Habedank⁵⁹ C. Haber^{18a} H. K. Hadavand⁸ A. Haddad⁴¹
 A. Hadeef⁵⁰ A. I. Hagan⁹² J. J. Hahn¹⁴⁶ E. H. Haines⁹⁷ M. Haleem¹⁷¹ J. Haley¹²³ G. D. Hallowell¹⁰³
 J. A. Hallford⁴⁸ K. Hamano¹⁷⁰ H. Hamdaoui¹⁶⁶ M. Hamer²⁵ S. E. D. Hammoud⁶⁶ E. J. Hampshire⁹⁶
 J. Han^{142a} L. Han^{113a} L. Han⁶² S. Han¹⁴ K. Hanagaki⁸³ M. Hance¹³⁸ D. A. Hangal⁴² H. Hanif¹⁴⁷
 M. D. Hank¹³⁰ J. B. Hansen⁴³ P. H. Hansen⁴³ T. Harenberg¹⁷⁶ S. Harkusha¹⁷⁸ M. L. Harris¹⁰⁴ Y. T. Harris²⁵
 J. Harrison¹³ P. F. Harrison¹⁷² M. L. E. Hart⁹⁷ N. M. Hartman¹¹¹ N. M. Hartmann¹¹⁰ R. Z. Hasan^{136,96}
 Y. Hasegawa¹⁴⁵ F. Haslbeck¹²⁸ S. Hassan¹⁷ R. Hauser¹⁰⁸ M. Haviernik¹³⁵ C. M. Hawkes²¹ R. J. Hawkins³⁷
 Y. Hayashi¹⁵⁸ D. Hayden¹⁰⁸ C. Hayes¹⁰⁷ R. L. Hayes¹¹⁶ C. P. Hays¹²⁸ J. M. Hays⁹⁵ H. S. Hayward⁹³
 M. He^{113c,14} Y. He⁴⁸ Y. He⁹⁷ N. B. Heatley⁹⁵ V. Hedberg⁹⁹ J. Heilman³⁵ S. Heim⁴⁸ T. Heim^{18a}
 J. J. Heinrich¹²⁵ L. Heinrich¹¹¹ J. Hejbal¹³³ M. Helbig⁵⁰ A. Held¹⁷⁵ S. Hellesund¹⁷ C. M. Helling¹⁶⁹
 S. Hellman^{47a,47b} A. M. Henriques Correia³⁷ H. Herde⁹⁹ Y. Hernández Jiménez¹⁵⁰ L. M. Herrmann²⁵
 T. Herrmann⁵⁰ G. Herten⁵⁴ R. Hertenberger¹¹⁰ L. Hervas³⁷ M. E. Hespings¹⁰¹ N. P. Hessey^{161a} J. Hessler¹¹¹
 M. Hidaoui^{36b} N. Hidic¹³⁵ E. Hill¹⁶⁰ T. S. Hillersoy¹⁷ S. J. Hillier²¹ J. R. Hinds¹⁰⁸ F. Hinterkeuser²⁵
 M. Hirose¹²⁶ S. Hirose¹⁶² D. Hirschbuehl¹⁷⁶ T. G. Hitchings¹⁰² B. Hiti⁹⁴ J. Hobbs¹⁵⁰ R. Hobincu^{28e}
 N. Hod¹⁷⁴ A. M. Hodges¹⁶⁷ M. C. Hodgkinson¹⁴⁴ B. H. Hodgkinson¹²⁸ A. Hoecker³⁷ D. D. Hofer¹⁰⁷
 J. Hofer¹⁶⁸ J. Hofner¹⁰¹ M. Holzbock³⁷ L. B. A. H. Hommels³³ V. Homsak¹²⁸ J. J. Hong⁶⁸ T. M. Hong¹³¹
 B. H. Hoerberman¹⁶⁷ W. H. Hopkins⁶ M. C. Hoppesch¹⁶⁷ Y. Horii¹¹² M. E. Horstmann¹¹¹ S. Hou¹⁵³
 M. R. Housenga¹⁶⁷ J. Howarth⁵⁹ J. Hoya⁶ M. Hrabovsky¹²⁴ T. Hryn'ova⁴ P. J. Hsu⁶⁵ S.-C. Hsu¹⁴¹
 T. Hsu⁶⁶ M. Hu^{18a} Q. Hu⁶² S. Huang³³ X. Huang^{113c,14} Y. Huang¹³⁵ Y. Huang^{113b} Y. Huang¹⁴
 Z. Huang⁶⁶ Z. Hubacek¹³⁴ F. Huegging²⁵ T. B. Huffman¹²⁸ M. Hufnagel Maranhã De Faria^{82a} C. A. Hugli⁴⁸
 M. Huhtinen³⁷ S. K. Huiberts¹²⁷ R. Hulsken¹⁰⁵ C. E. Hultquist^{18a} D. L. Humphreys¹⁰⁴ N. Huseynov¹²
 J. Huston¹⁰⁸ J. Huth⁶¹ L. Huth⁴⁸ R. Hyneman⁷ G. Iacobucci⁵⁶ G. Iakovidis³⁰ L. Iconomidou-Fayard⁶⁶
 J. P. Iddon³⁷ P. Iengo^{72a,72b} Y. Iiyama¹⁵⁸ T. Iizawa¹⁵⁸ Y. Ikegami⁸³ D. Iliadis¹⁵⁷ N. Ilic¹⁶⁰ H. Imam^{36a}
 G. Inacio Goncalves^{82d} S. A. Infante Cabanas^{139c} T. Ingebretsen Carlson^{47a,47b} J. M. Inglis⁹⁵ G. Introzzi^{73a,73b}
 M. Iodice^{77a} V. Ippolito^{75a,75b} R. K. Irwin⁹³ M. Ishino¹⁵⁸ W. Islam¹⁷⁵ C. Issever¹⁹ S. Istin^{22a,w}
 K. Itabashi¹²⁶ H. Ito¹⁷³ R. Iuppa^{78a,78b} A. Ivina¹⁷⁴ S. Izumiya¹¹² V. Izzo^{72a} P. Jacka¹³⁴ P. Jackson¹
 P. Jain⁴⁸ K. Jakobs⁵⁴ T. Jakoubek¹⁷⁴ J. Jamieson⁵⁹ W. Jang¹⁵⁸ S. Jankovych¹³⁵ M. Javurkova¹⁰⁴
 P. Jawahar¹⁰² L. Jeanty¹²⁵ J. Jejelava^{154a,x} P. Jenni^{54,y} C. E. Jessiman³⁵ C. Jia^{142a} H. Jia¹⁶⁹ J. Jia¹⁵⁰
 X. Jia^{111,113c} Z. Jia^{113a} C. Jiang⁵² Q. Jiang^{64b} S. Jiggins⁴⁸ M. Jimenez Ortega¹⁶⁸ J. Jimenez Pena¹³
 S. Jin^{113a} A. Jinaru^{28b} O. Jinnouchi¹⁴⁰ P. Johansson¹⁴⁴ K. A. Johns⁷ J. W. Johnson¹³⁸ F. A. Jolly⁴⁸
 D. M. Jones¹⁵¹ E. Jones⁴⁸ K. S. Jones⁸ P. Jones³³ R. W. L. Jones⁹² T. J. Jones⁹³ H. L. Joos⁵⁵ R. Joshi¹²¹
 J. Jovicevic¹⁶ X. Ju^{18a} J. J. Junggeburth³⁷ T. Junkermann^{63a} A. Juste Rozas^{13,u} M. K. Juzek⁸⁷ S. Kabana^{139f}
 A. Kaczmarska⁸⁷ S. A. Kadir¹⁴⁸ M. Kado¹¹¹ H. Kagan¹²¹ M. Kagan¹⁴⁸ A. Kahn¹³⁰ C. Kahra¹⁰¹ T. Kaji¹⁵⁸
 E. Kajomovitz¹⁵⁵ N. Kakati¹⁷⁴ N. Kakoty¹³ I. Kalaitzidou⁵⁴ S. Kandel⁸ N. Kanellos¹⁰ N. J. Kang¹³⁸
 D. Kar^{34e} E. Karentzos²⁵ K. Karki⁸ O. Karkout¹¹⁶ S. N. Karpov³⁹ Z. M. Karpova³⁹ V. Kartvelishvili^{154b,92}
 A. N. Karyukhin³⁸ E. Kasimi¹⁵⁷ J. Katzy⁴⁸ S. Kaur³⁵ K. Kawade¹⁴⁵ M. P. Kawale¹²² C. Kawamoto⁸⁸
 T. Kawamoto⁶² E. F. Kay³⁷ S. Kazakov¹⁰⁸ V. F. Kazanin³⁸ J. M. Keaveney^{34a} R. Keeler¹⁷⁰ G. V. Kehris⁶¹
 J. S. Keller³⁵ J. M. Kelly¹⁷⁰ J. J. Kempster¹⁵¹ O. Kepka¹³³ J. Kerr^{161b} B. P. Kerridge¹³⁶ B. P. Kerševan⁹⁴
 L. Keszezhova^{29a} R. A. Khan¹³¹ A. A. Khanov¹²³ A. G. Kharlamov³⁸ T. Kharlamova³⁸ E. E. Khoda¹⁴¹
 M. Kholodenko^{132a} T. J. Khoo¹⁹ G. Khorialuli¹⁷¹ Y. Khoulaki^{36a} Y. A. R. Khwaira¹²⁹ B. Kibirige^{34e} D. Kim⁶
 D. W. Kim^{18b} Y. K. Kim⁴⁰ N. Kimura⁹⁷ M. K. Kingston⁵⁵ A. Kirchhoff⁵⁵ C. Kirfel²⁵ F. Kirfel²⁵ J. Kirk¹³⁶
 A. E. Kiryunin¹¹¹ S. Kita¹⁶² O. Kivernyk²⁵ M. Klassen¹⁶³ C. Klein³⁵ L. Klein¹⁷¹ M. H. Klein⁴⁵
 S. B. Klein⁵⁶ U. Klein⁹³ A. Klimentov³⁰ T. Klioutchnikova³⁷ P. Kluit¹¹⁶ S. Kluth¹¹¹ E. Kneringer⁷⁹
 T. M. Knight¹⁶⁰ A. Knue⁴⁹ M. Kobel⁵⁰ D. Kobylanskii¹⁷⁴ S. F. Koch¹²⁸ M. Kocian¹⁴⁸ P. Kodyš¹³⁵
 D. M. Koeck¹²⁵ T. Koffas³⁵ O. Kolay⁵⁰ I. Koletsou⁴ T. Komarek⁸⁷ K. Köneke⁵⁵ A. X. Y. Kong¹
 T. Kono¹²⁰ N. Konstantinidis⁹⁷ P. Kontaxakis⁵⁶ B. Konya⁹⁹ R. Kopeliansky⁴² S. Koperny^{86a}
 R. Koppenhofer⁵⁴ K. Korcyl⁸⁷ K. Kordas^{157,z} A. Korn⁹⁷ S. Korn⁵⁵ I. Korolkov¹³ N. Korotkova³⁸
 B. Kortman¹¹⁶ O. Kortner¹¹¹ S. Kortner¹¹¹ W. H. Kostecka¹¹⁷ M. Kostov^{29a} V. V. Kostyukhin¹⁴⁶

- A. Kotsokechagia³⁷ A. Kotwal⁵¹ A. Koulouris³⁷ A. Kourkoumeli-Charalampidi^{73a,73b} C. Kourkoumelis⁹
 E. Kourlitis¹¹¹ O. Kovanda¹²⁵ R. Kowalewski¹⁷⁰ W. Kozanecki¹²⁵ A. S. Kozhin³⁸ V. A. Kramarenko³⁸
 G. Kramerberger⁹⁴ P. Kramer²⁵ M. W. Krasny¹²⁹ A. Krasznahorkay¹⁰⁴ A. C. Kraus¹¹⁷ J. W. Kraus¹⁷⁶
 J. A. Kremer⁴⁸ N. B. Kregel¹⁴⁶ T. Kresse⁵⁰ L. Kretschmann¹⁷⁶ J. Kretzschmar⁹³ P. Krieger¹⁶⁰ K. Krizka²¹
 K. Kroeninger⁴⁹ H. Kroha¹¹¹ J. Kroll¹³³ J. Kroll¹³⁰ K. S. Krowpman¹⁰⁸ U. Kruchonak³⁹ H. Krüger²⁵
 N. Krumnack⁸⁰ M. C. Kruse⁵¹ O. Kuchinskaia³⁹ S. Kuday^{3a} S. Kuehn³⁷ R. Kuesters⁵⁴ T. Kuhl⁴⁸
 V. Kukhtin³⁹ Y. Kulchitsky³⁹ S. Kuleshov^{139b,139d} J. Kull¹ E. V. Kumar¹¹⁰ M. Kumar^{34e} N. Kumari⁴⁸
 P. Kumari^{161b} A. Kupco¹³³ A. Kupich³⁸ O. Kuprash⁵⁴ H. Kurashige⁸⁵ L. L. Kurchaninov^{161a} O. Kurdysh⁴
 A. Kurova³⁸ M. Kuze¹⁴⁰ A. K. Kvam¹⁰⁴ J. Kvita¹²⁴ N. G. Kyriacou¹⁴¹ M. Laassiri³⁰ C. Lacasta¹⁶⁸
 F. Lacava^{75a,75b} H. Lacker¹⁹ D. Lacour¹²⁹ N. N. Lad⁹⁷ E. Ladygin³⁹ A. Lafarge⁴¹ B. Laforge¹²⁹
 T. Lagouri¹⁷⁷ F. Z. Lahbabi^{36a} S. Lai^{37,55} W. S. Lai⁹⁷ I. K. Lakomic⁵⁵ J. E. Lambert¹⁷⁰ S. Lammers⁶⁸
 W. Lampl⁷ C. Lampoudis^{157,z} G. Lamprinoudis¹⁷¹ A. N. Lancaster¹¹⁷ E. Lançon³⁰ U. Landgraf⁵⁴
 M. P. J. Landon⁹⁵ V. S. Lang⁵⁴ A. J. Lankford¹⁶⁴ F. Lanni³⁷ C. S. Lantz¹⁶⁷ K. Lantzsch²⁵ A. Lanza^{73a}
 M. Lanzac Berrocal¹⁶⁸ J. F. Laporte¹³⁷ T. Lari^{71a} D. Larsen¹⁷ L. Larson¹¹ F. Lasagni Manghi^{24b} M. Lassnig³⁷
 S. D. Lawlor¹⁴⁴ R. Lazaridou¹⁶⁴ M. Lazzaroni^{71a,71b} E. T. T. Le¹⁶⁴ H. D. M. Le¹⁰⁸ E. M. Le Boulicaut¹⁷⁷
 L. T. Le Pottier^{18a} B. Leban^{24a,24b} F. Ledroit-Guillon⁶⁰ T. F. Lee^{161b} L. L. Leeuw^{34c} M. Lefebvre¹⁷⁰
 C. Leggett^{18a} G. Lehmann Miotto³⁷ M. Leigh⁵⁶ W. A. Leight¹⁰⁴ W. Leinonen¹¹⁵ A. Leisos^{157,aa}
 M. A. L. Leite^{82c} C. E. Leitgeb¹⁹ R. Leitner¹³⁵ K. J. C. Leney⁴⁵ T. Lenz²⁵ S. Leone^{74a} C. Leonidopoulos⁵²
 A. Leopold¹⁴⁹ J. H. Lepage Bourbonnais³⁵ R. Les¹⁰⁸ C. G. Lester³³ M. Levchenko³⁸ J. Levêque⁴
 L. J. Levinson¹⁷⁴ G. Levrini^{24a,24b} M. P. Lewicki⁸⁷ C. Lewis¹⁴¹ D. J. Lewis⁴ L. Lewitt¹⁴⁴ A. Li³⁰ B. Li^{142a}
 C. Li¹⁰⁷ C-Q. Li¹¹¹ H. Li^{142a} H. Li¹⁰² H. Li¹⁵ H. Li⁶² H. Li^{142a} J. Li^{143a} K. Li¹⁴ L. Li^{143a} R. Li¹⁷⁷
 S. Li^{113c,14} S. Li^{143a,143b} T. Li⁵ X. Li¹⁰⁵ Y. Li¹⁴ Z. Li¹⁵⁸ Z. Li^{113c,14} Z. Li⁶² S. Liang^{113c,14} Z. Liang¹⁴
 M. Liberatore¹³⁷ B. Liberti^{76a} G. B. Libotte^{82d} K. Lie^{64c} J. Lieber Marin^{82e} H. Lien⁶⁸ H. Lin¹⁰⁷
 S. F. Lin¹⁵⁰ L. Linden¹¹⁰ R. E. Lindley⁷ J. H. Lindon³⁷ J. Ling⁶¹ E. Lipeles¹³⁰ A. Lipniacka¹⁷
 A. Lister¹⁶⁹ J. D. Little⁶⁸ B. Liu¹⁴ B. X. Liu^{113b} D. Liu¹⁵⁵ D. Liu¹³⁸ E. H. L. Liu²¹ J. K. K. Liu¹¹⁹
 K. Liu^{143b} K. Liu^{143a,143b} M. Liu⁶² M. Y. Liu⁶² P. Liu¹⁴ Q. Liu¹⁴⁸ S. Liu¹⁵⁰ X. Liu^{142a} Y. Liu^{113b,113c}
 Y. Liu¹⁶⁷ Y. L. Liu^{142a} Y. W. Liu⁶² Z. Liu^{66,ab} Z. Liu⁶² S. L. Lloyd⁹⁵ E. M. Lobodzinska⁴⁸ P. Loch⁷
 E. Lodhi¹⁶⁰ K. Lohwasser¹⁴⁴ E. Loiacono⁴⁸ J. D. Lomas²¹ J. D. Long⁴² I. Longarini¹⁶⁴ R. Longo¹⁶⁷
 A. Lopez Solis¹³ N. A. Lopez-canelas⁷ N. Lorenzo Martinez⁴ A. M. Lory¹¹⁰ M. Losada^{118a}
 G. Lösckche Centeno⁴ X. Lou^{47a,47b} X. Lou^{113c,14} A. Lounis⁶⁶ P. A. Love⁹² M. Lu⁶⁶ S. Lu¹³⁰ Y. J. Lu¹⁵³
 H. J. Lubatti¹⁴¹ C. Luci^{75a,75b} F. L. Lucio Alves^{113a} F. Luehring⁶⁸ B. S. Lunday¹³⁰ O. Lundberg¹⁴⁹ J. Lunde³⁷
 N. A. Luongo⁶ M. S. Lutz³⁷ A. B. Lux²⁶ D. Lynn³⁰ R. Lysak¹³³ V. Lysenko¹³⁴ E. Lytken⁹⁹
 V. Lyubushkin³⁹ T. Lyubushkina³⁹ M. M. Lyukova¹⁵⁰ H. Ma³⁰ K. Ma⁶² L. L. Ma^{142a} W. Ma⁶² Y. Ma¹²³
 J. C. MacDonald¹⁰¹ P. C. Machado De Abreu Farias^{82c} D. Macina³⁷ R. Madar⁴¹ T. Madula⁹⁷ J. Maeda⁸⁵
 T. Maeno³⁰ P. T. Mafa^{34c,ac} H. Maguire¹⁴⁴ M. Maheshwari³³ V. Maiboroda⁶⁶ A. Maio^{132a,132b,132d} K. Maj^{86a}
 O. Majersky⁴⁸ S. Majewski¹²⁵ R. Makhmanazarov³⁸ N. Makovec⁶⁶ V. Maksimovic¹⁶ B. Malaescu¹²⁹
 J. Malamant¹²⁷ Pa. Malecki⁸⁷ V. P. Maleev³⁸ F. Malek^{60,ad} M. Mali⁹⁴ D. Malito⁹⁶ A. Maloizel⁵ S. Maltezos¹⁰
 A. Malvezzi Lopes^{82d} S. Malyukov³⁹ J. Mamuzic⁹⁴ G. Mancini⁵³ M. N. Mancini²⁷ G. Manco^{73a,73b}
 J. P. Mandalia⁹⁵ S. S. Mandarriy¹⁵¹ I. Mandić⁹⁴ L. Manhaes de Andrade Filho^{82a} I. M. Maniatis¹⁷⁴
 J. Manjarres Ramos⁹⁰ D. C. Mankad¹⁷⁴ A. Mann¹¹⁰ T. Manoussos³⁷ M. N. Mantinan⁴⁰ S. Manzoni³⁷
 L. Mao^{143a} X. Mapekula^{34c} A. Marantis¹⁵⁷ R. R. Marcelo Gregorio⁹⁵ G. Marchiori⁵ C. Marcon^{71a}
 E. Maricic¹⁶ M. Marinescu⁴⁸ S. Marium⁴⁸ M. Marjanovic¹²² A. Markhoos⁵⁴ M. Markovitch⁶⁶
 M. K. Maroun¹⁰⁴ M. C. Marr¹⁴⁷ G. T. Marsden¹⁰² E. J. Marshall⁹² Z. Marshall^{18a} S. Marti-Garcia¹⁶⁸
 J. Martin⁹⁷ T. A. Martin¹³⁶ V. J. Martin⁵² B. Martin dit Latour¹⁷ L. Martinelli^{75a,75b} M. Martinez^{13,u}
 P. Martinez Agullo¹⁶⁸ V. I. Martinez Outschoorn¹⁰⁴ P. Martinez Suarez³⁷ S. Martin-Haugh¹³⁶ G. Martinovicova¹³⁵
 V. S. Martoiu^{28b} A. C. Martyniuk⁹⁷ A. Marzin³⁷ D. Mascione^{78a,78b} L. Masetti¹⁰¹ J. Masik¹⁰²
 A. L. Maslennikov³⁹ S. L. Mason⁴² P. Massarotti^{72a,72b} P. Mastrandrea^{74a,74b} A. Mastroberardino^{44a,44b}
 T. Masubuchi¹²⁶ T. T. Mathew¹²⁵ J. Matousek¹³⁵ D. M. Mattern⁴⁹ K. Mauer⁴⁸ J. Maurer^{28b} T. Maurin⁵⁹
 A. J. Maury⁶⁶ B. Maček⁹⁴ C. Mavungu Tsava¹⁰³ D. A. Maximov³⁸ A. E. May¹⁰² E. Mayer⁴¹ R. Mazini^{34e}
 I. Maznas¹¹⁷ S. M. Mazza¹³⁸ E. Mazzeo³⁷ J. P. Mc Gowan¹⁷⁰ S. P. Mc Kee¹⁰⁷ C. A. Mc Lean⁶
 C. C. McCracken¹⁶⁹ E. F. McDonald¹⁰⁶ A. E. McDougall¹¹⁶ L. F. Mcelhinney⁹² J. A. Mcfayden¹⁵¹
 R. P. McGovern¹³⁰ R. P. Mckenzie^{34e} T. C. Mclachlan⁴⁸ D. J. McLaughlin⁹⁷ S. J. McMahon¹³⁶
 C. M. Mcpartland⁹³ R. A. McPherson^{170,n} S. Mehlhase¹¹⁰ A. Mehta⁹³ D. Melini¹⁶⁸ B. R. Mellado Garcia^{34e}
 A. H. Melo⁵⁵ F. Meloni⁴⁸ A. M. Mendes Jacques Da Costa¹⁰² L. Meng⁹² S. Menke¹¹¹ M. Mentink³⁷
 E. Meoni^{44a,44b} G. Mercado¹¹⁷ S. Merianos¹⁵⁷ C. Merlassino^{69a,69c} C. Meroni^{71a,71b} J. Metcalfe⁶ A. S. Mete⁶
 E. Meuser¹⁰¹ C. Meyer⁶⁸ J-P. Meyer¹³⁷ Y. Miao^{113a} R. P. Middleton¹³⁶ M. Mihovilovic⁶⁶ L. Mijović⁵²
 G. Mikenberg¹⁷⁴ M. Mikestikova¹³³ M. Mikuž⁹⁴ H. Mildner¹⁰¹ A. Milic³⁷ D. W. Miller⁴⁰ E. H. Miller¹⁴⁸
 A. Milov¹⁷⁴ D. A. Milstead^{47a,47b} T. Min^{113a} A. A. Minaenko³⁸ I. A. Minashvili^{154b} A. I. Mincer¹¹⁹ B. Mindur^{86a}

- M. Mineev³⁹, Y. Mino⁸⁸, L. M. Mir¹³, M. Miralles Lopez⁵⁹, M. Mironova^{18a}, M. Missio⁴¹, A. Mitra¹⁷², V. A. Mitsou¹⁶⁸, Y. Mitsumori¹¹², O. Miu¹⁶⁰, P. S. Miyagawa⁹⁵, T. Mkrtychyan³⁷, M. Mlinarevic⁹⁷, T. Mlinarevic⁹⁷, M. Mlynarikova¹³⁵, L. Mlynarska^{86a}, C. Mo^{143a}, S. Mobius²⁰, M. H. Mohamed Farook¹¹⁴, S. Mohapatra⁴², M. F. Mohd Sober⁵², S. Mohiuddin¹²³, G. Mokgatitswane^{34e}, L. Moleri¹⁷⁴, U. Molinatti¹²⁸, L. G. Mollier²⁰, B. Mondal¹³³, S. Mondal¹³⁴, K. Mönig⁴⁸, E. Monnier¹⁰³, L. Monsonis Romero¹⁶⁸, J. Montejo Berlingen¹³, A. Montella^{47a,47b}, M. Montella¹²¹, F. Montekali^{77a,77b}, F. Monticelli⁹¹, S. Monzani^{69a,69c}, A. Morancho Tarda⁴³, N. Morange⁶⁶, A. L. Moreira De Carvalho⁴⁸, M. Moreno Llácer¹⁶⁸, C. Moreno Martinez⁵⁶, J. M. Moreno Perez^{23b}, P. Morettini^{57b}, S. Morgenstern³⁷, M. Morii⁶¹, M. Morinaga¹⁵⁸, M. Moritsu⁸⁹, F. Morodei^{75a,75b}, P. Moschovakos³⁷, B. Moser⁵⁴, M. Mosidze^{154b}, T. Moskalets⁴⁵, P. Moskvitina¹¹⁵, J. Moss³², P. Moszkowicz^{86a}, T. Motta Quirino^{82d}, A. Moussa^{36d}, Y. Moyal¹⁷⁴, H. Moyano Gomez¹³, E. J. W. Moyse¹⁰⁴, L. J. Mozarsky⁴², T. G. Mroz⁸⁷, S. Muanza¹⁰³, M. Mucha²⁵, J. Mueller¹³¹, R. Müller³⁷, G. A. Mullier¹⁶⁶, A. J. Mullin³³, J. J. Mullin⁵¹, A. C. Mullins⁴⁵, A. E. Mulski⁶¹, D. P. Mungo¹⁶⁰, D. Munoz Perez¹⁶⁸, F. J. Munoz Sanchez¹⁰², W. J. Murray^{136,172}, M. Muškinja⁹⁴, C. Mwewa⁴⁸, A. G. Myagkov^{38,j}, A. J. Myers⁸, G. Myers¹⁰⁷, M. Myska¹³⁴, B. P. Nachman¹⁴⁸, K. Nagai¹²⁸, K. Nagano⁸³, R. Nagasaka¹⁵⁸, J. L. Nagle^{30,ae}, E. Nagy¹⁰³, A. M. Nairz³⁷, Y. Nakahama⁸³, K. Nakamura⁸³, K. Nakkalil⁵, A. Nandi^{63b}, H. Nanjo¹²⁶, E. A. Narayanan⁴⁵, Y. Narukawa¹⁵⁸, I. Naryshkin³⁸, L. Nasella^{71a,71b}, S. Nasri^{118b}, C. Nass²⁵, G. Navarro^{23a}, A. Nayaz¹⁹, P. Y. Nechaeva³⁸, S. Nechaeva^{24a,24b}, F. Nechansky¹³³, L. Nedic¹²⁸, T. J. Neep²¹, A. Negri^{73a,73b}, M. Negrini^{24b}, C. Nellist¹¹⁶, C. Nelson¹⁰⁵, K. Nelson¹⁰⁷, S. Nemecek¹³³, M. Nessi^{37,af}, M. S. Neubauer¹⁶⁷, J. Newell⁹³, P. R. Newman²¹, Y. W. Y. Ng¹⁶⁷, B. Ngair^{118a}, H. D. N. Nguyen¹⁰⁹, J. D. Nichols¹²², R. B. Nickerson¹²⁸, R. Nicolaidou¹³⁷, J. Nielsen¹³⁸, M. Niemeyer⁵⁵, J. Niermann³⁷, N. Nikiforou³⁷, V. Nikolaenko^{38,j}, I. Nikolic-Audit¹²⁹, P. Nilsson³⁰, I. Ninca⁴⁸, G. Ninio¹⁵⁶, A. Nisati^{75a}, R. Nisius¹¹¹, N. Nitika¹⁷⁴, E. K. Nkadameng^{34b}, T. Nobe¹⁵⁸, D. Noll¹⁴⁸, T. Nommensen¹⁵², M. B. Norfolk¹⁴⁴, B. J. Norman³⁵, L. C. Nosler^{18a}, M. Noury^{36a}, J. Novak⁹⁴, T. Novak⁹⁴, R. Novotny¹³⁴, L. Nozka¹²⁴, K. Ntekas¹⁶⁴, D. Ntounis¹⁴⁸, N. M. J. Nunes De Moura Junior^{82b}, J. Ocariz¹²⁹, I. Ochoa^{132a}, A. Odella Rodriguez¹³, S. Oerdek^{48,ag}, J. T. Offermann⁴⁰, A. Ogrodnik⁸⁷, A. Oh¹⁰², C. C. Ohm¹⁴⁹, H. Oide⁸³, M. L. Ojeda³⁷, Y. Okumura¹⁵⁸, L. F. Oleiro Seabra^{132a}, I. Oleksiyuk⁵⁶, G. Oliveira Correa¹³, D. Oliveira Damazio³⁰, J. L. Oliver¹, R. Omar⁶⁸, Ö. O. Öncel⁵⁴, A. P. O'Neill²⁰, A. Onofre^{132a,132e,ah}, P. U. E. Onyisi¹¹, M. J. Oreglia⁴⁰, D. Orestano^{77a,77b}, R. Orlandini^{77a,77b}, R. S. Orr¹⁶⁰, L. M. Osojnak⁴², Y. Osumi¹¹², G. Otero y Garzon³¹, H. Otono⁸⁹, M. Ouchrif^{36d}, F. Ould-Saada¹²⁷, T. Ovsianikova¹⁴¹, M. Owen⁵⁹, R. E. Owen¹³⁶, V. E. Ozcan^{22a}, F. Ozturk⁸⁷, N. Ozturk⁸, S. Ozturk⁸¹, H. A. Pacey¹²⁸, K. Pachal^{161a}, A. Pacheco Pages¹³, C. Padilla Aranda¹³, G. Padovano^{75a,75b}, S. Pagan Griso^{18a}, J. Pampel²⁵, J. Pan¹⁷⁷, D. K. Panchal¹¹, C. E. Pandini⁶⁰, J. G. Panduro Vazquez¹³⁶, H. D. Pandya¹, H. Pang¹³⁷, P. Pani⁴⁸, G. Panizzo^{69a,69c}, L. Panwar¹²⁹, L. Paolozzi⁵⁶, S. Parajuli¹⁶⁷, A. Paramonov⁶, C. Paraskevopoulos⁵³, D. Paredes Hernandez^{64b}, S. R. Paredes Saenz⁵², A. Pareti^{73a,73b}, K. R. Park⁴², T. H. Park¹¹¹, F. Parodi^{57a,57b}, J. A. Parsons⁴², U. Parzefall⁵⁴, B. Pascual Dias⁴¹, L. Pascual Dominguez¹⁰⁰, E. Pasqualucci^{75a}, S. Passaggio^{57b}, F. Pastore⁹⁶, P. Patel⁸⁷, U. M. Patel⁵¹, J. R. Pater¹⁰², T. Pauly³⁷, F. Pauwels¹³⁵, C. I. Pazos¹⁶³, M. Pedersen¹²⁷, R. Pedro^{132a}, S. V. Peleganchuk³⁸, O. Penc¹³³, S. Peng¹⁵, G. D. Penn¹⁷⁷, K. E. Pensi¹¹⁰, M. Penzin³⁸, B. S. Peralva^{82d}, A. P. Pereira Peixoto¹⁴¹, L. Pereira Sanchez¹⁴⁸, D. V. Perepelitsa^{30,ae}, G. Perera¹⁰⁴, E. Perez Codina³⁷, M. Perganti¹⁰, H. Pernegger³⁷, S. Perrella^{75a,75b}, K. Peters⁴⁸, R. F. Y. Peters¹⁰², B. A. Petersen³⁷, T. C. Petersen⁴³, E. Petit¹⁰³, V. Petousis¹³⁴, A. R. Petri^{71a,71b}, C. Petridou^{157,z}, T. Petru¹³⁵, M. Pettee^{18a}, A. Petukhov⁸¹, K. Petukhova³⁷, R. Pezoa^{139g}, L. Pezzotti^{24a,24b}, G. Pezzullo¹⁷⁷, L. Pfaffenbichler³⁷, A. J. Pflieger⁷⁹, T. M. Pham¹⁷⁵, T. Pham¹⁰⁶, P. W. Phillips¹³⁶, G. Piacquadio¹⁵⁰, E. Pianori^{18a}, F. Piazza¹²⁵, R. Piegaia³¹, D. Pietreanu^{28b}, A. D. Pilkington¹⁰², M. Pinamonti^{69a,69c}, J. L. Pinfold², G. Pinheiro Matos⁴², B. C. Pinheiro Pereira^{132a}, J. Pinol Bel¹³, A. E. Pinto Pinoargote¹²⁹, L. Pintucci^{69a,69c}, K. M. Piper¹⁵¹, A. Pirttikoski⁵⁶, D. A. Pizzi³⁵, L. Pizzimento^{64b}, A. Plebani³³, M.-A. Pleier³⁰, V. Pleskot¹³⁵, E. Plotnikova³⁹, G. Poddar⁹⁵, R. Poettgen⁹⁹, L. Poggioli¹²⁹, S. Polacek¹³⁵, G. Polesello^{73a}, A. Poley¹⁴⁷, A. Polini^{24b}, C. S. Pollard¹⁷², Z. B. Pollock¹²¹, E. Pompa Pacchi¹²², N. I. Pond⁹⁷, D. Ponomarenko⁶⁸, L. Pontecorvo³⁷, S. Popa^{28a}, G. A. Popeneciu^{28d}, A. Poreba³⁷, D. M. Portillo Quintero^{161a}, S. Pospisil¹³⁴, M. A. Postill¹⁴⁴, P. Postolache^{28c}, K. Potamianos¹⁷², P. A. Potepa^{86a}, I. N. Potrap³⁹, C. J. Potter³³, H. Potti¹⁵², J. Poveda¹⁶⁸, M. E. Pozo Astigarraga³⁷, R. Pozzi³⁷, A. Prades Ibanez^{76a,76b}, S. R. Pradhan¹⁴⁴, J. Pretel¹⁷⁰, D. Price¹⁰², M. Primavera^{70a}, L. Primomo^{69a,69c}, M. A. Principe Martin¹⁰⁰, R. Privara¹²⁴, T. Procter^{86b}, M. L. Proffitt¹⁴¹, N. Proklova¹³⁰, K. Prokofiev^{64c}, G. Proto¹¹¹, J. Proudfoot⁶, M. Przybycien^{86a}, W. W. Przygoda^{86b}, A. Psallidas⁴⁶, J. E. Pudefoot¹⁴⁴, D. Pudzha⁵³, H. I. Purnell¹, D. Pyatizbyantseva¹¹⁵, J. Qian¹⁰⁷, R. Qian¹⁰⁸, D. Qichen¹²⁸, Y. Qin¹³, T. Qiu⁵², A. Quadt⁵⁵, M. Queitsch-Maitland¹⁰², G. Quetant⁵⁶, R. P. Quinn¹⁶⁹, G. Rabanal Bolanos⁶¹, D. Rafanoharana¹¹¹, F. Raffaelli^{76a,76b}, F. Ragusa^{71a,71b}, J. L. Rainbolt⁴⁰, S. Rajagopalan³⁰, E. Ramakoti³⁹, L. Rambelli^{57a,57b}, I. A. Ramirez-Berend³⁵, K. Ran^{107,113c}, D. S. Rankin¹³⁰, N. P. Rapheeha^{34e}, H. Rasheed^{28b}, A. Rastogi^{18a}, S. Rave¹⁰¹, S. Ravera^{57a,57b}, B. Ravina³⁷, I. Ravinovich¹⁷⁴, M. Raymond³⁷, A. L. Read¹²⁷, N. P. Readioff¹⁴⁴, D. M. Rebuffi^{73a,73b}, A. S. Reed⁵⁹, K. Reeves²⁷, D. Reikher³⁷, A. Rej⁴⁹, C. Rembser³⁷, H. Ren⁶², M. Renda^{28b}

F. Renner ⁴⁸, A. G. Rennie ⁵⁹, M. Repik ⁵⁶, A. L. Rescia ^{57a,57b}, S. Resconi ^{71a}, M. Ressegotti ^{57a,57b}, S. Rettie ¹¹⁶, W. F. Rettie ³⁵, M. M. Revering ³³, E. Reynolds ^{18a}, O. L. Rezanova ³⁹, P. Reznicek ¹³⁵, H. Riani ^{36d}, N. Ribaric ⁵¹, B. Ricci ^{69a,69c}, E. Ricci ^{78a,78b}, R. Richter ¹¹¹, S. Richter ^{47a,47b}, E. Richter-Was ^{86b}, M. Ridel ¹²⁹, S. Ridouani ^{36d}, P. Rieck ¹¹⁹, P. Riedler ³⁷, E. M. Riefel ^{47a,47b}, J. O. Rieger ¹¹⁶, M. Rijssenbeek ¹⁵⁰, M. Rimoldi ^{34c}, L. Rinaldi ^{24a,24b}, P. Rincke ^{166,55}, G. Ripellino ¹⁶⁶, I. Riu ¹³, J. C. Rivera Vergara ¹⁷⁰, F. Rizatdinova ¹²³, E. Rizvi ⁹⁵, B. R. Roberts ⁴⁰, S. S. Roberts ¹³⁸, D. Robinson ³³, A. Robson ⁵⁹, A. Rocchi ^{76a,76b}, C. Roda ^{74a,74b}, F. A. Rodriguez ¹¹⁷, S. Rodriguez Bosca ³⁷, Y. Rodriguez Garcia ^{23a}, A. M. Rodríguez Vera ¹¹⁷, S. Roe ³⁷, J. T. Roemer ³⁷, O. Røhne ¹²⁷, R. A. Rojas ³⁷, C. P. A. Roland ¹²⁹, A. Romaniouk ⁷⁹, E. Romano ^{73a,73b}, M. Romano ^{24b}, A. C. Romero Hernandez ¹⁶⁷, N. Rompotis ⁹³, L. Roos ¹²⁹, S. Rosati ^{75a}, B. J. Rosser ⁴⁰, E. Rossi ¹²⁸, E. Rossi ^{72a,72b}, L. P. Rossi ⁶¹, L. Rossini ⁵⁴, R. Rosten ¹²¹, M. Rotaru ^{28b}, D. Rousseau ⁶⁶, D. Rousso ⁴⁸, S. Roy-Garand ¹⁶⁰, A. Rozanov ¹⁰³, Z. M. A. Rozario ⁵⁹, Y. Rozen ¹⁵⁵, A. Rubio Jimenez ¹⁶⁸, V. H. Ruelas Rivera ¹⁹, T. A. Ruggeri ¹, A. Ruggiero ¹²⁸, A. Ruiz-Martinez ¹⁶⁸, A. Rummler ³⁷, G. B. Rupnik Boero ³⁷, Z. Rurikova ⁵⁴, N. A. Rusakovich ³⁹, S. Ruscelli ⁴⁹, H. L. Russell ¹⁷⁰, G. Russo ^{75a,75b}, J. P. Rutherford ⁷, S. Rutherford Colmenares ³³, M. Rybar ¹³⁵, P. Rybczynski ^{86a}, A. Ryzhov ⁴⁵, H.F.-W. Sadrozinski ¹³⁸, F. Safai Tehrani ^{75a}, S. Saha ¹, M. Sahinsoy ⁸¹, B. Sahoo ¹⁷⁴, A. Saibel ¹⁶⁸, B. T. Saifuddin ¹²², M. Saimpert ¹³⁷, G. T. Saito ^{82c}, M. Saito ¹⁵⁸, T. Saito ¹⁵⁸, A. Sala ^{71a,71b}, A. Salnikov ¹⁴⁸, J. Salt ¹⁶⁸, A. Salvador Salas ¹⁵⁶, F. Salvatore ¹⁵¹, A. Salzburger ³⁷, D. Sammel ⁵⁴, E. Sampson ⁹², D. Sampsonidis ^{157,z}, D. Sampsonidou ¹²⁵, M. A. A. Samy ⁵⁹, J. Sánchez ¹⁶⁸, V. Sanchez Sebastian ¹⁶⁸, H. Sandaker ¹²⁷, C. O. Sander ⁴⁸, J. A. Sandesara ¹⁷⁵, M. Sandhoff ¹⁷⁶, C. Sandoval ^{23b}, L. Sanfilippo ^{63a}, D. P. C. Sankey ¹³⁶, T. Sano ⁸⁸, A. Sansoni ⁵³, M. Santana Queiroz ^{18b}, L. Santi ³⁷, C. Santoni ⁴¹, H. Santos ^{132a,132b}, A. Santra ¹⁷⁴, E. Sanzani ^{24a,24b}, K. A. Saoucha ^{84b}, J. G. Saraiva ^{132a,132d}, J. Sardain ⁷, O. Sasaki ⁸³, K. Sato ¹⁶², C. Sauer ³⁷, E. Sauvan ⁴, P. Savard ^{160,t}, R. Sawada ¹⁵⁸, C. Sawyer ¹³⁶, L. Sawyer ⁹⁸, A. M. Sayed ²⁷, C. Sbarra ^{24b}, A. Sbrizzi ^{24a,24b}, T. Scanlon ⁹⁷, J. Schaarschmidt ¹⁴¹, U. Schäfer ¹⁰¹, A. C. Schaffer ^{45,66}, D. Schaile ¹¹⁰, R. D. Schamberger ¹⁵⁰, C. Scharf ¹⁹, M. M. Schefer ²⁰, V. A. Schegelsky ³⁸, D. Scheirich ¹³⁵, M. Schernau ^{139f}, C. Scheulen ⁵⁶, C. Schiavi ^{57a,57b}, M. Schioppa ^{44a,44b}, B. Schlag ¹⁴⁸, S. Schlenker ³⁷, J. Schmeing ¹⁷⁶, E. Schmidt ¹¹¹, M. A. Schmidt ¹⁷⁶, K. Schmieden ²⁵, C. Schmitt ¹⁰¹, N. Schmitt ¹⁰¹, S. Schmitt ⁴⁸, N. A. Schneider ¹¹⁰, L. Schoeffel ¹³⁷, A. Schoening ^{63b}, P. G. Scholer ³⁵, E. Schopf ¹⁴⁶, M. Schott ²⁵, S. Schramm ⁵⁶, T. Schroer ⁵⁶, H.-C. Schultz-Coulon ^{63a}, M. Schumacher ⁵⁴, B. A. Schumm ¹³⁸, Ph. Schune ¹³⁷, H. R. Schwartz ⁷, A. Schwartzman ¹⁴⁸, T. A. Schwarz ¹⁰⁷, Ph. Schwemling ¹³⁷, R. Schwienhorst ¹⁰⁸, F. G. Sciacca ²⁰, A. Sciandra ³⁰, G. Sciolla ²⁷, F. Scuri ^{74a}, C. D. Sebastiani ³⁷, K. Sedlaczek ¹¹⁷, S. C. Seidel ¹¹⁴, A. Seiden ¹³⁸, B. D. Seidlitz ⁴², C. Seitz ⁴⁸, J. M. Seixas ^{82b}, G. Sekhniaidze ^{72a}, L. Selem ⁶⁰, N. Semprini-Cesari ^{24a,24b}, A. Semushin ¹⁷⁸, D. Sengupta ⁵⁶, V. Senthilkumar ¹⁶⁸, L. Serin ⁶⁶, M. Sessa ^{72a,72b}, H. Severini ¹²², F. Sforza ^{57a,57b}, A. Sfyrla ⁵⁶, Q. Sha ¹⁴, H. Shaddix ¹¹⁷, A. H. Shah ³³, R. Shaheen ¹⁴⁹, J. D. Shahinian ¹³⁰, M. Shamim ³⁷, L. Y. Shan ¹⁴, M. Shapiro ^{18a}, A. Sharma ³⁷, A. S. Sharma ¹⁶⁹, P. Sharma ³⁰, P. B. Shatalov ³⁸, K. Shaw ¹⁵¹, S. M. Shaw ¹⁰², Q. Shen ¹⁴, D. J. Sheppard ¹⁴⁷, P. Sherwood ⁹⁷, L. Shi ⁹⁷, X. Shi ¹⁴, S. Shimizu ⁸³, I. P. J. Shipsey ^{128,p}, S. Shirabe ⁸⁹, M. Shiyakova ^{39,ai}, M. J. Shochet ⁴⁰, D. R. Shope ¹²⁷, B. Shrestha ¹²², S. Shrestha ^{121,aj}, I. Shreyber ³⁹, M. J. Shroff ¹⁷⁰, P. Sicho ¹³³, A. M. Sickles ¹⁶⁷, E. Sideras Haddad ^{165,34e}, A. C. Sidley ¹¹⁶, A. Sidoti ^{24b}, F. Siegert ⁵⁰, Dj. Sijacki ¹⁶, F. Sili ⁶², J. M. Silva ⁵², I. Silva Ferreira ^{82b}, M. V. Silva Oliveira ³⁰, S. B. Silverstein ^{47a}, S. Simion ⁶⁶, R. Simoniello ³⁷, E. L. Simpson ¹⁰², H. Simpson ¹⁵¹, L. R. Simpson ⁶, S. Simsek ⁸¹, S. Sindhu ⁵⁵, P. Sinervo ¹⁶⁰, S. N. Singh ²⁷, S. Singh ³⁰, S. Sinha ⁴⁸, S. Sinha ¹⁰², M. Sioli ^{24a,24b}, K. Sioulas ⁹, I. Siral ³⁷, E. Sitnikova ⁴⁸, J. Sjölin ^{47a,47b}, A. Skaf ⁵⁵, E. Skorda ²¹, P. Skubic ¹²², M. Slawinska ⁸⁷, I. Slazyk ¹⁷, I. Sliuser ¹²⁷, V. Smakhtin ¹⁷⁴, B. H. Smart ¹³⁶, S. Yu. Smirnov ^{139b}, Y. Smirnov ⁸¹, L. N. Smirnova ^{38,j}, O. Smirnova ⁹⁹, A. C. Smith ⁴², D. R. Smith ¹⁶⁴, J. L. Smith ¹⁰², M. B. Smith ³⁵, R. Smith ¹⁴⁸, H. Smitmans ¹⁰¹, M. Smizanska ⁹², K. Smolek ¹³⁴, P. Smolyanskiy ¹³⁴, A. A. Snesarev ³⁹, H. L. Snoek ¹¹⁶, R. M. Snyder ⁵¹, S. Snyder ³⁰, R. Sobie ^{170,n}, A. Soffer ¹⁵⁶, C. A. Solans Sanchez ³⁷, E. Yu. Soldatov ³⁹, U. Soldevila ¹⁶⁸, A. A. Solodkov ^{34e}, S. Solomon ²⁷, A. Soloshenko ³⁹, K. Solovieva ⁵⁴, O. V. Solovyanov ⁴¹, P. Sommer ⁵⁰, A. Sonay ¹³, A. Sopczak ¹³⁴, A. L. Sapiro ⁵², F. Sopkova ^{29b}, J. D. Sorenson ¹¹⁴, I. R. Sotarriva Alvarez ¹⁴⁰, V. Sothilingam ^{63a}, O. J. Soto Sandoval ^{139b,139c}, S. Sottocornola ⁶⁸, R. Soualah ^{84a}, Z. Soumami ^{36e}, D. South ⁴⁸, N. Soybelman ¹⁷⁴, S. Spagnolo ^{70a,70b}, D. Sperlich ⁵⁴, B. Spisso ^{72a,72b}, D. P. Spiteri ⁵⁹, L. Splendori ¹⁰³, M. Spousta ¹³⁵, E. J. Staats ³⁵, R. Stamen ^{63a}, E. Stanecka ⁸⁷, W. Stanek-Maslouska ⁴⁸, M. V. Stange ⁵⁰, B. Stanislaus ^{18a}, M. M. Stanitzki ⁴⁸, E. A. Starchenko ³⁸, G. H. Stark ¹³⁸, J. Stark ⁹⁰, P. Staroba ¹³³, P. Starovoitov ^{84b}, R. Staszewski ⁸⁷, C. Stauch ¹¹⁰, G. Stavropoulos ⁴⁶, A. Stefl ³⁷, A. Stein ¹⁰¹, P. Steinberg ³⁰, B. Stelzer ^{147,161a}, H. J. Stelzer ¹³¹, O. Stelzer ^{161a}, H. Stenzel ⁵⁸, T. J. Stevenson ¹⁵¹, G. A. Stewart ³⁷, J. R. Stewart ¹²³, G. Stoica ^{28b}, M. Stolarski ^{132a}, S. Stonjek ¹¹¹, A. Straessner ⁵⁰, J. Strandberg ¹⁴⁹, S. Strandberg ^{47a,47b}, M. Stratmann ¹⁷⁶, M. Strauss ¹²², T. Streblor ¹⁰³, P. Strizenec ^{29b}, R. Ströhmer ¹⁷¹, D. M. Strom ¹²⁵, R. Stroynowski ⁴⁵, A. Strubig ^{47a,47b}, S. A. Stucci ³⁰, B. Stugu ¹⁷, J. Stupak ¹²², N. A. Styles ⁴⁸, D. Su ¹⁴⁸, S. Su ⁶², X. Su ⁶², D. Suchy ^{29a}, A. D. Sudhakar Ponnu ⁵⁵, K. Sugizaki ¹³⁰, V. V. Sulim ³⁸, D. M. S. Sultan ¹²⁸, L. Sultanaliyeva ²⁵, S. Sultansoy ^{3b}, S. Sun ¹⁷⁵, W. Sun ¹⁴, N. Sur ⁹⁹, M. R. Sutton ¹⁵¹, M. Svatos ¹³³, P. N. Swallow ³³, M. Swiatlowski ^{161a}, A. Swoboda ³⁷, I. Sykora ^{29a}, M. Sykora ¹³⁵, T. Sykora ¹³⁵, D. Ta ¹⁰¹, K. Tackmann ^{48,ag}, A. Taffard ¹⁶⁴, R. Tafirout ^{161a}, Y. Takubo ⁸³, M. Talby ¹⁰³, A. A. Talyshv ³⁸

- K. C. Tam^{64b}, N. M. Tamir¹⁵⁶, A. Tanaka¹⁵⁸, J. Tanaka¹⁵⁸, R. Tanaka⁶⁶, M. Tanasini¹⁵⁰, Z. Tao¹⁶⁹, S. Tapia Araya^{139g}, S. Tapprogge¹⁰¹, A. Tarek Abouelfadl Mohamed³⁷, S. Tarem¹⁵⁵, K. Tariq¹⁴, G. Tarna³⁷, G. F. Tartarelli^{71a}, M. J. Tartarin⁹⁰, P. Tas¹³⁵, M. Tasevsky¹³³, E. Tassi^{44a,44b}, A. C. Tate¹⁶⁷, Y. Tayalati^{36e,ak}, G. N. Taylor¹⁰⁶, W. Taylor^{161b}, R. J. Taylor Vara¹⁶⁸, A. S. Tegetmeier⁹⁰, P. Teixeira-Dias⁹⁶, J. J. Teoh¹⁶⁰, K. Terashi¹⁵⁸, J. Terron¹⁰⁰, S. Terzo¹³, M. Testa⁵³, R. J. Teuscher^{160,n}, A. Thaler⁷⁹, O. Theiner⁵⁶, T. Thevenaux-Pelzer¹⁰³, D. W. Thomas⁹⁶, J. P. Thomas²¹, E. A. Thompson^{18a}, P. D. Thompson²¹, E. Thomson¹³⁰, R. E. Thornberry⁴⁵, C. Tian⁶², Y. Tian⁵⁶, V. Tikhomirov⁸¹, Yu. A. Tikhonov³⁹, S. Timoshenko³⁸, D. Timoshyn¹³⁵, E. X. L. Ting¹, P. Tipton¹⁷⁷, A. Tishelman-Charny³⁰, K. Todome¹⁴⁰, S. Todorova-Nova¹³⁵, L. Toffolin^{69a,69c}, M. Togawa⁸³, J. Tojo⁸⁹, S. Tokár^{29a}, O. Toldaiev⁶⁸, G. Tolkachev¹⁰³, M. Tomoto⁸³, L. Tompkins^{148,al}, E. Torrence¹²⁵, H. Torres⁹⁰, D. I. Torres Arza^{139g}, E. Torró Pastor¹⁶⁸, M. Toscani³¹, C. Toscirci⁴⁰, M. Tost¹¹, D. R. Tovey¹⁴⁴, T. Trefzger¹⁷¹, P. M. Tricarico¹³, A. Tricoli³⁰, I. M. Trigger^{161a}, S. Trincaz-Duvoid¹²⁹, D. A. Trischuk¹⁷⁰, A. Tropina³⁹, D. Truncali^{76a,76b}, L. Truong^{34c}, M. Trzebinski⁸⁷, A. Trzupek⁸⁷, F. Tsai¹⁵⁰, M. Tsai¹⁰⁷, A. Tsiamis¹⁵⁷, P. V. Tsiarehka³⁹, S. Tsigaridas^{161a}, A. Tsirigotis^{157,aa}, V. Tsiskaridze^{154a}, E. G. Tskhadadze^{154a}, Y. Tsujikawa⁸⁸, I. I. Tsukerman³⁸, V. Tsulaia^{18a}, S. Tsuno⁸³, K. Tsurii¹²⁰, D. Tsybychev¹⁵⁰, Y. Tu^{64b}, A. Tudorache^{28b}, V. Tudorache^{28b}, S. B. Tuncay¹²⁸, S. Turchikhin^{57a,57b}, I. Turk Cakir^{3a}, R. Turra^{71a}, T. Turtuvshin^{39,am}, P. M. Tuts⁴², S. Tzamarias^{157,z}, Y. Uematsu⁸³, F. Ukegawa¹⁶², P. A. Ulloa Poblete^{139b,139c}, E. N. Umaka³⁰, G. Unal³⁷, A. Undrus³⁰, G. Unel¹⁶⁴, J. Urban^{29b}, P. Urrejola^{139e}, G. Usai⁸, R. Ushioda¹⁵⁹, M. Usman¹⁰⁹, F. Ustuner⁵², Z. Uysal⁸¹, V. Vacek¹³⁴, B. Vachon¹⁰⁵, T. Vafeiadis³⁷, A. Vaitkus⁹⁷, C. Valderanis¹¹⁰, E. Valdes Santurio^{47a,47b}, M. Valente³⁷, S. Valentinetti^{24a,24b}, A. Valero¹⁶⁸, E. Valiente Moreno¹⁶⁸, A. Vallier⁹⁰, J. A. Valls Ferrer¹⁶⁸, D. R. Van Arneeman¹¹⁶, A. Van Der Graaf⁴⁹, H. Z. Van Der Schyf^{34e}, P. Van Gemmeren⁶, M. Van Rijnbach³⁷, S. Van Stroud⁹⁷, I. Van Vulpen¹¹⁶, P. Vana¹³⁵, M. Vanadia^{76a,76b}, U. M. Vande Voorde¹⁴⁹, W. Vandelli³⁷, E. R. Vandewall¹⁴⁸, D. Vannicola¹⁵⁶, L. Vannoli⁵³, R. Vari^{75a}, M. Varma¹⁷⁷, E. W. Varnes⁷, C. Varni⁷⁹, D. Varouchas⁶⁶, L. Varriale¹⁶⁸, K. E. Varvell¹⁵², M. E. Vasile^{28b}, L. Vaslin⁸³, M. D. Vassilev¹⁴⁸, A. Vasyukov³⁹, L. M. Vaughan¹²³, R. Vavricka¹³⁵, T. Vazquez Schroeder¹³, J. Veatch³², V. Vecchio¹⁰², M. J. Veen¹⁰⁴, I. Veliscek³⁰, I. Velkovska⁹⁴, L. M. Veloce¹⁶⁰, F. Veloso^{132a,132c}, A. G. Veltman⁵², S. Veneziano^{75a}, A. Ventura^{70a,70b}, A. Verbytskyi¹¹¹, M. Verducci^{74a,74b}, C. Vergis⁹⁵, M. Verissimo De Araujo^{82b}, W. Verkerke¹¹⁶, J. C. Vermeulen¹¹⁶, C. Vernieri¹⁴⁸, M. Vessella¹⁶⁴, M. C. Vetterli^{147,t}, A. Vgenopoulos¹⁰¹, N. Viaux Maira^{139g,an}, T. Vickey¹⁴⁴, O. E. Vickey Boeriu¹⁴⁴, G. H. A. Viehhauser¹²⁸, L. Vigani^{63b}, M. Vigil¹¹¹, M. Villa^{24a,24b}, M. Villaplana Perez¹⁶⁸, E. M. Villhauer⁴⁰, E. Vilucchi⁵³, M. Vincent¹⁶⁸, M. G. Vincter³⁵, A. Visibile¹¹⁶, A. Visive¹¹⁶, C. Vittori³⁷, I. Vivarelli^{24a,24b}, M. I. Vivas Albornoz⁴⁸, E. Voevodina¹¹¹, F. Vogel¹¹⁰, J. C. Voigt⁵⁰, P. Vokac¹³⁴, Yu. Volkotrub^{86b}, L. Vomberg²⁵, E. Von Toerne²⁵, B. Vormwald³⁷, K. Vorobev⁵¹, M. Vos¹⁶⁸, K. Voss¹⁴⁶, M. Vozak³⁷, L. Vozdecky¹²², N. Vranjes¹⁶, M. Vranjes Milosavljevic¹⁶, M. Vreeswijk¹¹⁶, N. K. Vu^{143a,143b}, R. Vuillermet³⁷, O. Vujanovic¹⁰¹, I. Vukotic⁴⁰, I. K. Vyas³⁵, J. F. Wack³³, S. Wada¹⁶², C. Wagner¹⁴⁸, J. M. Wagner^{18a}, W. Wagner¹⁷⁶, S. Wahdan¹⁷⁶, H. Wahlberg⁹¹, C. H. Waits¹²², J. Walder¹³⁶, R. Walker¹¹⁰, K. Walkingshaw Pass⁵⁹, W. Walkowiak¹⁴⁶, A. Wall¹³⁰, E. J. Wallin⁹⁹, T. Wamorkar^{18a}, K. Wandall-Christensen¹⁶⁸, A. Wang⁶², A. Z. Wang¹³⁸, C. Wang⁴⁸, C. Wang¹¹, H. Wang^{18a}, J. Wang^{64c}, P. Wang¹⁰², P. Wang⁹⁷, R. Wang⁶¹, R. Wang⁶, S. M. Wang¹⁵³, S. Wang¹⁴, T. Wang¹¹⁵, T. Wang⁶², W. T. Wang¹²⁸, W. Wang¹⁴, X. Wang¹⁶⁷, X. Wang^{143a}, X. Wang⁴⁸, Y. Wang¹⁵⁰, Y. Wang⁶², Z. Wang¹⁰⁷, Z. Wang^{143b}, Z. Wang¹⁰⁷, C. Wanotayaroj⁸³, A. Warburton¹⁰⁵, A. L. Warnerbring¹⁴⁶, S. Waterhouse⁹⁶, A. T. Watson²¹, H. Watson⁵², M. F. Watson²¹, E. Watton³⁷, G. Watts¹⁴¹, B. M. Waugh⁹⁷, J. M. Webb⁵⁴, C. Weber³⁰, M. S. Weber²⁰, S. M. Weber^{63a}, C. Wei⁶², Y. Wei⁵⁴, A. R. Weidberg¹²⁸, E. J. Weik¹¹⁹, J. Weingarten⁴⁹, C. Weiser⁵⁴, C. J. Wells⁴⁸, T. Wenaus³⁰, T. Wengler³⁷, N. S. Wenke¹¹¹, N. Wermes²⁵, M. Wessels^{63a}, A. M. Wharton⁹², A. S. White⁶¹, A. White⁸, M. J. White¹, D. Whiteson¹⁶⁴, L. Wickremasinghe¹²⁶, W. Wiedenmann¹⁷⁵, M. Wielers¹³⁶, R. Wierda¹⁴⁹, C. Wigglesworth⁴³, H. G. Wilkens³⁷, J. J. H. Wilkinson³³, D. M. Williams⁴², H. H. Williams¹³⁰, S. Williams³³, S. Willocq¹⁰⁴, B. J. Wilson¹⁰², D. J. Wilson¹⁰², P. J. Windischhofer⁴⁰, F. I. Winkel³¹, F. Winklmeier¹²⁵, B. T. Winter⁵⁴, M. Wittgen¹⁴⁸, M. Wobisch⁹⁸, T. Wojtkowski¹¹⁶, Z. Wolffs¹¹⁶, J. Wollrath³⁷, M. W. Wolter⁸⁷, H. Wolters^{132a,132c}, M. C. Wong¹³⁸, E. L. Woodward⁴², S. D. Worm⁴⁸, B. K. Wosiek⁸⁷, K. W. Woźniak⁸⁷, S. Wozniowski⁵⁵, K. Wraight⁵⁹, C. Wu¹⁶⁰, C. Wu²¹, J. Wu¹⁵⁸, M. Wu^{113b}, M. Wu¹¹⁵, S. L. Wu¹⁷⁵, S. Wu^{14,ao}, X. Wu⁶², Y. Q. Wu¹⁶⁰, Y. Wu⁶², Z. Wu⁴, Z. Wu^{113a}, J. Wuerzinger¹¹¹, T. R. Wyatt¹⁰², B. M. Wynne⁵², S. Xella⁴³, L. Xia^{113a}, M. Xie⁶², A. Xiong¹²⁵, D. Xu¹⁴, H. Xu⁶², L. Xu⁶², R. Xu¹³⁰, T. Xu¹⁰⁷, W. Xu^{113a}, Y. Xu¹⁴¹, Z. Xu⁵², R. Xue¹³¹, B. Yabsley¹⁵², S. Yacoob^{34a}, Y. Yamaguchi⁸³, E. Yamashita¹⁵⁸, H. Yamauchi¹⁶², T. Yamazaki^{18a}, Y. Yamazaki⁸⁵, S. Yan⁵⁹, Z. Yan¹⁰⁴, H. J. Yang^{143a,143b}, H. T. Yang⁶², S. Yang⁶², T. Yang^{64c}, X. Yang³⁷, X. Yang¹⁴, Y. Yang¹⁵⁸, Y. Yang⁶², W-M. Yao^{18a}, C. L. Yardley¹⁵¹, J. Ye¹⁴, S. Ye³⁰, X. Ye⁶², Y. Yeh⁹⁷, I. Yeletsikh³⁹, B. Yeo^{18b}, M. R. Yexley⁹⁷, T. P. Yildirim¹²⁸, K. Yorita¹⁷³, C. J. S. Young³⁷, C. Young¹⁴⁸, I. N. L. Young⁵⁹, N. D. Young¹²⁵, Y. Yu⁶², J. Yuan^{113c,14}, M. Yuan¹⁰⁷, R. Yuan^{143b}, L. Yue⁹⁷, M. Zaazoua⁶², B. Zabinski⁸⁷, I. Zahir^{36a}, A. Zaio^{57a,57b}, Z. K. Zak⁸⁷, T. Zakareishvili¹⁶⁸, S. Zambito⁵⁶, J. A. Zamora Saa^{139d}, J. Zang¹⁵⁸, R. Zanzottera^{71a,71b}, O. Zaplatilek¹³⁴, C. Zeitnitz¹⁷⁶, H. Zeng¹⁴, D. T. Zenger, Jr.²⁷, O. Zenin³⁸, T. Ženiš^{29a}, S. Zenz⁹⁵, D. Zerwas⁶⁶

D. F. Zhang¹⁴⁴, G. Zhang^{14,ao}, J. Zhang^{142a}, J. Zhang⁶, L. Zhang⁶², L. Zhang^{113a}, P. Zhang^{113c,14}, R. Zhang^{113a}, S. Zhang⁹⁰, T. Zhang¹⁵⁸, Y. Zhang¹⁴¹, Y. Zhang⁹⁷, Y. Zhang⁶², Y. Zhang^{113a}, Z. Zhang^{18a}, Z. Zhang^{142a}, Z. Zhang⁶⁶, H. Zhao¹⁴¹, T. Zhao^{142a}, Y. Zhao³⁵, Z. Zhao⁶², Z. Zhao⁶², A. Zhemchugov³⁹, J. Zheng^{113a}, K. Zheng¹⁶⁷, X. Zheng⁶², Z. Zheng¹⁴⁸, D. Zhong¹⁶⁷, B. Zhou¹⁰⁷, B. Zhou^{143b}, H. Zhou⁷, N. Zhou^{143a}, Y. Zhou¹⁵, Y. Zhou^{113a}, Y. Zhou⁷, J. Zhu¹⁰⁷, X. Zhu^{143b}, Y. Zhu^{143a}, Y. Zhu⁶², X. Zhuang¹⁴, K. Zhukov⁶⁸, N. I. Zimine³⁹, J. Zinsser^{63b}, M. Ziolkowski¹⁴⁶, L. Živković¹⁶, A. Zoccoli^{24a,24b}, K. Zoch⁶¹, A. Zografos³⁷, T. G. Zorbas¹⁴⁴, O. Zornpa⁴⁶, and L. Zwalinski³⁷

(ATLAS Collaboration)

¹*Department of Physics, University of Adelaide, Adelaide, Australia*

²*Department of Physics, University of Alberta, Edmonton, Alberta, Canada*

^{3a}*Department of Physics, Ankara University, Ankara, Türkiye*

^{3b}*Division of Physics, TOBB University of Economics and Technology, Ankara, Türkiye*

⁴*LAPP, Université Savoie Mont Blanc, CNRS/IN2P3, Annecy, France*

⁵*APC, Université Paris Cité, CNRS/IN2P3, Paris, France*

⁶*High Energy Physics Division, Argonne National Laboratory, Argonne, Illinois, USA*

⁷*Department of Physics, University of Arizona, Tucson, Arizona, USA*

⁹*Physics Department, National and Kapodistrian University of Athens, Athens, Greece*

¹⁰*Physics Department, National Technical University of Athens, Zografou, Greece*

¹¹*Department of Physics, University of Texas at Austin, Austin, Texas, USA*

¹²*Institute of Physics, Azerbaijan Academy of Sciences, Baku, Azerbaijan*

¹³*Institut de Física d'Altes Energies (IFAE), Barcelona Institute of Science and Technology, Barcelona, Spain*

¹⁴*Institute of High Energy Physics, Chinese Academy of Sciences, Beijing, China*

¹⁵*Physics Department, Tsinghua University, Beijing, China*

¹⁶*Institute of Physics, University of Belgrade, Belgrade, Serbia*

¹⁷*Department for Physics and Technology, University of Bergen, Bergen, Norway*

^{18a}*Physics Division, Lawrence Berkeley National Laboratory, Berkeley, California, USA*

^{18b}*University of California, Berkeley, California, USA*

¹⁹*Institut für Physik, Humboldt Universität zu Berlin, Berlin, Germany*

²⁰*Albert Einstein Center for Fundamental Physics and Laboratory for High Energy Physics, University of Bern, Bern, Switzerland*

²¹*School of Physics and Astronomy, University of Birmingham, Birmingham, United Kingdom*

^{22a}*Department of Physics, Bogazici University, Istanbul, Türkiye*

^{22b}*Department of Physics Engineering, Gaziantep University, Gaziantep, Türkiye*

^{22c}*Department of Physics, Istanbul University, Istanbul, Türkiye*

^{23a}*Facultad de Ciencias y Centro de Investigaciones, Universidad Antonio Nariño, Bogotá, Colombia*

^{23b}*Departamento de Física, Universidad Nacional de Colombia, Bogotá, Colombia*

^{24a}*Dipartimento di Fisica e Astronomia A. Righi, Università di Bologna, Bologna, Italy*

^{24b}*INFN Sezione di Bologna, Bologna, Italy*

²⁵*Physikalisches Institut, Universität Bonn, Bonn, Germany*

²⁶*Department of Physics, Boston University, Boston MA, USA*

²⁷*Department of Physics, Brandeis University, Waltham MA, USA*

^{28a}*Transilvania University of Brasov, Brasov, Romania*

^{28b}*Horia Hulubei National Institute of Physics and Nuclear Engineering, Bucharest, Romania*

^{28c}*Department of Physics, Alexandru Ioan Cuza University of Iasi, Iasi, Romania*

^{28d}*National Institute for Research and Development of Isotopic and Molecular Technologies, Physics Department, Cluj-Napoca, Romania*

^{28e}*National University of Science and Technology Politehnica, Bucharest, Romania*

^{28f}*West University in Timisoara, Timisoara, Romania*

^{28g}*Faculty of Physics, University of Bucharest, Bucharest, Romania*

^{29a}*Faculty of Mathematics, Physics and Informatics, Comenius University, Bratislava, Slovakia*

^{29b}*Department of Subnuclear Physics, Institute of Experimental Physics of the Slovak Academy of Sciences, Kosice, Slovak Republic*

³⁰*Physics Department, Brookhaven National Laboratory, Upton NY, USA*

³¹*Universidad de Buenos Aires, Facultad de Ciencias Exactas y Naturales, Departamento de Física, y CONICET, Instituto de Física de Buenos Aires (IFIBA), Buenos Aires, Argentina*

³²*California State University, California, USA*

³³*Cavendish Laboratory, University of Cambridge, Cambridge, United Kingdom*

^{34a}*Department of Physics, University of Cape Town, Cape Town, South Africa*

^{34b}*iThemba Labs, Western Cape, South Africa*

- ^{34c}Department of Mechanical Engineering Science, *University of Johannesburg*, Johannesburg, South Africa
- ^{34d}National Institute of Physics, *University of the Philippines Diliman*, Diliman, Quezon City, Philippines
- ^{34e}School of Physics, *University of the Witwatersrand*, Johannesburg, South Africa
- ³⁵Department of Physics, *Carleton University*, Ottawa, Ontario, Canada
- ^{36a}Faculté des Sciences Ain Chock, *Université Hassan II de Casablanca*, Casablanca, Morocco
- ^{36b}Faculté des Sciences, *Université Ibn-Tofail*, Kénitra, Morocco
- ^{36c}Faculté des Sciences Semlalia, *Université Cadi Ayyad*, LPHEA-Marrakech, Morocco
- ^{36d}LPMR, Faculté des Sciences, *Université Mohamed Premier*, Oujda, Morocco
- ^{36e}Faculté des Sciences, *Université Mohammed V*, Rabat, Morocco
- ^{36f}Institute of Applied Physics, *Mohammed VI Polytechnic University*, Ben Guerir, Morocco
- ³⁷CERN, Geneva, Switzerland
- ³⁸Affiliated with an institute formerly covered by a cooperation agreement with CERN
- ³⁹Affiliated with an international laboratory covered by a cooperation agreement with CERN
- ⁴⁰Enrico Fermi Institute, *University of Chicago*, Chicago, Illinois, USA
- ⁴¹LPC, *Université Clermont Auvergne*, CNRS/IN2P3, Clermont-Ferrand, France
- ⁴²Nevis Laboratory, *Columbia University*, Irvington, New York, USA
- ⁴³Niels Bohr Institute, *University of Copenhagen*, Copenhagen, Denmark
- ^{44a}Dipartimento di Fisica, *Università della Calabria*, Rende, Italy
- ^{44b}INFN Gruppo Collegato di Cosenza, Laboratori Nazionali di Frascati, Italy
- ⁴⁵Physics Department, *Southern Methodist University*, Dallas Texas, USA
- ⁴⁶National Centre for Scientific Research “Demokritos”, Agia Paraskevi, Greece
- ^{47a}Department of Physics, *Stockholm University*, Stockholm, Sweden
- ^{47b}Oskar Klein Centre, *Stockholm*, Sweden
- ⁴⁸Deutsches Elektronen-Synchrotron DESY, Hamburg and Zeuthen, Germany
- ⁴⁹Fakultät Physik, *Technische Universität Dortmund*, Dortmund, Germany
- ⁵⁰Institut für Kern- und Teilchenphysik, *Technische Universität Dresden*, Dresden, Germany
- ⁵¹Department of Physics, *Duke University*, Durham NC; USA
- ⁵²SUPA - School of Physics and Astronomy, *University of Edinburgh*, Edinburgh, United Kingdom
- ⁵³INFN e Laboratori Nazionali di Frascati, *Frascati*, Italy
- ⁵⁴Physikalisches Institut, *Albert-Ludwigs-Universität Freiburg*, Freiburg, Germany
- ⁵⁵II. Physikalisches Institut, *Georg-August-Universität Göttingen*, Göttingen, Germany
- ⁵⁶Département de Physique Nucléaire et Corpusculaire, *Université de Genève*, Genève, Switzerland
- ^{57a}Dipartimento di Fisica, *Università di Genova*, Genova, Italy
- ^{57b}INFN Sezione di Genova, *Genova*, Italy
- ⁵⁸II. Physikalisches Institut, *Justus-Liebig-Universität Giessen*, Giessen, Germany
- ⁵⁹SUPA - School of Physics and Astronomy, *University of Glasgow*, Glasgow, United Kingdom
- ⁶⁰LPSC, *Université Grenoble Alpes*, CNRS/IN2P3, Grenoble INP, Grenoble, France
- ⁶¹Laboratory for Particle Physics and Cosmology, *Harvard University*, Cambridge, Massachusetts USA
- ⁶²Department of Modern Physics and State Key Laboratory of Particle Detection and Electronics, *University of Science and Technology of China*, Hefei, China
- ^{63a}Kirchhoff-Institut für Physik, *Ruprecht-Karls-Universität Heidelberg*, Heidelberg, Germany
- ^{63b}Physikalisches Institut, *Ruprecht-Karls-Universität Heidelberg*, Heidelberg, Germany
- ^{64a}Department of Physics, *Chinese University of Hong Kong*, Shatin, New Territories, Hong Kong, China
- ^{64b}Department of Physics, *University of Hong Kong*, Hong Kong, China
- ^{64c}Department of Physics and Institute for Advanced Study, *Hong Kong University of Science and Technology*, Clear Water Bay, Kowloon, Hong Kong, China
- ⁶⁵Department of Physics, *National Tsing Hua University*, Hsinchu, Taiwan
- ⁶⁶IJCLab, *Université Paris-Saclay*, CNRS/IN2P3, 91405, Orsay, France
- ⁶⁷Centro Nacional de Microelectrónica (IMB-CNM-CSIC), *Barcelona*, Spain
- ⁶⁸Department of Physics, *Indiana University*, Bloomington IN; USA
- ^{69a}INFN Gruppo Collegato di Udine, Sezione di Trieste, *Udine*, Italy
- ^{69b}ICTP, *Trieste*, Italy
- ^{69c}Dipartimento Politecnico di Ingegneria e Architettura, *Università di Udine*, Udine, Italy
- ^{70a}INFN Sezione di Lecce, *Lecce*, Italy
- ^{70b}Dipartimento di Matematica e Fisica, *Università del Salento*, Lecce, Italy
- ^{71a}INFN Sezione di Milano, *Milano*, Italy
- ^{71b}Dipartimento di Fisica, *Università di Milano*, Milano, Italy
- ^{72a}INFN Sezione di Napoli, *Napoli*, Italy
- ^{72b}Dipartimento di Fisica, *Università di Napoli*, Napoli, Italy

- ^{73a}*INFN Sezione di Pavia, Pavia, Italy*
^{73b}*Dipartimento di Fisica, Università di Pavia, Pavia, Italy*
^{74a}*INFN Sezione di Pisa, Pisa, Italy*
^{74b}*Dipartimento di Fisica E. Fermi, Università di Pisa, Pisa, Italy*
^{75a}*INFN Sezione di Roma, Roma, Italy*
^{75b}*Dipartimento di Fisica, Sapienza Università di Roma, Roma, Italy*
^{76a}*INFN Sezione di Roma Tor Vergata, Roma, Italy*
^{76b}*Dipartimento di Fisica, Università di Roma Tor Vergata, Roma, Italy*
^{77a}*INFN Sezione di Roma Tre, Roma, Italy*
^{77b}*Dipartimento di Matematica e Fisica, Università Roma Tre, Roma, Italy*
^{78a}*INFN-TIFPA, Povo, Italy*
^{78b}*Università degli Studi di Trento, Trento, Italy*
⁷⁹*Universität Innsbruck, Department of Astro and Particle Physics, Innsbruck, Austria*
⁸*Department of Physics, University of Texas at Arlington, Arlington, Texas, USA*
⁸⁰*Department of Physics and Astronomy, Iowa State University, Ames, Iowa, USA*
⁸¹*Istinye University, Sariyer, Istanbul, Türkiye*
^{82a}*Departamento de Engenharia Elétrica, Universidade Federal de Juiz de Fora (UFJF), Juiz de Fora, Brazil*
^{82b}*Universidade Federal do Rio De Janeiro COPPE/EE/IF, Rio de Janeiro, Brazil*
^{82c}*Instituto de Física, Universidade de São Paulo, São Paulo, Brazil*
^{82d}*Rio de Janeiro State University, Rio de Janeiro, Brazil*
^{82e}*Federal University of Bahia, Bahia, Brazil*
⁸³*KEK, High Energy Accelerator Research Organization, Tsukuba, Japan*
^{84a}*Khalifa University of Science and Technology, Abu Dhabi, United Arab Emirates*
^{84b}*University of Sharjah, Sharjah, United Arab Emirates*
⁸⁵*Graduate School of Science, Kobe University, Kobe, Japan*
^{86a}*AGH University of Krakow, Faculty of Physics and Applied Computer Science, Krakow, Poland*
^{86b}*Marian Smoluchowski Institute of Physics, Jagiellonian University, Krakow, Poland*
⁸⁷*Institute of Nuclear Physics Polish Academy of Sciences, Krakow, Poland*
⁸⁸*Faculty of Science, Kyoto University, Kyoto, Japan*
⁸⁹*Research Center for Advanced Particle Physics and Department of Physics, Kyushu University, Fukuoka, Japan*
⁹⁰*L2IT, Université de Toulouse, CNRS/IN2P3, UPS, Toulouse, France*
⁹¹*Instituto de Física La Plata, Universidad Nacional de La Plata and CONICET, La Plata, Argentina*
⁹²*Physics Department, Lancaster University, Lancaster, United Kingdom*
⁹³*Oliver Lodge Laboratory, University of Liverpool, Liverpool, United Kingdom*
⁹⁴*Department of Experimental Particle Physics, Jožef Stefan Institute and Department of Physics, University of Ljubljana, Ljubljana, Slovenia*
⁹⁵*Department of Physics and Astronomy, Queen Mary University of London, London, United Kingdom*
⁹⁶*Department of Physics, Royal Holloway University of London, Egham, United Kingdom*
⁹⁷*Department of Physics and Astronomy, University College London, London, United Kingdom*
⁹⁸*Louisiana Tech University, Ruston, Louisiana, USA*
⁹⁹*Fysiska institutionen, Lunds universitet, Lund, Sweden*
¹⁰⁰*Departamento de Física Teórica C-15 and CIAFF, Universidad Autónoma de Madrid, Madrid, Spain*
¹⁰¹*Institut für Physik, Universität Mainz, Mainz, Germany*
¹⁰²*School of Physics and Astronomy, University of Manchester, Manchester, United Kingdom*
¹⁰³*CPPM, Aix-Marseille Université, CNRS/IN2P3, Marseille, France*
¹⁰⁴*Department of Physics, University of Massachusetts, Amherst, Massachusetts, USA*
¹⁰⁵*Department of Physics, McGill University, Montreal, Quebec, Canada*
¹⁰⁶*School of Physics, University of Melbourne, Victoria, Australia*
¹⁰⁷*Department of Physics, University of Michigan, Ann Arbor, Michigan, USA*
¹⁰⁸*Department of Physics and Astronomy, Michigan State University, East Lansing, Michigan, USA*
¹⁰⁹*Group of Particle Physics, University of Montreal, Montreal, Quebec, Canada*
¹¹⁰*Fakultät für Physik, Ludwig-Maximilians-Universität München, München, Germany*
¹¹¹*Max-Planck-Institut für Physik (Werner-Heisenberg-Institut), München, Germany*
¹¹²*Graduate School of Science and Kobayashi-Maskawa Institute, Nagoya University, Nagoya, Japan*
^{113a}*Department of Physics, Nanjing University, Nanjing, China*
^{113b}*School of Science, Shenzhen Campus of Sun Yat-sen University, Shenzhen, China*
^{113c}*University of Chinese Academy of Science (UCAS), Beijing, China*
¹¹⁴*Department of Physics and Astronomy, University of New Mexico, Albuquerque, New Mexico, USA*
¹¹⁵*Institute for Mathematics, Astrophysics and Particle Physics, Radboud University/Nikhef, Nijmegen, Netherlands*
¹¹⁶*Nikhef National Institute for Subatomic Physics and University of Amsterdam, Amsterdam, Netherlands*

- ¹¹⁷*Department of Physics, Northern Illinois University, DeKalb, Illinois, USA*
^{118a}*New York University Abu Dhabi, Abu Dhabi, United Arab Emirates*
^{118b}*United Arab Emirates University, Al Ain, United Arab Emirates*
¹¹⁹*Department of Physics, New York University, New York, New York, USA*
¹²⁰*Ochanomizu University, Otsuka, Bunkyo-ku, Tokyo, Japan*
¹²¹*Ohio State University, Columbus, Ohio, USA*
- ¹²²*Homer L. Dodge Department of Physics and Astronomy, University of Oklahoma, Norman, Oklahoma, USA*
¹²³*Department of Physics, Oklahoma State University, Stillwater, Oklahoma, USA*
¹²⁴*Palacký University, Joint Laboratory of Optics, Olomouc, Czech Republic*
¹²⁵*Institute for Fundamental Science, University of Oregon, Eugene, Oregon, USA*
¹²⁶*Graduate School of Science, University of Osaka, Osaka, Japan*
¹²⁷*Department of Physics, University of Oslo, Oslo, Norway*
¹²⁸*Department of Physics, Oxford University, Oxford, United Kingdom*
¹²⁹*LPNHE, Sorbonne Université, Université Paris Cité, CNRS/IN2P3, Paris, France*
¹³⁰*Department of Physics, University of Pennsylvania, Philadelphia, Pennsylvania, USA*
¹³¹*Department of Physics and Astronomy, University of Pittsburgh, Pittsburgh, Pennsylvania, USA*
^{132a}*Laboratório de Instrumentação e Física Experimental de Partículas - LIP, Lisboa, Portugal*
^{132b}*Departamento de Física, Faculdade de Ciências, Universidade de Lisboa, Lisboa, Portugal*
^{132c}*Departamento de Física, Universidade de Coimbra, Coimbra, Portugal*
^{132d}*Centro de Física Nuclear da Universidade de Lisboa, Lisboa, Portugal*
^{132e}*Departamento de Física, Escola de Ciências, Universidade do Minho, Braga, Portugal*
^{132f}*Departamento de Física Teórica y del Cosmos, Universidad de Granada, Granada, Spain*
^{132g}*Departamento de Física, Instituto Superior Técnico, Universidade de Lisboa, Lisboa, Portugal*
¹³³*Institute of Physics of the Czech Academy of Sciences, Prague, Czech Republic*
¹³⁴*Czech Technical University in Prague, Prague, Czech Republic*
¹³⁵*Charles University, Faculty of Mathematics and Physics, Prague, Czech Republic*
¹³⁶*Particle Physics Department, Rutherford Appleton Laboratory, Didcot, United Kingdom*
¹³⁷*IRFU, CEA, Université Paris-Saclay, Gif-sur-Yvette, France*
- ¹³⁸*Santa Cruz Institute for Particle Physics, University of California Santa Cruz, Santa Cruz, California, USA*
^{139a}*Departamento de Física, Pontificia Universidad Católica de Chile, Santiago, Chile*
^{139b}*Millennium Institute for Subatomic Physics at High Energy Frontier (SAPHIR), Santiago, Chile*
^{139c}*Instituto de Investigación Multidisciplinario en Ciencia y Tecnología, y Departamento de Física, Universidad de La Serena, La Serena, Chile*
^{139d}*Universidad Andres Bello, Department of Physics, Santiago, Chile*
^{139e}*Universidad San Sebastian, Recoleta, Chile*
^{139f}*Instituto de Alta Investigación, Universidad de Tarapacá, Arica, Chile*
^{139g}*Departamento de Física, Universidad Técnica Federico Santa María, Valparaíso, Chile*
¹⁴⁰*Department of Physics, Institute of Science, Tokyo, Japan*
- ¹⁴¹*Department of Physics, University of Washington, Seattle, Washington, USA*
- ^{142a}*Institute of Frontier and Interdisciplinary Science and Key Laboratory of Particle Physics and Particle Irradiation (MOE), Shandong University, Qingdao, China*
^{142b}*School of Physics, Zhengzhou University, Zhengzhou, China*
- ^{143a}*State Key Laboratory of Dark Matter Physics, School of Physics and Astronomy, Shanghai Jiao Tong University, Key Laboratory for Particle Astrophysics and Cosmology (MOE), SKLPPC, Shanghai, China*
^{143b}*State Key Laboratory of Dark Matter Physics, Tsung-Dao Lee Institute, Shanghai Jiao Tong University, Shanghai, China*
- ¹⁴⁴*Department of Physics and Astronomy, University of Sheffield, Sheffield, United Kingdom*
¹⁴⁵*Department of Physics, Shinshu University, Nagano, Japan*
¹⁴⁶*Department Physik, Universität Siegen, Siegen, Germany*
¹⁴⁷*Department of Physics, Simon Fraser University, Burnaby, British Columbia, Canada*
¹⁴⁸*SLAC National Accelerator Laboratory, Stanford, California, USA*
¹⁴⁹*Department of Physics, Royal Institute of Technology, Stockholm, Sweden*
- ¹⁵⁰*Departments of Physics and Astronomy, Stony Brook University, Stony Brook, New York, USA*
¹⁵¹*Department of Physics and Astronomy, University of Sussex, Brighton, United Kingdom*
¹⁵²*School of Physics, University of Sydney, Sydney, Australia*
¹⁵³*Institute of Physics, Academia Sinica, Taipei, Taiwan*
- ^{154a}*E. Andronikashvili Institute of Physics, Iv. Javakhishvili Tbilisi State University, Tbilisi, Georgia*
^{154b}*High Energy Physics Institute, Tbilisi State University, Tbilisi, Georgia*
^{154c}*University of Georgia, Tbilisi, Georgia*
- ¹⁵⁵*Department of Physics, Technion, Israel Institute of Technology, Haifa, Israel*

- ¹⁵⁶*Raymond and Beverly Sackler School of Physics and Astronomy, Tel Aviv University, Tel Aviv, Israel*
- ¹⁵⁷*Department of Physics, Aristotle University of Thessaloniki, Thessaloniki, Greece*
- ¹⁵⁸*International Center for Elementary Particle Physics and Department of Physics, University of Tokyo, Tokyo, Japan*
- ¹⁵⁹*Graduate School of Science and Technology, Tokyo Metropolitan University, Tokyo, Japan*
- ¹⁶⁰*Department of Physics, University of Toronto, Toronto, Ontario, Canada*
- ^{161a}*TRIUMF, Vancouver, British Columbia, Canada*
- ^{161b}*Department of Physics and Astronomy, York University, Toronto, Ontario, Canada*
- ¹⁶²*Division of Physics and Tomonaga Center for the History of the Universe, Faculty of Pure and Applied Sciences, University of Tsukuba, Tsukuba, Japan*
- ¹⁶³*Department of Physics and Astronomy, Tufts University, Medford, Massachusetts, USA*
- ¹⁶⁴*Department of Physics and Astronomy, University of California Irvine, Irvine, California, USA*
- ¹⁶⁵*University of West Attica, Athens, Greece*
- ¹⁶⁶*Department of Physics and Astronomy, University of Uppsala, Uppsala, Sweden*
- ¹⁶⁷*Department of Physics, University of Illinois, Urbana, Illinois, USA*
- ¹⁶⁸*Instituto de Física Corpuscular (IFIC), Centro Mixto Universidad de Valencia - CSIC, Valencia, Spain*
- ¹⁶⁹*Department of Physics, University of British Columbia, Vancouver, British Columbia, Canada*
- ¹⁷⁰*Department of Physics and Astronomy, University of Victoria, Victoria, British Columbia, Canada*
- ¹⁷¹*Fakultät für Physik und Astronomie, Julius-Maximilians-Universität Würzburg, Würzburg, Germany*
- ¹⁷²*Department of Physics, University of Warwick, Coventry, United Kingdom*
- ¹⁷³*Waseda University, Tokyo, Japan*
- ¹⁷⁴*Department of Particle Physics and Astrophysics, Weizmann Institute of Science, Rehovot, Israel*
- ¹⁷⁵*Department of Physics, University of Wisconsin, Madison, Wisconsin, USA*
- ¹⁷⁶*Fakultät für Mathematik und Naturwissenschaften, Fachgruppe Physik, Bergische Universität Wuppertal, Wuppertal, Germany*
- ¹⁷⁷*Department of Physics, Yale University, New Haven, Connecticut, USA*
- ¹⁷⁸*Yerevan Physics Institute, Yerevan, Armenia*

^aAlso at Department of Physics, King's College London, London, United Kingdom.

^bAlso at Institute of Physics, Azerbaijan Academy of Sciences, Baku, Azerbaijan.

^cAlso at Imam Mohammad Ibn Saud Islamic University, Saudi Arabia.

^dAlso at Department of Physics, University of Thessaly, Greece.

^eAlso at An-Najah National University, Nablus, Palestine.

^fAlso at Department of Physics, University of Fribourg, Fribourg, Switzerland.

^gAlso at Department of Physics, Westmont College, Santa Barbara, USA.

^hAlso at Departament de Física de la Universitat Autònoma de Barcelona, Barcelona, Spain.

ⁱAlso at University of Siena, Siena, Italy.

^jAlso at Affiliated with an institute formerly covered by a cooperation agreement with CERN.

^kAlso at The Collaborative Innovation Center of Quantum Matter (CICQM), Beijing, China.

^lAlso at Faculty of Physics, Sofia University, 'St. Kliment Ohridski', Sofia, Bulgaria.

^mAlso at Università di Napoli Parthenope, Napoli, Italy.

ⁿAlso at Institute of Particle Physics (IPP), Canada.

^oAlso at Department of Physics, Bolu Abant İzzet Baysal University, Bolu, Türkiye.

^pDeceased.

^qAlso at Faculty of Physics, University of Bucharest, Bucharest, Romania.

^rAlso at Borough of Manhattan Community College, City University of New York, New York, New York, USA.

^sAlso at Department of Financial and Management Engineering, University of the Aegean, Chios, Greece.

^tAlso at TRIUMF, Vancouver, British Columbia, Canada.

^uAlso at Institutio Catalana de Recerca i Estudis Avancats, ICREA, Barcelona, Spain.

^vAlso at Henan University, Henan, China.

^wAlso at Yeditepe University, Physics Department, Istanbul, Türkiye.

^xAlso at Institute of Theoretical Physics, Ilia State University, Tbilisi, Georgia.

^yAlso at CERN, Geneva, Switzerland.

^zAlso at Center for Interdisciplinary Research and Innovation (CIRI-AUTH), Thessaloniki, Greece.

^{aa}Also at Hellenic Open University, Patras, Greece.

^{ab}Also at Department of Modern Physics and State Key Laboratory of Particle Detection and Electronics, University of Science and Technology of China, Hefei, China.

^{ac}Also at Department of Mathematical Sciences, University of South Africa, Johannesburg, South Africa.

^{ad}Also at Department of Physics, Stellenbosch University, South Africa.

^{ae}Also at Department of Physics, University of Colorado Boulder, Boulder, Colorado, USA.

^{af}Also at Département de Physique Nucléaire et Corpusculaire, Université de Genève, Genève, Switzerland.

^{ag}Also at Institut für Experimentalphysik, Universität Hamburg, Hamburg, Germany.

^{ah} Also at Centre of Physics of the Universities of Minho and Porto (CF-UM-UP), Portugal.

^{ai} Also at Institute for Nuclear Research and Nuclear Energy (INRNE) of the Bulgarian Academy of Sciences, Sofia, Bulgaria.

^{aj} Also at Washington College, Chestertown, Maryland, USA.

^{ak} Also at Institute of Applied Physics, Mohammed VI Polytechnic University, Ben Guerir, Morocco.

^{al} Also at Department of Physics, Stanford University, Stanford, California, USA.

^{am} Also at Institute of Physics and Technology, Mongolian Academy of Sciences, Ulaanbaatar, Mongolia.

^{an} Also at Millennium Institute for Subatomic Physics at High Energy Frontier (SAPHIR), Santiago, Chile.

^{ao} Also at University of Chinese Academy of Sciences (UCAS), Beijing, China.